Baffin Bay Sediment Core Profiling for Historical Water Quality

Final Report by:

Mark Besonen, Principal Investigator
Earth System Science Laboratory
Texas A&M University—Corpus Christi
6300 Ocean Drive, Unit 5892
Corpus Christi, TX 78412
E-mail: Mark.Besonen@tamucc.edu

Erin M. Hill, Co-Principal Investigator
Center for Coastal Studies
Texas A&M University—Corpus Christi
6300 Ocean Drive, NRC Suite 3200
Corpus Christi, TX 78412
E-mail: Erin.Hill@tamucc.edu

Philippe Tissot, Co-Principal Investigator
Conrad Blucher Institute
Sediment Analysis and Radioanalysis Laboratory
Texas A&M University—Corpus Christi
6300 Ocean Drive, NRC Suite 2801
Corpus Christi, TX 78412
E-mail: Philippe.Tissot@tamucc.edu

Baffin Bay Sediment Core Profiling for Historical Water Quality Project 1514
Reporting period: 1 September 2014 to 31 March 2016
Date of submission: 8 April 2016

SUBMITTED TO:

Coastal Bend Bays & Estuaries Program
615 N. Upper Broadway, Suite 1200
Corpus Christi, TX 78401

CBBEP - 109

A. Executive Summary

The recent deterioration of water quality conditions in Baffin Bay is of great concern. Increased nutrient loading from human impact in the watershed is an obvious factor that must be considered. But preliminary work on sediment cores from the Cayo del Grullo tributary bay showed that algal blooms and elevated chlorophyll concentrations were already occurring long before the most recent period of deterioration (Besonen, unpublished data). Thus, natural factors such as periods of wetter/drier climate, the very restricted circulation of Baffin Bay, and other elements are also important factors that moderate the water quality health of the system. A longer-term perspective is needed to understand these natural factors, and the goal of this project is to provide that perspective.

This project used a multiproxy suite of complementary indicators to study 12 sediment cores from Baffin Bay, and reconstruct a detailed history of water quality and sedimentation changes over the last ~150 years. Five sediment core were extracted from the main basin, three each from the Alazan and Cayo del Grullo secondary bays, and one from the Laguna Salada. Sedimentation in the tributary bays is highly variable due to the shallow waters and fluvial/terrestrial influence. Overall, stratigraphy throughout the system is well-preserved, but the main basin contains a more continuously complete record of sedimentation than the tributary bays.

^{137}Cs/^{210}Pb radioisotope analysis was used to provide chronologic control for three sediment cores—one from the main basin, and one each from the Alazan and Cayo del Grullo tributary bays. The main basin core yielded a ^{137}Cs-based sedimentation rate of 0.57 cm/year, with a complementary ^{210}Pb result. The tributary bays yielded calculated sedimentation rates that were much lower (~1/2 and ~1/5 of the main basin), which reaffirms that the main basin contains a much more continuously complete record of sedimentation. Radioisotope analyses were supplemented by the results of proxy analyses to further refine the chronology.

Grain size analyses (Figure 1) show an expected trend with main basin cores generally being composed of >= ~90% mud (mixed silt and clay size fractions, i.e. <63 microns), and the remainder portion sand (i.e. 63-2000 micron size range). Mud still dominates the sediment cores from the tributary bays, but sand content reaches 20-30% given the shallower water, and greater fluvial influence. No gravel-sized mineral grains (i.e. >= 2000 microns) were encountered in any of the samples.

Results from magnetic susceptibility analysis show a pronounced variability in sediment cores from the tributary bays, and this is related to the strong fluvial/terrestrial influence there. Overall, most cores show a shift towards decreasing magnetic susceptibility values from the base upwards, and this probably indicates a progressive, relative increase in autochthonous, biologic, water column-derived sediment production vs. fluvial/terrestrial inputs through time.

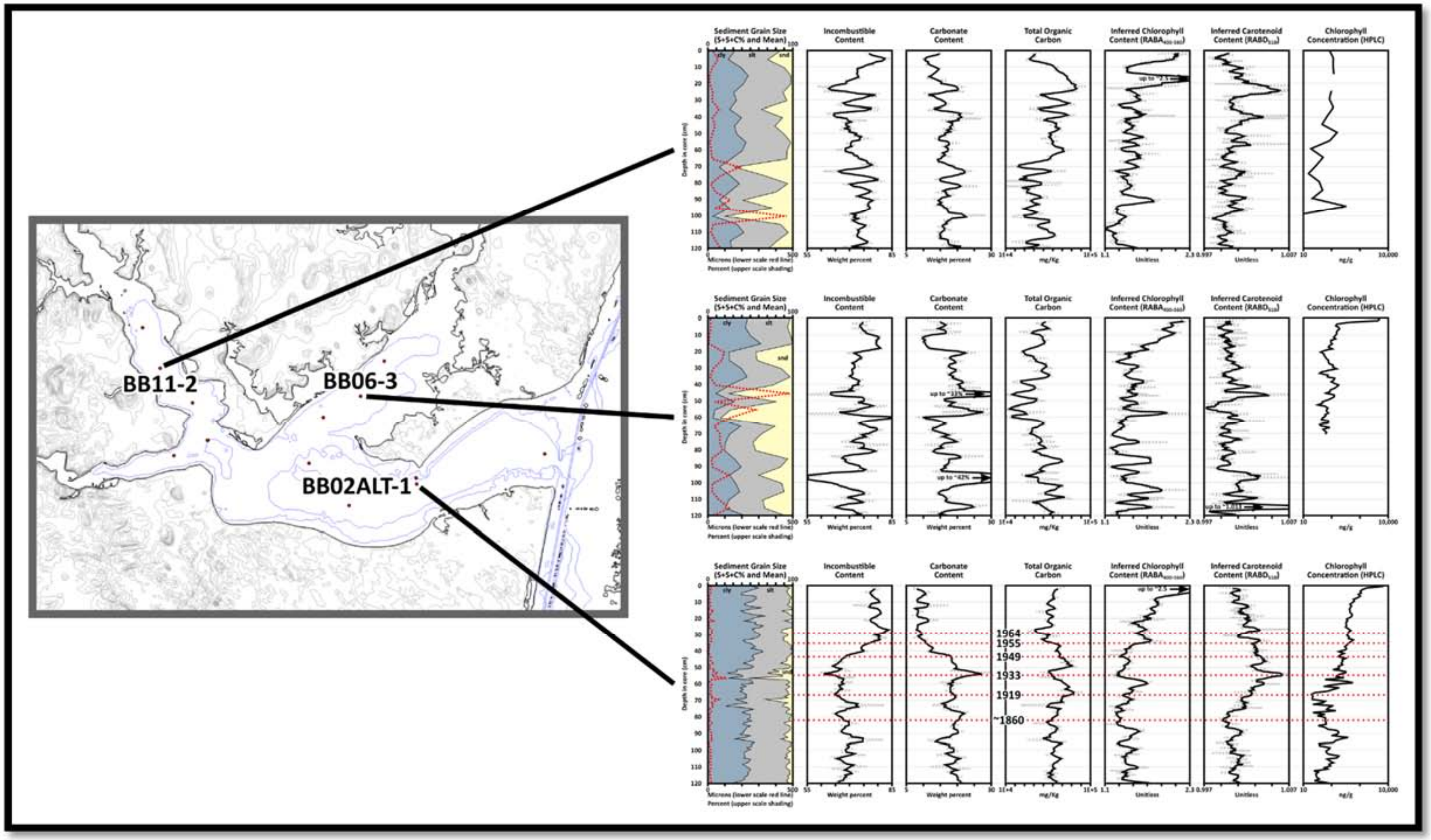

Figure 1—Multiproxy Results Panels from Main Basin, Alazan Bay, and Cayo del Grullo

This figure shows results panels for core BB02ALT-1 from the main basin (lower panel), core BB06-3 from Alazan Bay (middle panel), and BB11-2 from Cayo del Grullo. This is a subset of the analysis results that available for each core including (from left to right) grain size, incombustible content, carbonate content, total organic carbon, inferred chlorophyll content, inferred carotenoid content, and HPLC-measured chlorophyll content. Note the dated chronological time lines for the BB02ALT-1 curve. The trend towards ever increasing chlorophyll values as seen in core BB02ALT-1 starts around AD ~1860. Also, note that the long-term trends for chlorophyll and carotenoids initially covary, but then diverge about AD 1930. This suggests a long-term shift towards better preservation conditions, which favors chlorophyll, and probably represents a progressive, long-term decrease in oxygenation of the water column due to eutrophication of the basin. Finally, the incombustible and carbonate contents show a strong, mode-like shift to higher and lower values, respectively, and this is related to the opening of the ICW, which increased circulation, and lowered alkalinity in the basin.

Results for incombustible content (siliciclastic mineral matter), and mixed carbonate content vary inversely (Figure 1). The strongest trend is visible in sediments cores from the main basin. An abrupt, mode-like change occurs, and simultaneously increases incombustible content, and decreases carbonate content, by ~20 weight percent in the upper half of the cores. This is not due to an absolute increase in mineral matter—instead, it is linked to a reduction in carbonate. Dating pegs this abrupt shift to the opening of the Intracoastal Waterway in AD 1949, which increased water exchange with the ocean, and consequently greatly reduced alkalinity in the basin.

Sediment cores showed very high values of total organic carbon (TOC) with whole core averages ranging between 4.10-6.66% for all the cores (Figure 1). Long-term trends in TOC do not tightly mirror the chlorophyll content trends as initially expected, but similar results have been reported from other estuaries with high TOC values like Baffin Bay.

Diffuse color reflectance scanning was used to produce high-resolution curves showing inferred chlorophyll and carotenoid pigment concentrations down core (Figure 1). To verify the legitimacy of these reflectance-based, inferred chlorophyll content measurements, a comparison was made with a sediment core for which chlorophyll concentrations had been determined by traditional, high performance liquid chromatography (HPLC). Results from both analyses show very strong correspondence, and a simple, empirically-derived mathematical transform to convert reflectance-based, inferred chlorophyll values to approximate HPLC equivalents was suggested.

Chlorophyll concentrations show a generally increasing trend in most sediment cores from the base upwards with a very strong peak at the tops of all cores (Figure 1). The well-dated core from the main basin shows an initial decreasing trend, but then a shift to continuously increasing values up to the present day. Based on the radioisotope dating results, and recognition that establishment of the King Ranch in AD 1853 marked the beginning of significant land use changes in the watershed that has only increased through time, this transition to progressively increasing pigment values is dated to AD ~1860.

The long-term trends of chlorophyll and carotenoid pigment concentrations initially covary, but then diverge about mid core (Figure 1). The chlorophyll values continue to rise while carotenoid values fall. Chlorophylls are much more susceptible to alteration than carotenoids, thus, this divergence can be interpreted as a long-term shift towards better preservation conditions, which favors chlorophyll. This shift probably represents a progressive, long-term decrease in oxygenation of the water column due to eutrophication of the basin, and the start of this change is dated to AD ~1930.

Several chlorophyll content peaks are superimposed on the long-term trend of constantly rising chlorophyll values. One of the largest peaks is dated to AD 1954-1958, which exactly corresponds with the peak of the regional, catastrophic drought in the 1950's. A straightforward causal mechanism is suggested—decreased fresh water flow reduced flushing, and led to nutrient accumulation that drove primary productivity levels higher.

The modern chlorophyll peak in all cores reaches very high values—in one core it reaches 20,387 ng/g as measured by HPLC. This is undoubtedly related to an increasing nutrient load to the basin, but like the catastrophic drought in the 1950's, which reduced flushing, and led to an accumulation of nutrients, the modern chlorophyll peak is probably related to the strong drought which started in 2010. One appreciated implication of this observation is that as this modern drought recedes, chlorophyll values will probably be reduced, too, due to increased flushing.

This study makes it possible to comment on how the system functions as a whole with respect to water quality and sedimentation. The sediment cores from the eastern part of the main basin archive the most continuously complete records, they show excellent coordination with one another, and they show the strongest impact of the ICW opening at least with respect to sediment composition. Cores from the western part of the main basin reflect a mix of both main basin dynamics, and what is happening in the tributary bays. Cores from Alazan Bay generally seem to reflect what is happening in that tributary bay. The curious exception is the core farthest in towards the bay head—it shows trends similar to the main basin cores, which indicates that water quality changes in the main basin can be clearly noted deep into Alazan Bay. Cores from Cayo del Grullo generally seem to reflect what is happening in that tributary bay. The core farthest in towards the bay head in that branch, however, shows very strong fluvial/deltaic influence. Finally, the core from the Laguna Salada shows trends that are somewhat unique throughout the whole system, and this may have some significance with respect to the initiation of algal blooms such as brown tide. Since blooms are apparently not initiated in the main basin, and Alazan Bay seems to be affected by water quality changes seen in the main basin, it might not be the most likely candidate for the initiation of blooms. Instead, it is speculated that the Laguna Salada, might be a more likely candidate because it functions somewhat independently.

B. Table of Contents

List of Figures

List of Tables

C. Introduction and Background

The deterioration of water quality conditions in Baffin Bay has become of great concern with particular issues including the trend towards eutrophic conditions, elevated chlorophyll concentrations, the occurrence of nuisance brown tide blooms, and a potential disruption of the aquatic food web (possibly evidenced by emaciated black drum). TCEQ has Baffin Bay listed as a concern for chlorophyll-a according to the 2013 Basin Highlights Summary Report published by the Nueces River Authority (NRA, 2013). Much effort is now being dedicated to monitoring the current water quality conditions around the bay, and the nutrient inputs into the system, which may be driving the current problems. While these modern observations provide a critical body of evidence for understanding the current state of the system, pilot sediment cores retrieved from the Cayo del Grullo tributary bay show that algal blooms and periods of elevated chlorophyll concentrations existed there prior to 1990, and perhaps even 1850. Understanding the natural variability and long-term evolution of the system is necessary to put the modern condition into perspective. The goal of this project was to use sediment cores to provide the needed perspective, and look back in time to track the evolution and development of water quality and chlorophyll concentrations in the bay system over the last ~150 years.

Using radiometric dating techniques to provide actual calendar ages for the stratigraphy, we have created a timeline that shows how water quality and chlorophyll concentrations have evolved over the last ~150 years due to human impact. We examined a network of sediment cores from both the main bay and the tributary bays to extend the spatial coverage, and understand how the system has evolved as a whole instead of at just one particular spot. This longer term perspective provides a fundamental context for understanding the modern state of the system, and provides a basis for making the most informed management decisions and recommendations for the future.

D. Objective

The objective of this project was to use sediment cores to document how water quality and chlorophyll concentrations in the Baffin Bay system have changed through time with a primary focus from AD 1850 to the present. This period of time corresponds with the start of significant human impact, and thus, increased loadings from farming, grazing, and other land use changes.

E. Sampling and Analysis Methods

Sediment Coring and Retrieval

Multiple sediment cores were retrieved with a hammer/percussion coring system at twelve stations distributed around the main basin and tributary bays of the Baffin Bay complex (Figure 2). The coring system used polycarbonate tubes with a 6.7 cm inner diameter, and up to ~2.40 m in length. Sediment cores were transported back to the TAMUCC Earth System Science Lab in an upright, vertical orientation, and stored in a locked, walk-in refrigerator at 3-4°C in the same orientation until processing.

Sediment Core Workflow and Processing

Sediment cores were split longitudinally down their lengths yielding two semi-cylindrical halves—the first and second core halves. The first core half underwent immediate processing to ensure the best preservation of pigments as described below while the second core half was reserved for subsequent processing usually within a couple days of splitting.

Initial Non-Destructive Analyses on First Core Half (Diffuse Color Reflectance, Photography, and Magnetic Susceptibility)

First core halves underwent a rapid, initial suite of non-destructive analyses at high resolution to document the stratigraphy and basic physical sedimentology of the cores before being sectioned for pigment and radioisotope dating analysis as described further below. Immediately after splitting, the surface of the core half was cleaned off with aluminum flashing, and a depth scale was established with non-reactive glass beads. The sediment core was covered with plastic wrap making sure to minimize air bubbles, and a Konica-Minolta CM-2600d spectrophotometer with a 0.3 mm aperture was used to gather a diffuse color reflectance profile (further details in Inferred Pigments via Diffuse Color Reflectance Scanning section below) down the length of the core at 0.5-cm resolution. Following the diffuse color reflectance scan, the core surface was once again cleaned off, and high resolution, colored-balanced, manual exposure images were acquired down the length of the core with a custom, rolling light box, and a DSLR camera. The central "sweet spot" of each frame (minimum optical distortion) was used at a later time to manually stitch together seamless, high resolution photomosaics of each sediment core. Following the photo image acquisition, a Bartington MS3 susceptibility meter coupled with a high resolution MS2E surface scanner was used to produce a magnetic susceptibility profile down the length of the core at 0.5-cm resolution.

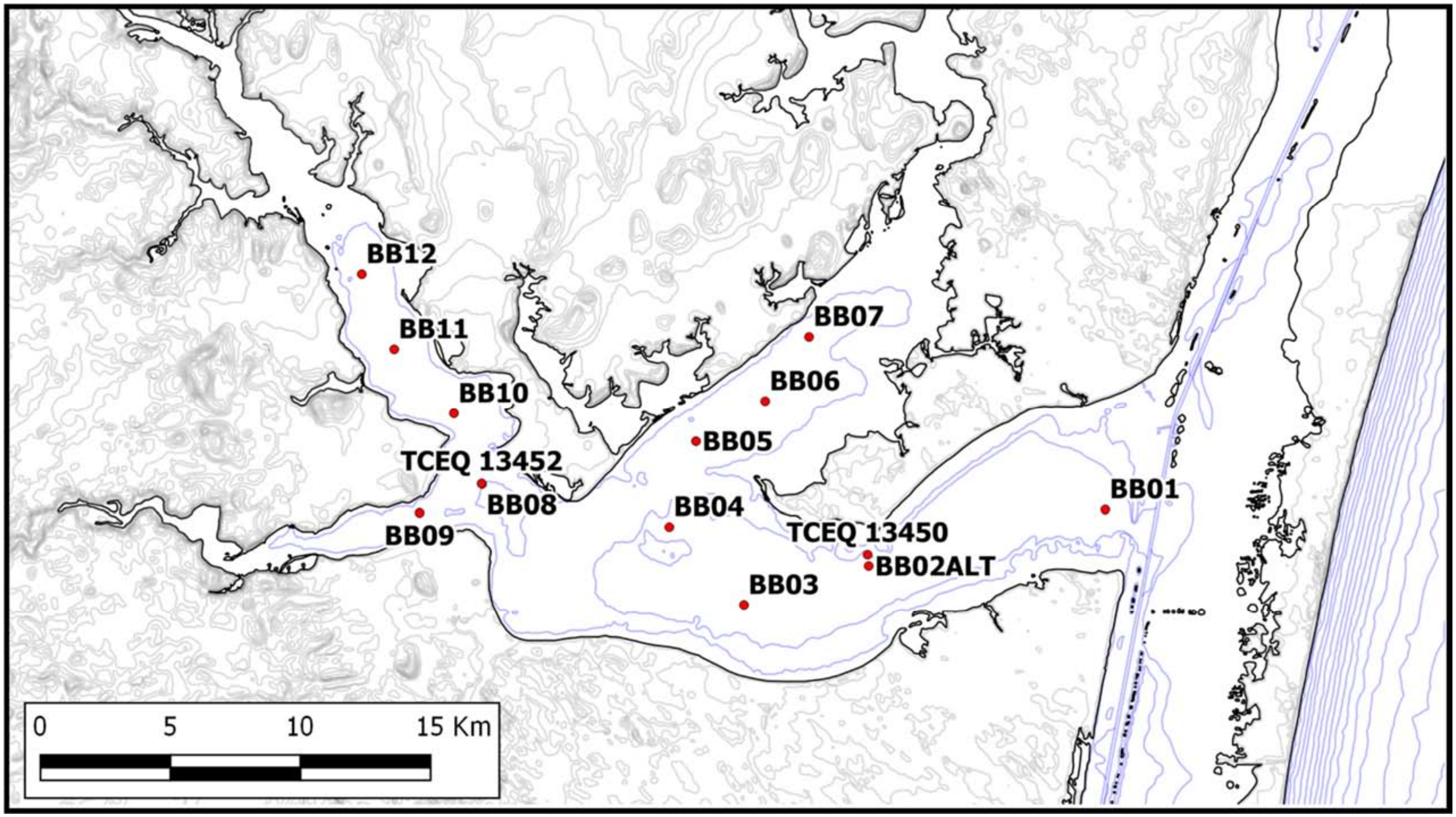

Figure 2—Map of Baffin Bay Sediment Core Locations
This map shows the locations of the 12 stations from which sediment cores were retrieved for this project. Station BB08 was coordinated with TCEQ long-term monitoring station 13452, and they are represented by a single red circle on the map above. Station BB02ALT was established about 400 m to the south of TCEQ long-term monitoring station 13450 towards the center of the main basin (two red circles on the map above). Exact coordination with TCEQ station 13450 was not possible because the sediments at that location consist of coarse, littoral drift as further explained in the Sediment Coring Stations section of the main Results section below.

Final Destructive Analyses on First Core Half (Pigment and $^{137}Cs/^{210}Pb$ Sampling and Storage)

Immediately following the non-destructive analysis chain mention above, the same sediment core half was subsampled into 1-cm thick slices using a custom, semi-circular spatula tool. The 1-cm slices were placed in preweighed, plastic ziplock bags, weighed for an estimate of wet bulk density, and then frozen and stored in a -80°C freezer in preparation for freeze drying. After freeze drying, the bags were reweighed for an estimate of dry bulk density, and the samples were gently homogenized by hand. Approximately 1g of dry sediment was removed to 15ml centrifuge tubes for pigment analysis, and the remainder of the sample made available for $^{137}Cs/^{210}Pb$ and other analyses. Throughout the entire processing chain involving pigment samples, working conditions were "lights out", and samples were kept in the freezer, and worked on in small batches so as to avoid degradation of the pigments by light and temperature.

Destructive Analyses on Second Core Half (Bulk Density/Loss-on-Ignition/TOC Chain, and Sediment Grain Size Analysis)

Following work on the first core half, the second core half was sampled down its length at 1-cm resolution using a custom, 1-cm^3 constant volume sampler. Sample plugs were gathered into preweighed plastic scintillation vials, and via a processing chain, determinations of wet/dry bulk density (second estimate), and loss-on-ignition (Dean, 1974) for organic carbon, carbonate minerals, and the incombustible fraction were made. Organic matter results via loss-on-ignition were converted to estimates of total organic carbon following guidance by Pribyl (2010).

Samples of ~2-3g of wet sediment were later taken down the same core half at 5-cm resolution for grain size analysis using a Beckman-Coulter LS 13 320 Laser Diffraction Particle Size Analyzer. For one sediment core (BB02ALT-1) samples were extracted at 1-cm resolution. To clean organic matter from the wet sediments, and disaggregate them, samples were digested in 5% H_2O_2 in a 50°C water bath until no reaction remained, and then were rinsed and centrifuged before analysis. Samples were manually homogenized into a slurry with the consistency of a soft pudding so as to insure that a representative sample involving all grain sizes in a given sample was extracted and used for analysis.

Inferred Pigments via Diffuse Color Reflectance Scanning

Diffuse color reflectance analysis is a rapid, non-destructive tool that can be used to determine the compositional characteristics of a sediment sample. This includes minerogenic matter, biogenic matter such as pigments, and essentially any material or sedimentological change that would alter the color reflectance of a sample even if the change is so subtle that it is not perceptible to the naked eye. It works on the simple principle that different materials do not uniformly reflect all wavelengths of light in the visible spectrum from 400-700 nm, i.e. materials may show preferential absorption bands at different wavelengths. Thus, by continuously scanning down the length of a sediment core, and quantifying the absorption bands in the resulting reflectance spectra, one may develop a profile that shows changing fluxes of mineral and biogenic matter, or other environmental changes, back in time. This tool has been used extensively in studies of oceanic sediments, and more recently adopted for high-resolution paleoenvironmental and paleoclimate studies by the lacustrine community. But it has been completely underutilized, perhaps "undiscovered", for similar studies in coastal/estuarine settings. Figure 3 shows four example reflectance spectra from Baffin Bay sediments, and they were chosen to simply illustrate the concept discussed above.

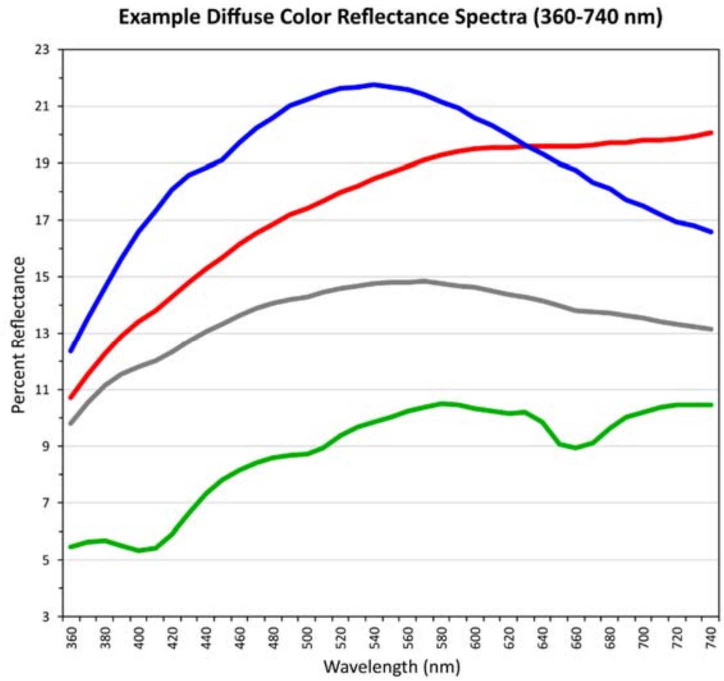

Figure 3—Example Diffuse Color Reflectance Spectra

The figure above shows example reflectance spectra in the visual range (400-700 nm) for four different sediment samples from Baffin Bay. The gray line shows the reflectance spectrum of a homogenous gray mud—reflectance varies from 10-15% at all wavelengths, which is much more uniform than the other samples. The red line shows the spectral response of a sand layer—there is a greater amount of reflectance (i.e. less absorption) at longer wavelengths. The blue line shows the reflectance spectrum for a green-gray mud found at depth in one of the tributary bays. Finally, the green line represents a sample with a high inferred pigment content. Notice the overall lower reflectivity value, but importantly, the absorption troughs at around 410 nm, 510 nm, and 660 nm. The two absorption troughs at 410 and 660 nm are related to chlorophyll and its derivate/breakdown products, which have absorption maxima at those wavelengths. Similarly, the trough at 510 nm is related to the presence of a carotenoid pigment, which has a local absorption maximum at that wavelength.

This study uses two parameters calculated from reflectance spectra that were defined by Rein and Sirocko (2002). The first one is the $RABA_{400\text{-}560}$ parameter, which is a calculation of the relative absorption band area from 400-560 nm beneath the local maximum at 590 nm. Rein and Sirocko (2002) related this parameter to the total pigment content of their samples, which was dominated by chlorophyll. Thus, this parameter is used as a measure of inferred chlorophyll content in the sediments for the present study. Use as such is justified by comparison with a chlorophyll *a* profile determined by traditional, high performance liquid chromatography (HPLC) in the Verification of Inferred Chlorophyll Content Versus HPLC-Determined Chlorophyll portion of the Results section. This report also uses the $RABD_{510}$ parameter, which is a calculation of the relative absorption band depth for the absorption trough centered on 510 nm. Rein and Sirocko (2002) relate this trough to a local absorption maximum for carotenoid pigments, and thus, this report uses the parameter as a measure of inferred carotenoid pigment content in the sediments. The green curve in Figure 3 shows the reflectance spectrum from a sample which shows these pigment absorption troughs.

Overall, the results in this report make a strong case for using diffuse color reflectance scanning analysis with estuarine sediments just like it has already been embraced for use with oceanic and lacustrine sediments. Though there is an initial cost associated with the purchase of a reflectance spectrophotometer, once the equipment acquired, it is low maintenance and low cost except for the occasional replacement of a light source or strobe. Second, this analysis is completely non-destructive. After acquiring a very rich data set about the compositional and physical characteristics a sediment core, 100% of the sediment core is still available for other analyses. Third, and this is especially true if pigments are the target of interest, there is essentially no preparation needed—no need to freeze-dry the samples, no chemicals needed for pigment extractions, and thus, no chemical waste to deal with later. In fact, preparation for reflectance scanning simply involves splitting open a core, cleaning off the surface, and covering it with plastic wrap before using the reflectance scanner. An extension of this point is that since the process is so quick and low cost, collecting rich, high-resolution (0.5-cm resolution, for example) data sets for every single sediment core in a large project actually becomes a distinct reality. In the present study, for example, 0.5-cm resolution diffuse color reflectance scans for all sediment cores were acquired, but it was necessary to keep HPLC chlorophyll assessments at 5-cm resolution for most of the cores because of time and funding considerations. In a hybrid scenario, diffuse reflectance scans can potentially be used to provide an initial "roadmap" for focusing other analyses that are more time-, effort-, and resource-intensive.

Of course, like any tool, there are some detractions, too. In fact, what makes the analysis so quick, i.e. the lack of sample preparation, also means that some adjustments to raw results are often necessary. For example, water content generally reduces reflectively so when scanning a wet sediment core, adjusting for changes in water content down core is necessary. Second, there is presently not a strong knowledgebase and general know-how as compared to more traditional analytical techniques. This carries over to the post-scanning, data processing part of the work because the analysis generates very large numerical data sets given its spectral nature. In fact, every measurement actually consists of 39 numerical values (i.e. reflectance values in 10 nm bins from 360-740 nm), and the large numerical matrices that are a result can potentially be challenging to process and analyze given the general lack of a large community knowledgebase. Finally, until this tool becomes better known and understood like traditional analytical techniques, some level of verification or calibration with traditional analytical results is usually necessary. Nonetheless, the attraction of rich, cheap, fast, high-resolution, non-destructive data sets makes this tool incredibly appealing.

Pigment Analysis via High Performance Liquid Chromatography (HPLC)

Phytoplankton community composition was assessed by pigment analysis using the HPLC methodology as described by Zimba et al. (1999). Pigments (carotenoids and chlorophylls) were quantified using a HP1100 equipped with DAD and fluorescence detectors (Agilent Technologies, Palo Alto, CA). Identification of specific divisions of algae was possible using taxon-specific pigment biomarkers. A pigment library was used to identify samples; unknown samples were quantified by linear regression of known commercial standards (Zimba et al., 2002).

^{137}Cs/^{210}Pb Sediment Dating

Sample Preparation

Freeze dried sediment samples from the first core halves of three sediment cores (BB02ALT-1, BB06-3, and BB11-2) were analyzed for ^{137}Cs/^{210}Pb at the Sediment Analysis and Radioanalysis Laboratory at the Conrad Blucher Institute (TAMUCC).

Samples were crushed into small particles and filled into wear-resistant 55 mm long Nylon tubes of 9.52 mm outer diameter (OD) and 7.94 mm inner diameter (ID) with sample material. After filling, the vial tubes were capped on each end with 7.94 mm diameter x ~3 mm nylon pieces and sealed hermetically with a layer of epoxy. The weight of the samples was measured as part of the process. All preparation equipment was cleaned and dried prior to contact with samples and work was conducted on a clean surface such as a large Kimwipe® which was replaced after each individual sample processing.

Equipment Specifications and Details

The spectrometer equipment and experimental geometry are presented in Figure 4. The central piece of the spectrometer is an EG&G Ortec High Purity Germanium (HPGe) well detector, model GWL-120-10-LB-AWT, with an OFHC copper Endcap and high purity aluminum well tube. The well tube has a diameter of 10 mm and a depth for 40 mm. The HPGe crystal has an active volume of 120 cm^3. The manufacturer specifications for the energy resolution (FWHM) of the detector are better than 1.2 keV at 122 keV and better than 2.10 keV at 1.333 MeV. Operational FWHM were regularly measured between 1.2 and 1.4 keV for the 1.772 MeV and 1.332 MeV Co-60 lines of the check source during the duration of the project. Other parts of the system include a low-background streamline side-looking cryostat, EG&G Electronics (detector power, bias, pre-amplifier), a very low background shield including a 2 tons pre-WWII lead shroud with a graded Z shield (Copper & Cadmium). The signal from the spectrometer was analyzed by an ORTEC DSPEC LF digital signal processor Multi Channel Analyzer and the Maestro®-32 Software.

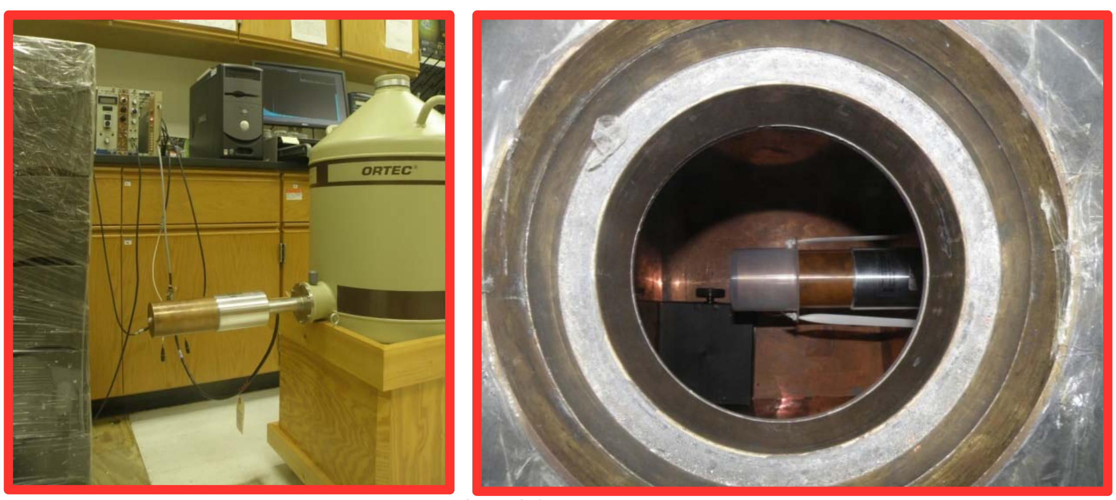

Figure 4—Spectrometer Equipment Used for ^{137}Cs/^{210}Pb Analysis
This figure shows the spectroscopy station (left image) and the experimental geometry without lid (right image) used for the ^{137}Cs/^{210}Pb analysis.

Gamma Ray Analysis

Gamma ray analysis of the samples was performed for counting times varying depending on the portion of the core and the radionuclides of interest. For the upper portions of the cores counting time was typically two days to measure with sufficient precision ^{137}Cs and ^{210}Pb activities. Once ^{137}Cs was no longer detected, counting time was decreased to about 1-day to record ^{210}Pb activities past their fast decrease and the other radionuclides of interest ^{40}K, ^{214}Bi, ^{214}Pb, ^{208}Tl. For some samples at the bottom of core BB11-2, counting times were reduced to less than a day sufficient to measure the activity of the radionuclides of interest at these depths, ^{40}K and ^{214}Bi. For each spectrum the following lines in the gamma ray spectra were analyzed: ^{210}Pb (46 keV), ^{214}Pb (295 keV), ^{214}Pb (351 keV), ^{208}Tl (583keV), ^{214}Bi (609 keV), ^{137}Cs (662 keV), and ^{40}K (1,460 keV). For gamma ray lines influenced by the background of the spectrometer, ^{214}Pb, ^{214}Bi, ^{208}Tl and ^{40}K, background counts were subtracted based on the spectrum acquisition time. Uncertainty in the count rates was computed based on the estimated standard deviation of the counts and expressed graphically with error bars representing +/- 1 standard deviation as is customary (Knoll 1989). Uncertainty related to the efficiency calibration of the spectrometer was not included in the graphics as the compositions and densities of the core materials are relatively similar for each of the cores as compared to the variety of standards used for the calibration of the system hence leading to small fluctuations in detection efficiencies.

Counts were above the detection limit of the system for all the above lines except for most of the ^{137}Cs measurements. For all ^{137}Cs measurements the Minimum Detectable Activity (MDA) was computed. MDA is defined as the smallest net count that can be reported with a 95% confidence that the counts represent a true activity from a sample and not a statistical variation of the background. MDA was computed with customary expression {1} below (Tsoulfanidis 1995) with "Counts" representing either the cumulative counts of the portion of the spectrum equivalent to the Full Width at Half Maximum of a ^{137}Cs 661.3 Kev line or the equivalent spectral energy span on either side of the ^{137}Cs line.

$$\text{MDA} = 2.71 + 4.66\ \text{SQRT (Counts)} \quad \{1\}$$

The MDA estimates were used to verify that once ^{137}Cs activities decreased below the detection limit of the system no further detectable ^{137}Cs activities were measured confirming the onset of the ^{137}Cs signal corresponding to year 1955.

Estimates of the radionuclide activities were computed based on a set of Standard Reference Materials from the National Institute of Standards and Technology (NIST) and the International Atomic Energy Agency (IAEA). The Standard Reference Materials used for the system calibration are presented in Table 1. Two general efficiency curves, one for low energies (up to 351 keV) and the other for higher energies (above 351 keV) were calibrated. Additionally for energies calibrated with several standards (46 keV, 583 keV, 609 keV, 662 keV, 1,460 keV and 2,614 keV) the general calibration was updated to match the average efficiency of the standards. The respective counts in the SRM and core sample were compared while taking into account the respective materials mass, spectrum acquisition time and for short half-life radionuclides the decay of the standard material. Materials from the standards were prepared similarly to the study samples, i.e. the standard materials were sealed in the same vials and placed in the HPGe gamma ray spectrometer with identical geometry. For reference materials with relatively short half-lives such as ^{137}Cs the activity of the materials was adjusted to take into account the time difference between the materials reference date and the date of the spectrum. For quality control, ^{60}Co spectra were measured at regular intervals to verify the stability of the efficiency calibration of the system during the project.

Table 1—Standard Reference Materials Used for Radioanalysis and Sediment Dating
Standard reference materials from the National Institute of Standard and Technology (NIST) and the International Atomic Energy Agency (IAEA) were used for the efficiency calibration of the gamma ray spectrometer/

Standard	Description	Reference Date
NIST 4350b	River Sediment	9/9/1981
NIST 4354	Lake Sediment	2/14/1986
NIST 4357	Ocean Sediment Environmental Radioactivity	2/6/1994
IAEA-312	Ra-226, Th, U in Stream Sediments	1/30/1988
IAEA-313	Ra-226, Th, U in Stream Sediments	1/30/1988
IAEA-314	Ra-226, Th, U in Stream Sediments	1/30/1988
IAEA-315	Radionuclides in Marine Sediment	1/1/1993
IAEA-375	Radionuclides and Trace Elements in Soil	12/31/1991
IAEA-385	Irish Sea Sediment	1/1/1996
IAEA-434	Ra-226, Th and U in stream sediment	1/1/2008
IAEA-447	Natural and Artificial Radionuclides in Most Soil	11/15/2009
IAEA RGK-1	Potassium Sulfate	
IAEA RGU-1	Uranium Ore	
IAEA RGTH-1	Thorium Ore	
IAEA SL-2	Lake Sediment	1/31/1986
IAEA Soil-6	Radionuclides in Soil	1/30/1983

F. Results

Sediment Coring Stations

Twelve sediment coring stations (Figure 2 and Table 2) were established in the Baffin Bay complex between the main basin, and the tributary bays (Alazan Bay, Cayo del Grullo, and Laguna Salada). The main basin stations include BB01, BB02ALT, BB03, BB04, and BB08. Stations in the tributary bays include BB05, BB06, and BB07 in Alazan Bay, BB09 in Laguna Salada, and BB10, BB11, and BB12 in Cayo del Grullo.

Stations BB02ALT and BB08 were specifically chosen at the same locations as TCEQ monitoring stations where some longer term water quality monitoring records are available. Station BB08 was established within ~20 m of the official location of TCEQ station 13452. An initial attempt was made to establish station BB02 at the location of TCEQ station 13450. However, sediment cores from that location showed just a thin layer (~20 cm) of muddy material capping littoral drift (sand and shell hash) for the remainder of the cores. Therefore, station BB02ALT was established about 400 m to the south towards the main basin center to avoid this littoral drift.

Table 2—Sediment Coring Stations and Core Details
This table provides information about the sediment coring stations and actual sediment cores used in this project. Though the sediment cores reached up to 171 cm in length, the focus of this report is on the upper 120 cm of each core given the time frame of interest.

Station ID	Latitude/ Longitude of Station	Water Depth (m)	Number of sediment cores retrieved	Which Sediment Core Analyzed?	Length of Sediment Core Analyzed	Notes
BB01	27° 16.924'N 97° 25.676'W	2.30	3	BB01-2	144 cm	
BB02ALT	27° 15.892'N 97° 30.578'W	2.55	3	BB02ALT-1	153 cm	400 m south of TCEQ station 13450
BB03	27° 15.174'N 97° 33.162'W	1.90	3	BB03-3	138 cm	
BB04	27° 16.605'N 97° 34.710'W	2.20	3	BB04-3	138 cm	
BB05	27° 18.177'N 97° 34.156'W	1.90	3	BB05-3	156 cm	
BB06	27° 18.914'N 97° 32.723'W	1.60	3	BB06-3	160 cm	
BB07	27° 20.098'N 97° 31.814'W	1.55	3	BB07-1	149 cm	
BB08	27° 17.392'N 97° 38.591'W	1.90	3	BB08-1	161 cm	coincident with TCEQ station 13452
BB09	27° 16.863'N 97° 39.885'W	1.90	3	BB09-3	150 cm	
BB10	27° 18.691'N 97° 39.174'W	1.90	3	BB10-2	171 cm	
BB11	27° 19.871'N 97° 40.411'W	1.75	2	BB11-2	155 cm	
BB12	27° 21.241'N 97° 41.083'W	1.45	3	BB12-1	169 cm	

Nature of the Sedimentation and Stratigraphy

The sediments in the system down to the depth penetrated by the cores for this study are predominantly muddy (mixed silt and clay) in nature with sand becoming more dominant in the tributary bays as would be expected due to the shallower water and greater fluvial influence. Sediment cores from station BB04 bottomed out in shell hash, but consist of ~60 cm of muds above the hash, and were kept for study. Further discussion about the sediment grain size distributions is reserved for the dedicated Sediment Grain Size section below.

A compilation of high resolution photomosaics from the 12 sediment cores used in this study is provided Figure 5 below. Stratigraphy is clearly visible—it is generally well-preserved at depth, and is largely on the scale from centimeters to multiple centimeters in thickness (Figure 6). In some cases, in particular, a zone in the upper part of the sediment cores from the Laguna Salada and Cayo del Grullo tributary bays, and the BB04-3 core at the mouth of Alazan Bay, finely laminated stratigraphy is also preserved (Figure 7).

The stratigraphy becomes visually much less distinct to even completely absent in the last 5-10 cm of sedimentation in the sediment cores from all stations (Figure 8). In cores from the deeper water stations, it becomes much less distinct, and part of this is related to higher water content and less compaction towards the core tops. But as seen in the lower image of Figure 8, there seems to be essentially mixing, probably via bioturbation, in some of the sediment cores from the tributary bays. Good, intact sediment/water interface contacts were observed in all cores on retrieval. Furthermore, immediately following retrieval while still on the water, the core tops were protected by siphoning off the excess water, and setting the tops with floral foam. It is still possible that some disturbance to the core tops could have occurred during transport either while still on the water, or during the return road trip to TAMUCC. Or it is possible, but unlikely, that every single core hit a previously disturbed patch of bay bottom (like an area of anchor dragging). But a more likely explanation is that there has been a significant change in depositional or preservational conditions throughout the basin in recent times.

Though the stratigraphy is generally well-preserved at depth whether in the main basin or tributary bays, sand/shell hash layers and erosional contacts are also common, but more so in the stratigraphy of the tributary bays (Figure 9). This is expected as the shallower water and greater fluvial influence in tributary bays probably leaves the bottom more subject to higher energy events. Sand layers (lesser amounts of shell hash) and erosional contacts are also present in the cores from the main basin, but they are less frequent as expected due to the deeper water depths. An implication of this relationship, especially for the stratigraphy in the tributary bays, is that simple, visual-only, one-to-one matching between layers from even adjacent sediment cores is very difficult if at all possible. While some clear, visual-only, one-to-one layer matches/correlations between cores may be possible for some features of the core, such matching is not possible over large vertical ranges of stratigraphic section. Visual-only matching is still a useful complementary analysis when combined with the results from the various other analyses undertaken for this project, allowing for correlations between main basin and tributary bay sediment cores by looking at the longer-term trends.

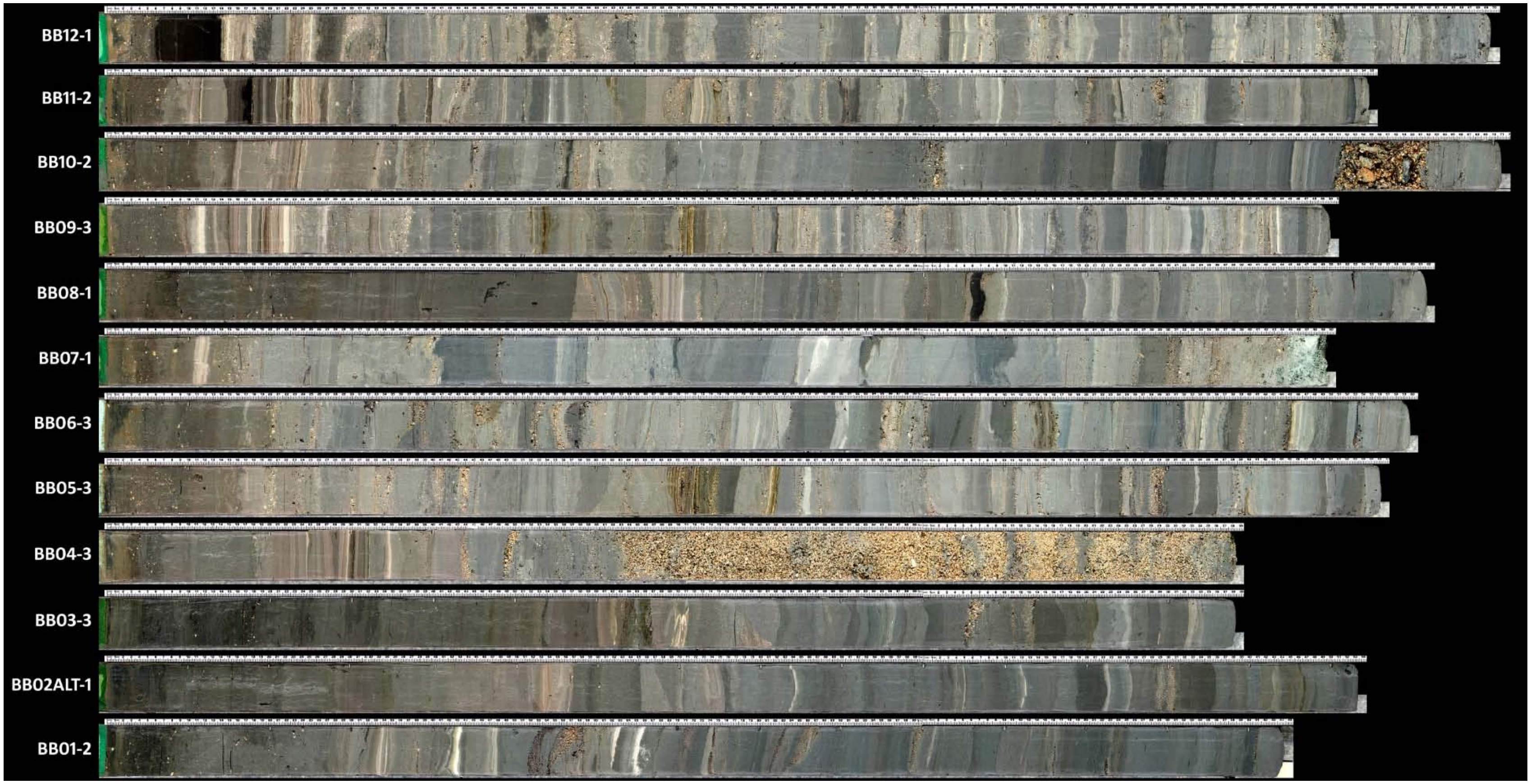

Figure 5—Compilation of High Resolution Sediment Core Photomosaics
The above image is a compilation of the high resolution, seamless photomosaics of the sediment cores used in this study. The tops of the sediment cores, i.e. the modern sediment/water interface, is at the left side of the image. The green object seen at the core tops is the floral foam used to set the core top on retrieval. The contrast of this image has been enhanced to accentuate the stratigraphy, but color-balanced and documented original images are available. Overall, the stratigraphy in the basin is well-preserved at depth, and appears to record generally continuous sedimentation especially for sediment cores taken from the eastern part of main basin (stations BB01, BB02ALT, and BB03). Stratigraphy in sediment cores from the tributary bays is also well-preserved, too. However, erosional contacts are more common as might be expected due to the shallower water, and greater fluvial influence.

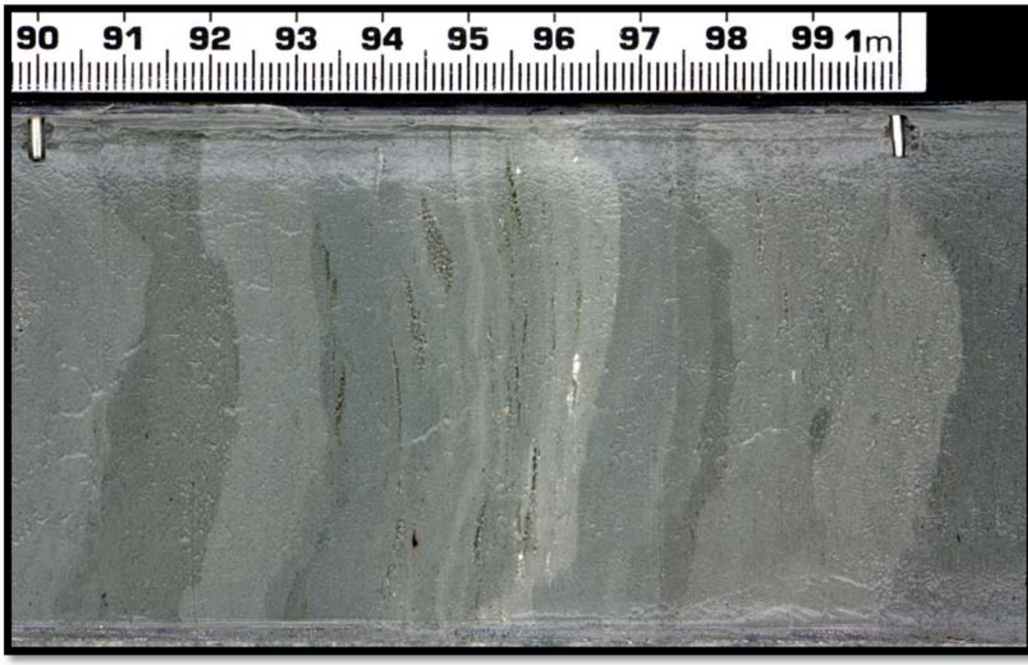

Figure 6—Example of Generally Well-Preserved Stratigraphy
The above image from approximately 90-101 cm depth in sediment core BB03-3 (note ruler at top of image) shows the nature of the generally well-preserved stratigraphy at depth throughout the basin. Note that the contrast in the image has been enhanced to accentuate visibility of the stratigraphy. A couple of microfaults, probably due to compressive stress while coring, are visible with a particularly stunning example showing ~0.5 cm of apparent offset on either side of the core from ~95-98 cm depth.

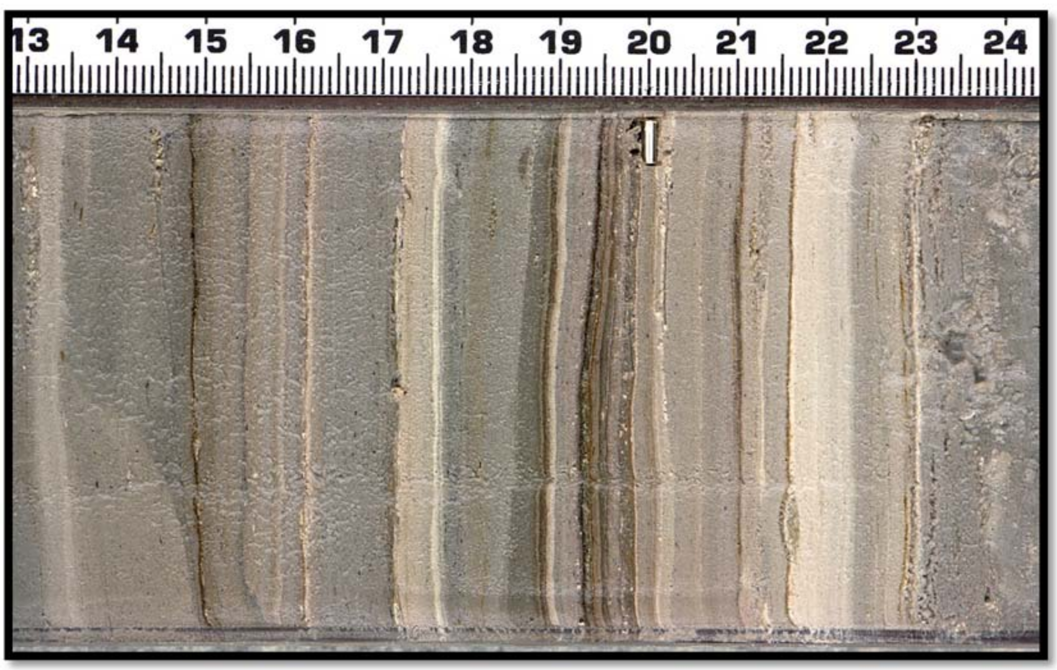

Figure 7—Example of Finely Laminated Stratigraphy
The above image from approximately 13-24 cm depth in sediment core BB09-3 (note ruler at top of image) shows an example of some of the finely laminated stratigraphy seen in the upper part of a few sediment cores from the basin. Note that the contrast in the image has been enhanced to accentuate visibility of the stratigraphy.

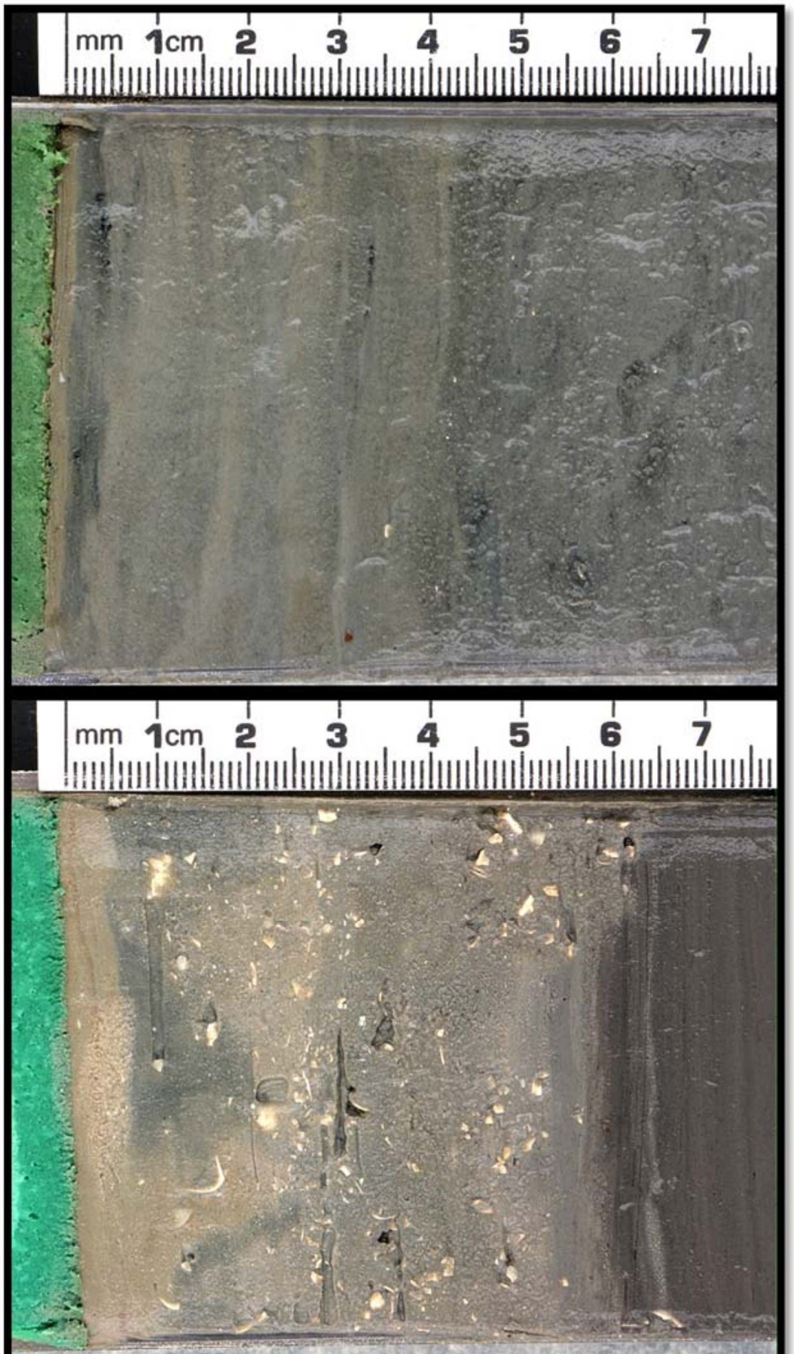

Figure 8—Example of Uppermost Stratigraphy in Two Sediment Cores
The above images show the uppermost ~7.5 cm of sediment accumulation in two sediment cores—one from the deeper main basin (core BB03-3, upper image), and one from the shallower Cayo del Grullo (core BB12-1, lower image). The green object at 0 cm depth in both cores is the floral foam used to fix the core top on retrieval while in the field. The stratigraphy in the BB03-3 image is much less distinct than the stratigraphy at depth in the same core. In the BB12-1 image, good stratigraphy (even millimeter-scale laminations) can be seen up to about 5.5 cm depth, but above that, the sediment accumulation appears to be mixed and homogenized.

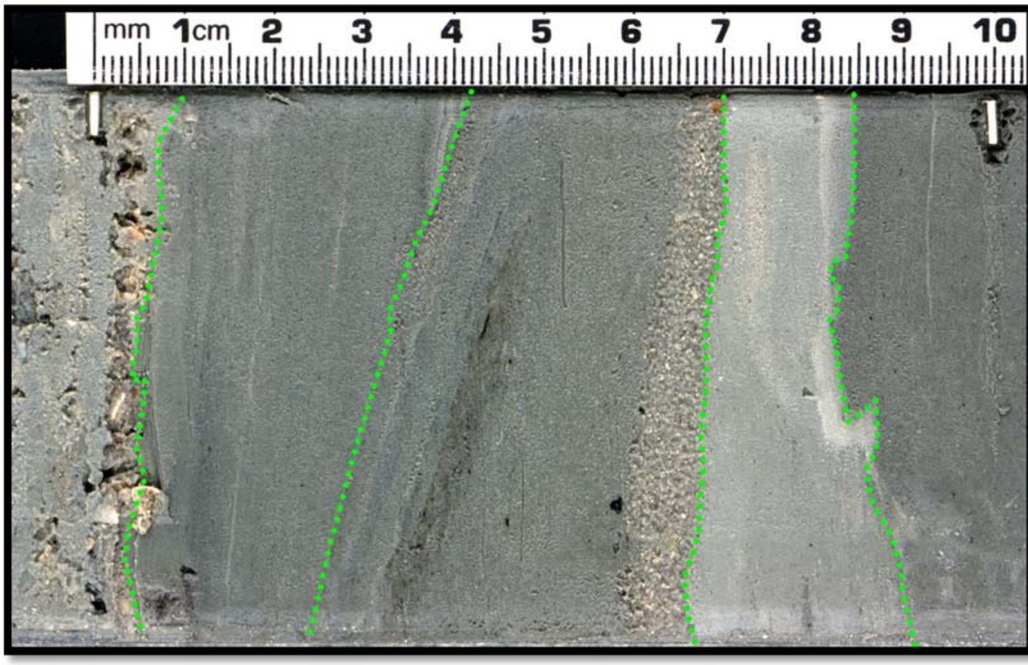

Figure 9—Example of Sand Layer and Erosional Contacts in Stratigraphy
The above image from approximately 100-110 cm depth in sediment core BB06-3 (note ruler at top of image) shows an example of a sand layer (at ~6.5-7 cm on ruler) and several erosional contacts indicated by the dotted green lines. Note that the contrast in the image has been enhanced to accentuate visibility of the stratigraphy.

An important further implication of the above, especially for interpretations of chronology and proxy evidence, is that the sediment cores from the main basin contain a more continuously complete record of sedimentation versus the sediment cores from the tributary bays. Indeed, this inference is clearly supported by calculated sedimentation rates from the radioisotope dating work as further discussed below. Overall, the variability of sediment accumulation throughout the basin reinforces the need to study the system from a broad, geospatial perspective.

Sediment Grain Size

Sediment grain size results are summarized graphically for all 12 sediment cores in Figure 10, on a core-by-core basis in the Appendix section, and as numerical averages in Table 3 below.

In general, grain size results show, as expected, finer sediments in the deeper water of the main basin, and coarser grain size distributions in the shallower tributary bays. Based on whole core averages of all samples in the 0-120 cm depth range, cores from the main basin (stations BB02ALT, BB03, BB04, and BB08) are composed of >= ~90% mud (mixed silt and clay size fractions, i.e. <63 microns) with the remainder as sand (i.e. 63-2000 micron size range). Station BB01 is also positioned in deeper water in the main basin, but given its location at the mouth of Baffin Bay, it also receives occasional inputs of sand from the Laguna Madre. That core averages ~23% sand per sample with a correspondingly lower mud content.

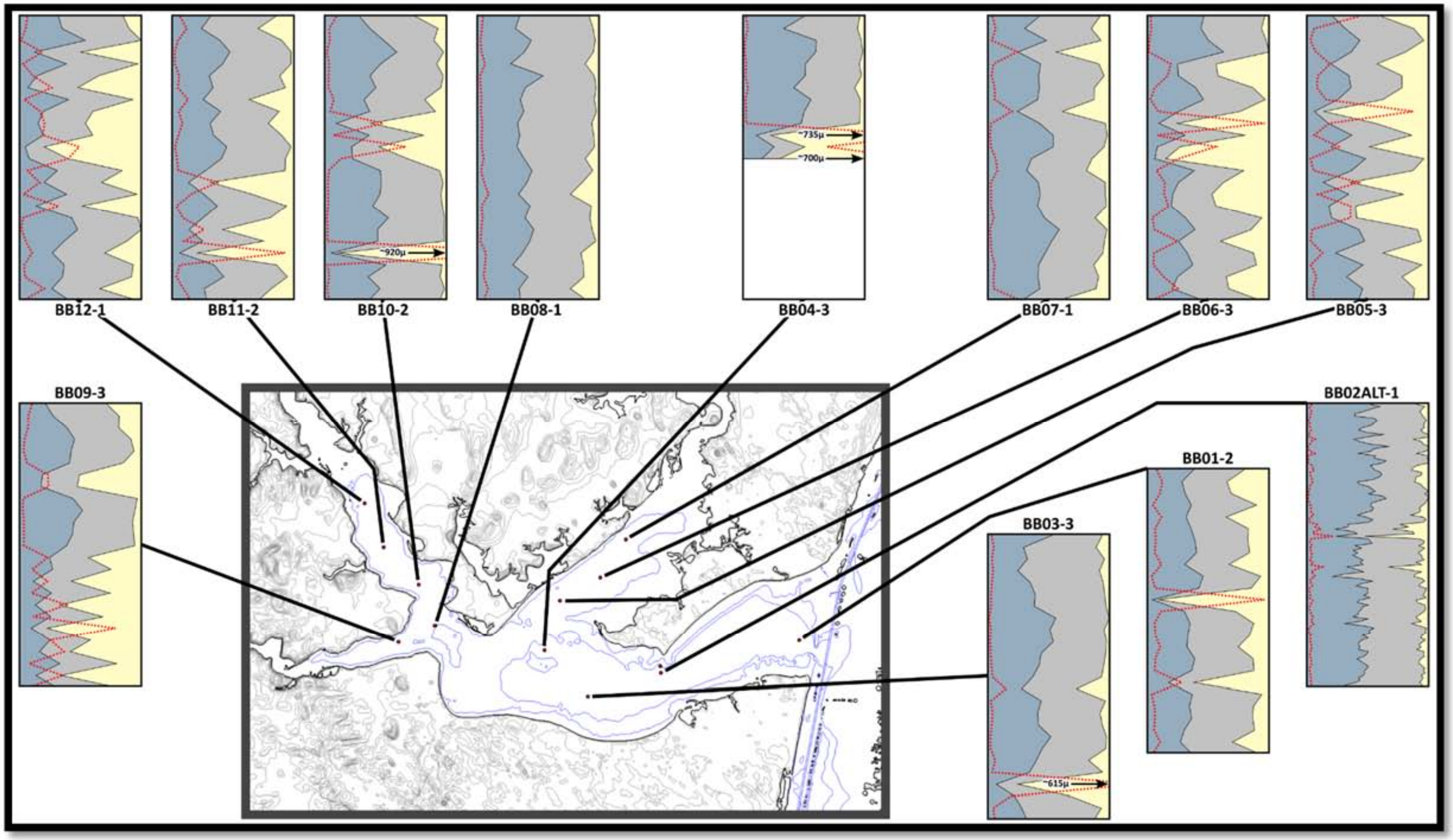

Figure 10—Synopsis Diagram of Grain Size Results

These plots show clay, silt, and sand percentages (blue, gray, and yellow shading, respectively) down core to 1.2 m depth at 5-cm intervals, except for sediment core BB02ALT-1, for which grain size analysis was undertaken at 1-cm intervals. The red dotted line in each plot represents the mean grain size with the width of the plot representing 0-500 microns diameter. Cores from the main basin (stations BB02ALT, BB03, BB04, and BB08), and from tributary bay station BB07 are characterized by mostly clay and silt, as expected, with occasional sand layers probably representing high energy events. Sand represents a larger percentage of the cores taken in the shallower tributary bays due to fluvial input, and near the mouth of bay at station BB01 given sand input from the Laguna Madre.

Grain size results from sediment cores taken in the tributary bays (stations BB05, BB06, BB09, BB10, BB11, and BB12) are significantly coarser with sand composing generally 20-30% of the samples, and the remainder being mud. Core BB10-2 grain sizes are finer than expected given the location of this station well into the Cayo del Grullo tributary bay. It averages only ~15% sand with the remaining 85% mud.

Sediment core BB07-1 is also located in a tributary bay, and, in fact, it was retrieved at the furthest most station deep into Alazan Bay (Figure 2). The water depth there is also very shallow—only 1.55 cm depth, which is the second most shallow water depth at any of the 12 stations used in this study (Table 2). Consequently, a generally coarser grain size distribution similar to the other tributary bay sediment cores was expected. However, the results show there is surprisingly little sand, just 12% on average, with the remainder mud. This places it in a range very similar to the main basin cores as described above, which is unexpected given its position deep in the tributary.

Regarding gravel-sized mineral grains, i.e. >2000 microns diameter, no such grains were encountered in any of the samples from any of the cores during analysis using the laser particle size analyzer machine. All samples were filtered through a 2 mm sieve while being loaded into the machine, and while occasional shell fragments were trapped, no gravel-sized mineral grains were ever retained.

Table 3—Average Sand, Silt, and Clay Percentages by Core

This table lists the average sand, silt, and clay percentages by core based on results from all samples in the 0-120 cm depth range. For core BB04-3, only samples down to 45 cm depth were considered because that core bottoms out in shell hash. It is important to stress that the values represent averages based on all samples over the 0-120 cm depth range (except for core BB04-3 as mentioned above). Thus, if one were to consider just samples taken from discrete sand layers, the results would appear significantly coarser.

Core	Avg. Sand %	Avg. Silt %	Avg. Clay %
BB01-2	23.1	43.7	33.2
BB02ALT-1	8.2	46.6	45.2
BB03-3	10.4	51.6	38.0
BB04-3	4.1	45.7	50.1
BB05-3	28.5	40.2	31.3
BB06-3	27.9	40.8	31.3
BB07-1	12.0	46.3	41.6
BB08-1	8.3	53.7	38.1
BB09-3	30.3	40.4	29.2
BB10-2	15.2	46.9	37.9
BB11-2	21.3	48.0	30.8
BB12-1	25.3	46.8	27.9

Regarding long-term trends in grain size data, the 5-cm sampling resolution unfortunately undersamples the centimeter-scale stratigraphy. But nonetheless, core BB09-3 appears to show a fining upwards trend from 120 cm up to 60 cm depth, and a slight coarsening in final 20 cm of sedimentation. And cores BB05-3, BB06-3, and BB12-1 show subtle trends towards coarsening from the base upwards to mid-core, followed by a gradual return to finer sedimentation. Finally, results from the high density, 1-cm sampling for core BB02ALT-1 seem relatively consistent when viewed on the sand-silt-clay percentage plots, but a subtle shift in clay percentages is visible at about 50 cm depth in the stratigraphy. Clay-sized particles represent on average ~41.5% of the samples for the 50-120 cm depths in the core, but the average clay content is substantially higher, ~52.7%, for the upper portion of the core from 0-50 cm. Overall, long-term trends in grain size for this core seem somewhat small indicating stability of the environment; the greatest variability is related to the occasional event-based, coarser beds seen in the stratigraphy.

Magnetic Susceptibility

Magnetic susceptibility results are summarized graphically for all 12 sediment cores in Figure 11, and on a core-by-core basis in the Appendix section. Magnetic susceptibility essentially measures the ability of a sediment to take on a magnetization by inducing a magnetic field in the sample, and examining the response. Sediments containing iron-bearing minerals such as those from fluvial/terrestrial sources generally produce a strong magnetic susceptibility signal. In turn, sediments with a high water/organic content such as those resulting from autochthonous, biologic production in the water column generally produce a weaker (and even negative) response. This is an excellent tool for the correlation of stratigraphy between sediment cores, but given the above explanation, it can also be interpreted as a general index between allochthonous, fluvial/terrestrial inputs versus autochthonous, biologic sediment production in the water column.

Susceptibility was measured at 0.5-cm resolution, but the results were smoothed by a 5-point centered running mean to reduce variability, and better show the trends. Susceptibility generally ranges from 0 to 5E-5 SI units for the 5-point centered running mean data for most cores except BB09-3, BB11-2, and BB12-1. These three cores are located in the Laguna Salada and Cayo del Grullo tributary bays, where fluvial influence is much greater. These cores, therefore, have much stronger magnetic susceptibility response signals, and doubling the plot range up to 1E-4 SI units was necessary to accommodate plotting the results.

One clear observation is that the magnetic susceptibility signal has a much more pronounced variability in sediment cores from the tributary bays versus those from the main basin. This observation is expected because the tributaries are more strongly influenced by fluvial/terrestrial sediment inputs. Furthermore, this interpretation supports the observations described in the Nature of the Sedimentation and Stratigraphy section above.

Most cores show a subtle but overall shift towards decreasing magnetic susceptibility values from the base upwards. The exception are cores that are very strongly influenced by fluvial/deltaic activity such as BB12-1 at the head of the Cayo del Grullo tributary bay. The decreasing trend is obvious in the results from some cores like (BB01-2, BB03-3, BB04-4, BB08-1, BB09-3, and BB11-2), but it is also present in other cores where it is not obvious on initial observation. This is the case, for example, with core BB02ALT-1. Though the long-term, up core decreasing trend is hard to notice, this is simply due to the plot scale—a common axis scale that worked well for most cores was used in order to facilitate comparisons. If a custom plot scale that visually expands that data set over its maximum range is used, the up core decreasing trend in magnetic susceptibility response becomes more obvious as illustrated in Figure 12.

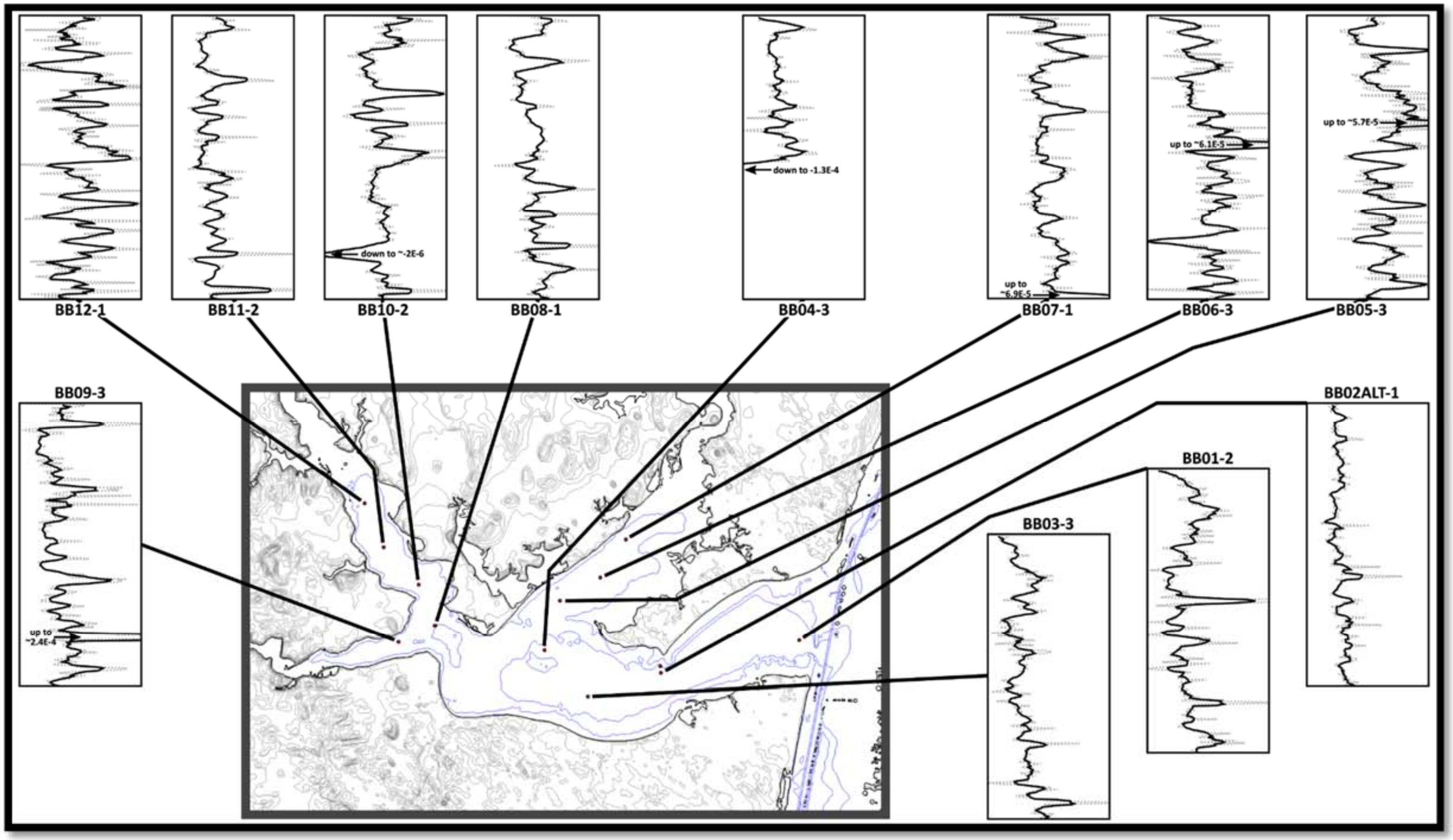

Figure 11—Synopsis Diagram of Magnetic Susceptibility Results
These plots show the magnetic susceptibility response down core to 1.2 m depth. Besides simply being used for correlation of stratigraphy, this is interpreted as essentially an index between allochthonous, fluvial/terrestrial inputs, and autochtonous, organic-rich sediment produced in the water. The former produces a strong signal because of iron-bearing minerals, and the latter a weaker (or even negative) response. Analyses were run at 0.5-cm intervals (dotted light gray lines in background), but the results were smoothed by a 5-point centered running mean (solid black lines) to better show the trends. All plots share an identical scale from 0 to 5E-5 SI units except cores BB09-3, BB11-2, and BB12-1 for which the range is doubled to 1E-4 SI units to accommodate the much stronger signals in those cores. All cores show a subtle but overall shift towards decreasing values from the base upwards, and this long-term shift probably indicates a progressive, relative increase in autochthonous, water column-derived sediment production vs. fluvial/terrestrial inputs throughout the system.

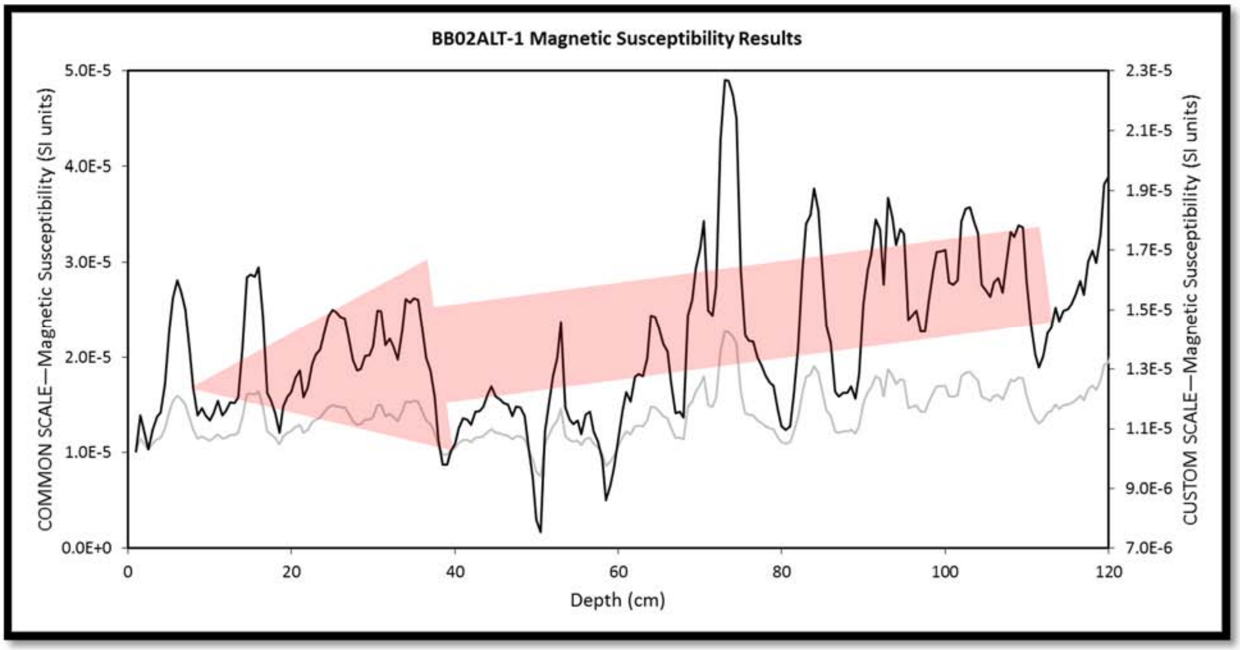

Figure 12—BB02ALT-1 Magnetic Susceptibility Results Scaling Explanation
This plot shows the 5-point centered running mean magnetic susceptibility results for core BB02ALT-1. The gray curve and left vertical axis show the data plotted at the common axis scale used for most of the cores in Figure 11, i.e. the synopsis diagram for this proxy. Using this scale, the long-term trend towards progressively lower magnetic susceptibility value from 120 cm depth upwards is less obvious (the same can be said for several other cores as presented in the summary diagram). However, if a custom scale is used to visually expand the range of the very same data set (black curve and right vertical axis), the long-term, up core trend towards progressively lower values becomes more obvious (semi-transparent red arrow).

This long-term shift seen in all cores probably indicates a progressive, relative increase in autochthonous, water column-derived sediment production vs. fluvial/terrestrial inputs throughout the system. This shift can be interpreted in multiple ways—for example, fluvial/terrestrial input could have stayed the same, and autochthonous water column production increased thereby changing the relative contributions of both components. Or autochthonous water column production could have stayed the same while fluvial/terrestrial input was decreased. Both scenarios result in the same relative change.

Two cores from the main basin (stations BB01 and BB03) show an increase and then decrease in the magnetic susceptibility signal over the final ~35 cm of sedimentation. The same change, but less well-developed, is potentially seen in core BB02ALT-1 if a custom range to visually expand the data set is used (Figure 12), and the reason behind this shift is currently undetermined.

Incombustible Content

Incombustible content results are summarized graphically for all 12 sediment cores in Figure 13, and on a core-by-core basis in the Appendix section. Incombustible content is back-calculated from loss-on-ignition results as 100% - weight % organics – weight % carbonate; thus, it represents the sediment fraction that was not combusted even at 1000°C. It is nominally interpreted as mineral matter of non-organic origin, i.e. siliciclastic mineral material like quartz and feldspar.

But it also potentially includes biogenic silica, which would lose structural water, but would otherwise be incombustible at 1000°C.

Incombustible content results are available at 1-cm resolution, but the results were smoothed by a 3-point centered running mean to reduce variability, and better show the trends. Incombustible content generally ranges between 55-85% by weight in the 3-point centered running mean results from most cores, but reaches almost 90% in sand layers that are present in the stratigraphy towards the tops of core BB09-3 and BB12-1.

As an initial note, there is a very strong and obvious inverse relationship between the incombustible and carbonate content results when they are seen side-by-side such as in the Appendix section. This is completely expected because they are the two main components in percentage data calculations from loss-on-ignition analysis, and as one increases, the other must consequently decrease to maintain 100%. Organic matter is also involved in the calculation, but it composes < ~20% by weight (~10% TOC equivalent; further details below) so it has a more muted effect.

Regarding incombustible content, there is significant variability in this data set especially towards the tributary bays as would be expected, and also at the mouth of Baffin Bay due to inputs from the Laguna Madre. But nonetheless, most cores sees to show a shift towards higher values towards the present though it happens at different depths, and with different amounts of abruptness. Perhaps the most obvious trend is visible in results from sediment cores in the main basin (stations BB01, BB02ALT, BB03, and BB04). In those cores, there is a trend towards reduced values from the base upwards, then a relatively abrupt shift to higher values that persist to the tops of the core. The abrupt shifts starts at ~42.5 cm, ~43.5 cm, ~53 cm, and ~21 cm depth in cores BB01-2, BB02ALT-1, BB03-3, and BB04-3, respectively. Core BB08-1 shows a somewhat similar response starting at about ~60.5 cm depth, but the shift is not as visually pronounced as for the previously mentioned four cores because the values preceding the shift are generally higher initially. The results from core BB07-1 also can be interpreted to show a similar trend starting about ~27-28 cm depth, but the shift is less abrupt.

Cores BB09-3 and BB11-2 from the Laguna Salada and Cayo del Grullo tributaries, respectively, show a long-term decrease in incombustible content from 120 cm depth upwards, but then a rather abrupt shift to high values over the last ~15 and ~22 cm of sedimentation at the tops of the cores. Cores BB05-3, BB06-3, and BB10-2 show the opposite trend towards a generally increasing amount of incombustible content up core, but a shift towards even higher incombustible content values towards the core tops starting at about ~32, ~20.5, and ~23 cm, depth, respectively. Given the high degree of variability in these cores, and layers of shell hash which cause carbonate to peak, and consequently lower incombustible content given they are part of the same percentage data set, some of the starting depths mentioned above could arguably be shifted. Also, while first impressions might suggest correlating these shifts in the tributary bays with those seen in the main basin, it is not certain that they are correlative because the shift is much higher stratigraphically, and less mode-like. A detailed transect of cores from the main basin and into the tributary bays could probably answer this question.

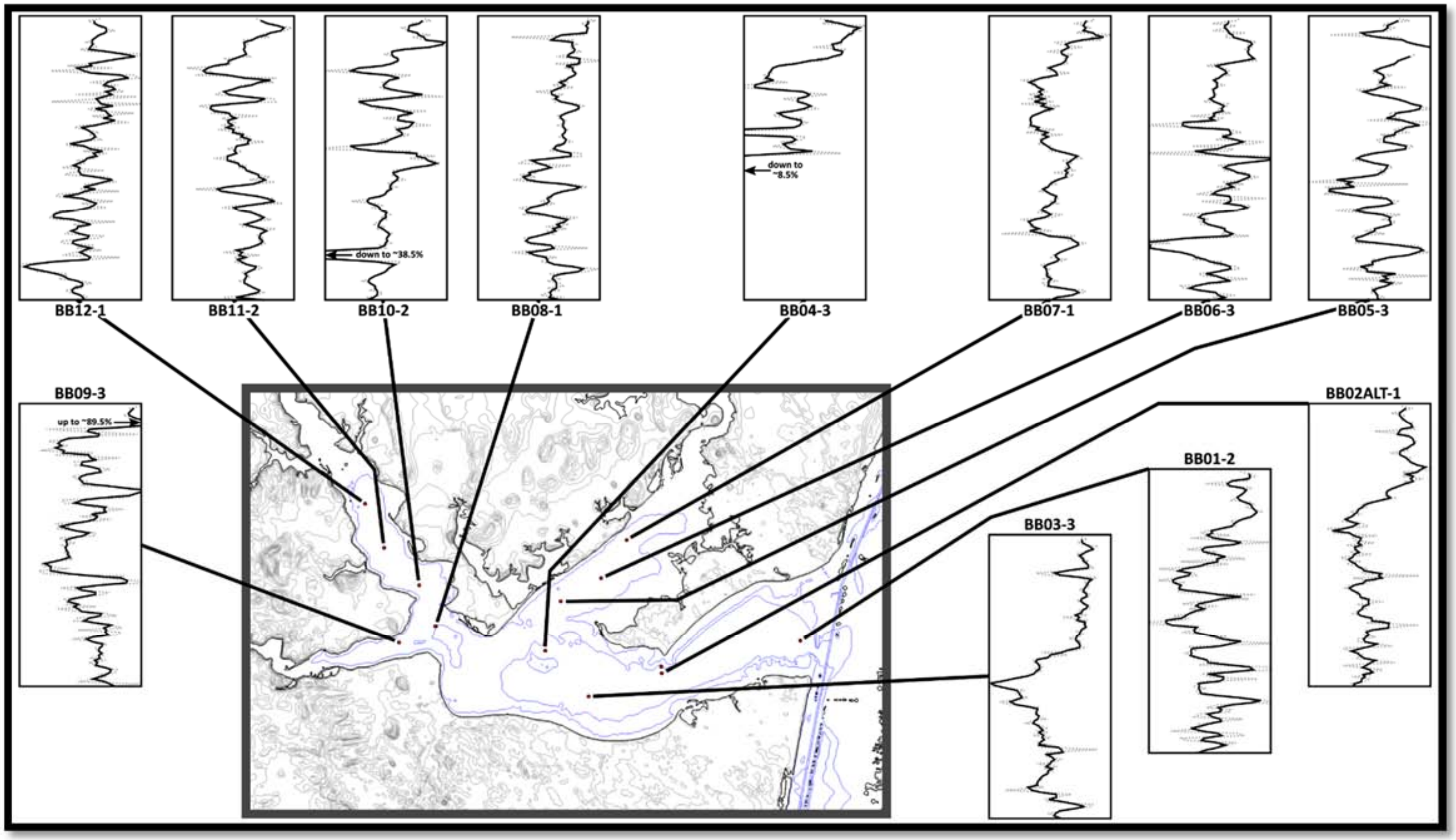

Figure 13—Synopsis Diagram of Incombustible Content Results

These plots show the weight percent of incombustible content down core to 1.2 m depth. Incombustible content is nominally siliciclastic mineral matter, but also potentially includes biogenic silica. Analyses were run at 1-cm intervals (dotted light gray lines in background), but the results were smoothed by a 3-point centered running mean (solid black lines) to better show the trends. The width of each plot represents an identical scale ranging from 55-85% dry weight of the sample with the exception of BB12-1, in which the scale runs from 60-90%. Several clear, long-term trends are visible with perhaps the most obvious trend seen in the sediment cores from the main basin (stations BB01, BB02ALT, BB03, and BB04). In those cores, there is a trend towards reduced values from the base upwards, then a relatively abrupt shift to higher values that persist to the tops of the core.

Finally, the results from core BB12-1 are different in that they do not show an obvious increase in incombustible content towards the core top like all of the other stations, but they do show a clear increasing trend over the length of the core. Given the position of this station deep within the Cayo del Grullo tributary bay, this long-term trend probably represents an ever stronger influence of fluvial/deltaic sedimentation at that station as the delta at the bay head has prograded into the basin.

Carbonate Content

Carbonate content results are summarized graphically for all 12 sediment cores in Figure 14, and on a core-by-core basis in the Appendix section. Carbonate content was determined via loss-on-ignition, and it reflects mixed source contributions which may potentially include hard parts from organisms, carbonate that was authigenically precipitated in the water column, and detrital/sedimentary carbonate.

Carbonate content results are available at 1-cm resolution, but the results were smoothed by a 3-point centered running mean to reduce variability, and better show the trends. It generally composes between 5-30% by weight of samples from most cores, but logically increases in shell hash layers, and can reach values of almost ~90% (for example, at the base of core BB04-3).

Long-term trends in carbonate content values can be grouped by station approximately similar to the incombustible content results. Sediment cores from the main basin (stations BB01, BB02ALT, BB03, BB04, and BB08) generally begin with carbonate content in the range of 15-25%, shift to lower values starting around ~42.5 cm, ~43.5 cm, ~53 cm, ~22 cm, and ~60.5 cm depth, respectively, and become reestablished around 10% by weight for the remainder of the core upwards. Carbonate results from BB07-1 show a similar trend starting at ~27-28 cm depth, but again, the signal is more muted than the main basin results. Note that there is a strong spike in carbonate content centered on ~15 cm depth, and thus, the identification of ~27-28 cm as the start point for the shift in that core may be questioned. But this carbonate spike is clearly due to a bunch of shell fragments present in the stratigraphy, and the shift really does happen at ~27-28 cm depth on closer inspection.

Cores BB09-3, BB10-2, and BB11-2 show a subtle general trend towards decreasing carbonate content values from 120 cm upwards, but also a marked drop around ~15 cm, ~23 cm, and ~22 cm. Long-term carbonate trends for cores BB05-3 and BB06-3 are not very prominent at the scale used for the plot, but nonetheless, mirroring the observations about incombustible content, a shift to lower carbonate values can be recognized at ~32 cm and ~20.5 cm depth, respectively. But the high degree of variability in the tributary bays makes correlating these shift with the main basin somewhat uncertain, and more work is needed to clear this up.

Finally, similar to what was noted with the incombustible content, core BB12-1 shows a clear, long-term decreasing trend in carbonate content, and this is probably due to the ever increasing fluvial/deltaic influence at that station.

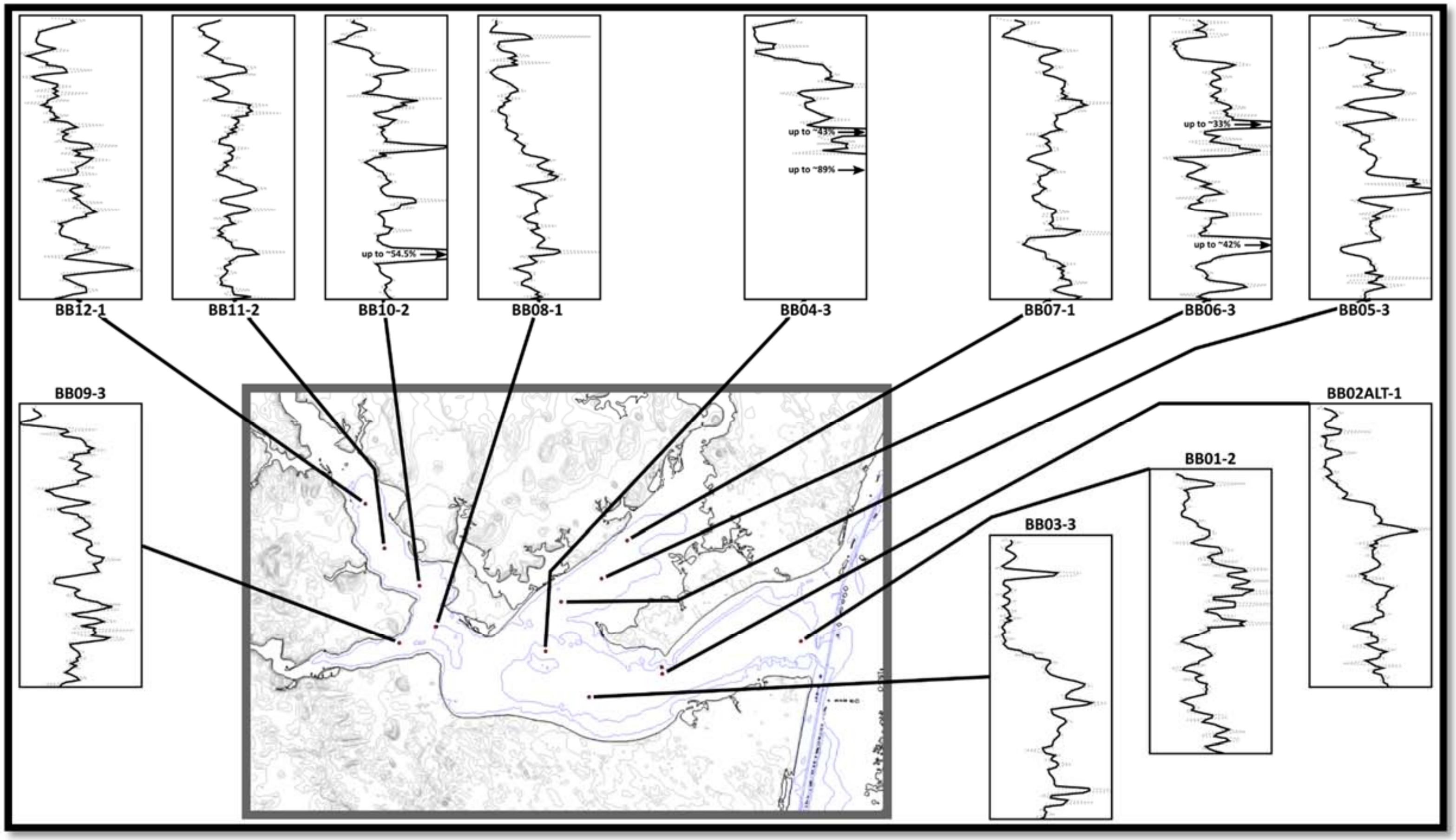

Figure 14—Synopsis Diagram of Carbonate Content Results
These plots show the carbonate content down core to 1.2 m depth as determined via loss-on-ignition analysis. Carbonate content reflects mixed source contributions which may potentially include hard parts from organisms, carbonate that was authigenically precipitated in the water column, and detrital/sedimentary carbonate. Analyses were run at 1-cm intervals (dotted light gray lines in background), but the results were smoothed by a 3-point centered running mean (solid black lines) to better show the trends. The width of each plot represents an identical scale ranging from 5 to 30 weight percent. In instances where peaks significantly exceed the maximum scale value, arrows show the approximate peak value reached. All cores show a general decrease in carbonate content from the base upwards, but in some cases the shift is more abrupt, and in other, more gradual.

Total Organic Carbon

Total organic carbon (TOC) results are summarized graphically for all 12 sediment cores in Figure 15, on a core-by-core basis in the Appendix section, and as numerical averages in Table 4 below. TOC is essentially the total amount of carbon in a sample from all organic sources, which includes mixed contributions from water column biomass, organic detritus, organic compounds, etc. TOC for this study was determined based on the organic matter results from loss-on-ignition, which were converted to estimated TOC values following guidance in Pribyl (2010).

Table 4—Average TOC Values by Core

This table lists the average TOC values by core based on results from all samples in the 0-120 cm depth range. For core BB04-3, only samples down to 70 cm depth were considered because that core bottoms out in shell hash. It is important to stress that the values represent averages based on all samples over the 0-120 cm depth range (except for core BB04-3 as mentioned above).

Core	Estimated TOC (mg/Kg) from 0-120 cm	Estimated TOC (% dry weight) from 0-120 cm
BB01-2	5.89E+4	5.89
BB02ALT-1	6.22E+4	6.22
BB03-3	6.66E+4	6.66
BB04-3	5.33E+4	5.33
BB05-3	4.22E+4	4.22
BB06-3	4.45E+4	4.45
BB07-1	5.88E+4	5.88
BB08-1	5.55E+4	5.55
BB09-3	5.16E+4	5.16
BB10-2	5.79E+4	5.79
BB11-2	5.29E+4	5.29
BB12-1	4.10E+4	4.10

TOC results are available at 1-cm resolution, but the results were smoothed by a 3-point centered running mean to reduce variability, and better show the trends. Values generally fall within the range of 2.0E4 to 8.0E4 mg/Kg (i.e. 2-8% dry weight) in the 3-point centered running mean results. The four highest average values for 0-120 cm depth range from 5.88-6.66%, and include the main basin cores BB01-2, BB02ALT-1, and BB03-3, as well as BB07-1 from the Alazan Bay tributary. The four lowest values range from 4.10-5.16%, and are all from cores in the tributary bays including BB05-3, BB06-3, BB09-3, and BB12-1. Better preservation potential in the deeper waters of the main basin may explain this difference.

Several strong and noticeable long-term trends can be recognized in the TOC values. Cores from the main basin (stations BB01, BB01ALT, BB03, BB04, and BB08), and one from Alazan Bay (station BB07) show a gradual increase in TOC values from 120 cm upwards, an inflection point about mid-core, and then a gradual decrease in TOC values to the core tops. The inflection point for cores BB07-1 and BB08-1 is more gradual than the other cores, but it is noticeable.

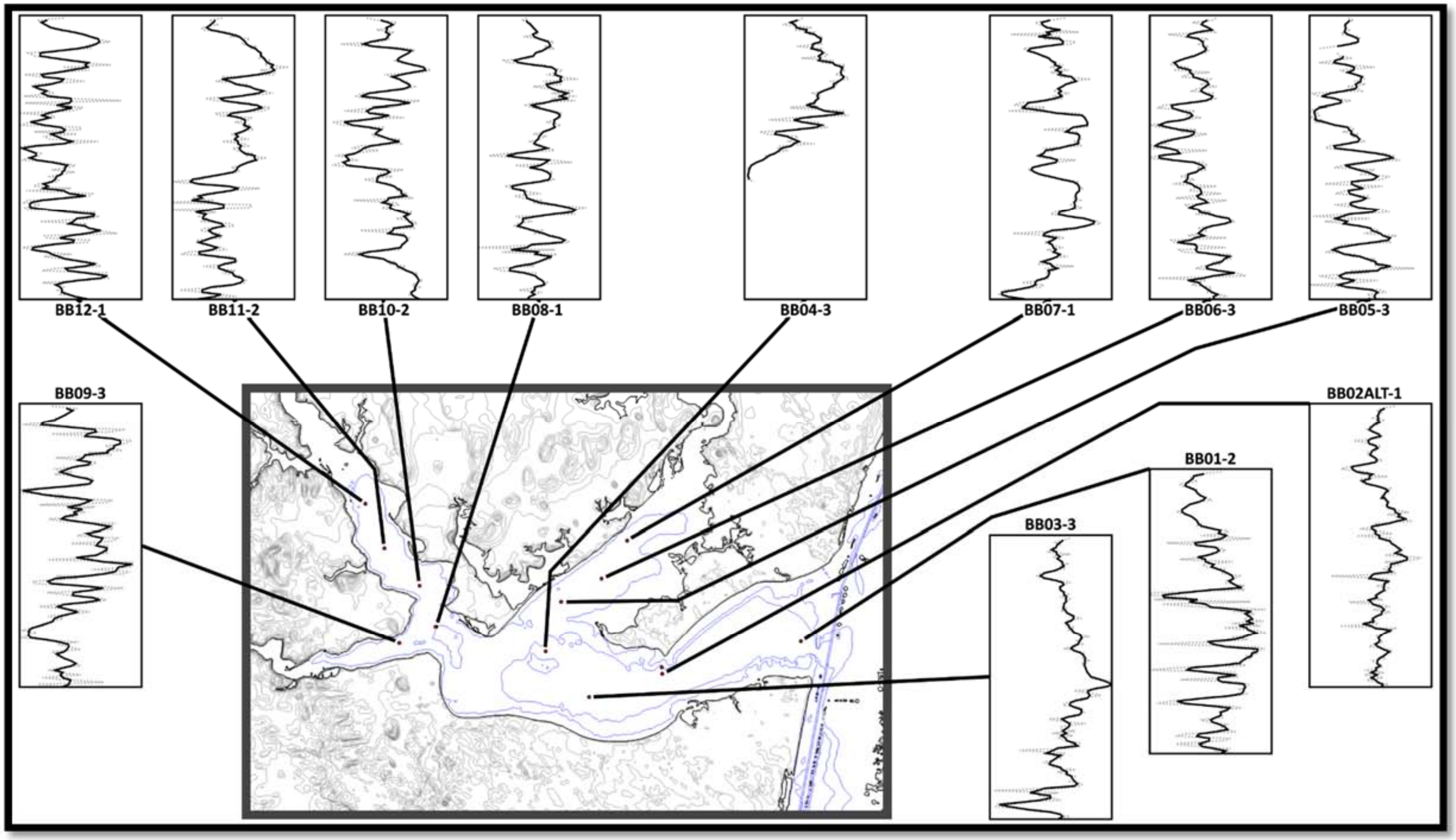

Figure 15—Synopsis Diagram of Total Organic Carbon Results
These plots show total organic carbon (TOC) as estimated via loss-on-ignition down core to 1.2 m depth. Analyses were run at 1-cm intervals (dotted light gray lines in background), but the results were smoothed by a 3-point centered running mean (solid black lines) to better show the trends. The width of each plot represents an identical scale ranging from 10,000 to 100,000 mg/Kg (i.e. 1-10%) dry weight TOC. In general, the trend in the main basin is first towards progressively higher values, and then a transition to progressively lower values towards the core top. In turn, an inverse pattern is generally noticeable in the results from the tributary bays.

In turn, TOC values from most sediment cores from the tributaries (stations BB05, BB06, BB10, BB11, and BB12) show the inverse relationship, but with more overall variability as expected in the tributaries. Values generally decrease from 120 cm upwards, and then around mid-core, make a shift, and start trending towards higher values. Trends in TOC values in core BB09-3 are also recognizable, but they are seemingly more complex than a simple decreasing→increasing trend like for the other tributary bay cores.

Verification of Inferred Chlorophyll Content Versus HPLC-Determined Chlorophyll

Inferred chlorophyll content ($RABA_{400-560}$ parameter of Rein and Sirocko 2002) results and trends are reported in the next section below, but here, we provide a verification that these diffuse color reflectance scanning results actually reflect traditionally-measured chlorophyll concentrations in the sediments. We do this by comparing a reflectance-based, inferred chlorophyll content profile against an HPLC-determined concentration profile on the same sediment core from the main basin, core BB02ALT-1.

Results from the diffuse color reflective scanning analysis are available at 0.5-cm resolution, but to reduce high-frequency variability, and better show the trends for comparison, the results were smoothed by a 5-point centered running mean. Thus, each inferred chlorophyll point in the Figure 16 plots below represents the average of results from five, consecutive, 3-mm diameter surface scans along 2.5 cm of the split core surface (an areal target). HPLC results are available at 1-cm resolution, but for the same reasons as mentioned above, they were smoothed with a 3-point centered running mean. Thus, each HPLC-determined chlorophyll point in the Figure 16 plots represents an average of results from three, consecutive, 1-cm thick, homogenized slabs from a 3.0-cm thick, semicylindrical volume of sediment core.

With no adjustments whatsoever, but simply using independent scales to accommodate the natural range of values in both data sets, the two chlorophyll curves show very strong correspondence (Figure 16 left plot). There are a few apparent lacks of correspondence between the curves including peaks in one curve, but not in the other. But some inconsistencies are actually expected and easily explained as discussed further below. If the reflectance-based, inferred chlorophyll values are divided by their bulk density measurements to help normalize for water content with the reflection scanning data, the match is even better. Indeed, via simple trial and error visual curve fitting, a simple mathematical transform that converts the reflection scanning data values into results that are approximately equivalent to the HPLC-determined values (Figure 16 right plot) was encountered. That simple, empirical, mathematical relationship is:

$$((RABA_{400\text{-}560} \text{ inferred chl value})/(\text{dry bulk density}))^{3.2} \approx \text{HPLC-determined chl value}$$

Future efforts will be directed towards developing a more formal, rigorous calibration and mathematical transform that will hopefully provide even better results. But nonetheless, it is clear that the inferred chlorophyll content values as determined by diffuse color reflectance scanning do indeed reflect chlorophyll concentrations in the sediments as measured by traditional techniques like HPLC. Therefore, the diffuse color scanning reflectance inferred chlorophyll content values in this study is interpreted with the same confidence as with HPLC-determined values, but with the major additional benefit of being essentially 10x the resolution (i.e. 0.5-cm resolution vs. 5-cm resolution).

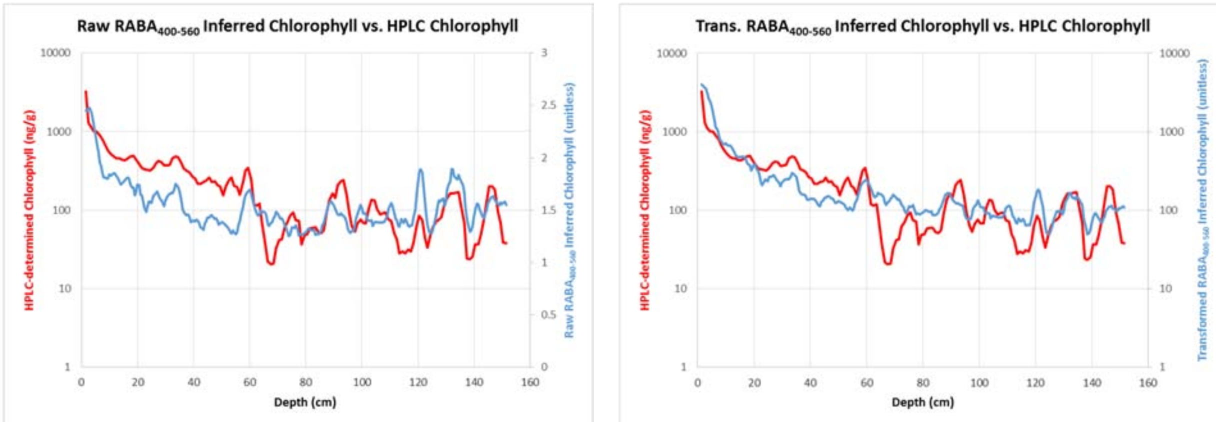

Figure 16—RABA$_{400-560}$ Inferred Chlorophyll Content vs. HPLC-Determined Chlorophyll
The above plots show the results of two different chlorophyll concentration analyses down the length of sediment core BB02ALT-1. The plot on the left shows raw RABA$_{400-560}$ inferred chlorophyll values (blue) vs. HPLC-determined chlorophyll concentrations (red). Note that the vertical axes have different numerical scales for this plot. In this case, the inferred chlorophyll values are completely raw, and no adjustments have been made. In the case of the plot on the right, the HPLC data (red) is still the same, but the inferred chlorophyll data (blue) has been normalized against measured bulk density values to account for differences in water content, and the values have also been mathematically transformed by the relationship mentioned in the text. Given that the vertical axis here is logarithmic, it is more important that the higher values show a closer match than the lower values. Several small inconsistencies can be noted between the curve including the low HPLC value centered on 67.5 cm depth, the slightly offset peaks between the two curves from 90-95 cm depth, and the high HPLC values at about 103 and 145 cm depth. These inconsistencies are readily explained by stratigraphic defects that have a seemingly large effect because of the different targets used by both analyses (i.e. area-based vs. volume-based targets). The text provides a detailed discussion about these inconsistencies.

While the overall shape and positions of peaks/troughs between the inferred chlorophyll and HPLC-determined chlorophyll curves show strong correspondence, there are several small inconsistencies between the curves including the low HPLC value centered on 67.5 cm depth, the slightly offset peaks between the two curves from 90-95 cm depth, and the high HPLC values at about 103 and 145 cm depth. These small inconsistencies are expected, easily explained, and represent true measured differences between the two different analyses despite them being run on the same sediment core half. This is admittedly unintuitive, but a straightforward explanation follows.

The different results between the analyses (even on the same sediment core half) can by readily explained the by the completely different targets samples these analyses use. In particular, the diffuse color reflection scanning analysis measures a 3 mm diameter circular exposure of the sediment core surface—this is an area-based target. But the HPLC-determined values are based on homogenizing a 1-cm thick, semicylindrical slab of sediment core, and extracting a subsample for analysis—this is a volume-based target. Therefore, unless every stratigraphic layer in the cores is perfectly horizontal and uniform in thickness, or the sediments are completely homogenized (i.e. no stratigraphy), both methods may still be making true and accurate measurements, but ending up with different results because of the significant difference in analysis targets (i.e. area vs. volume). In fact, this can be clearly seen with the four small inconsistencies that were pointed out for the curves with core BB02ALT-1. There are small stratigraphic defects visible at the depths indicated for the deepest three inconsistences (microfaults; see Figure 6 for an example), and a very large and obvious erosional/angular contact diagonally running across the core from 67-69 cm depth (Figure 17), which is responsible for the larger inconsistency centered on 67.5 cm depth.

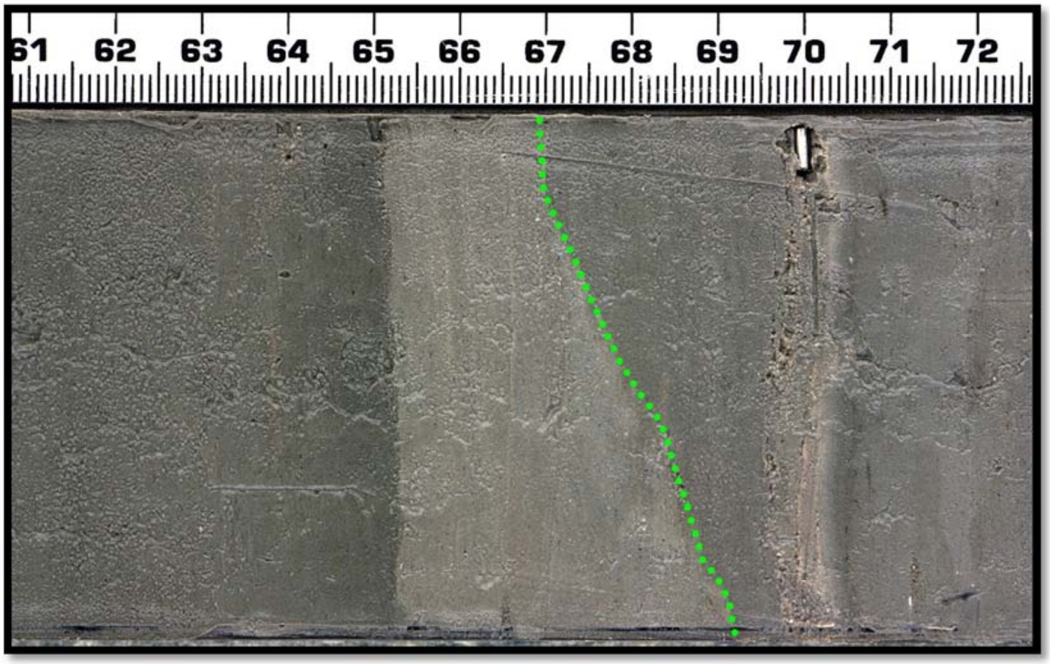

Figure 17—Erosional/Angular Contact in Core BB02ALT-1
There is an inconsistency in the results between the inferred chlorophyll content based on reflectance scanning and the HPLC-determined chlorophyll content at about 67.5 cm depth in core BB02ALT-1. This difference can be readily explained by an obvious erosional/angular contact at that depth, and the fact that one analysis uses a small area-based target on the surface of the core while the other uses a volume-based target from a 1-cm thick slab. For example, a 1-cm thick slab taken from the 67-68 cm depth range will partially bisect both the upper light gray and lower dark gray layer. Also, this is only what is visible on the core surface—it is probable that the boundary marked by the dotted green line is not perfectly vertical in 3D space, and continues into the core at an angle. Therefore, the surface-based reflectance measurement would be very different from volumetric HPLC measurement despite being made on the very same sediment core half.

Inferred Chlorophyll Content (RABA$_{400\text{-}560}$)

Inferred chlorophyll content (RABA$_{400\text{-}560}$ parameter of Rein and Sirocko 2002) results are summarized graphically for all 12 sediment cores in Figure 18, and on a core-by-core basis in the Appendix section. Inferred chlorophyll content was measured via diffuse color reflectance scanning as explained in the Sampling and Analysis Methods section above, and is interpreted to primarily reflect the amount of photosynthetic/algal biomass in the water column at the time a particular sediment layer was accumulated.

Inferred chlorophyll content results are available at 0.5-cm resolution, but the results were smoothed by a 5-point centered running mean to reduce variability, and better show the trends. The RABA$_{400\text{-}560}$ values generally fall between 1.1 and 2.3 for all cores, but some higher value peaks are present generally towards core tops. These numbers are unitless/dimensionless because they are calculated as simple ratios between wavelengths.

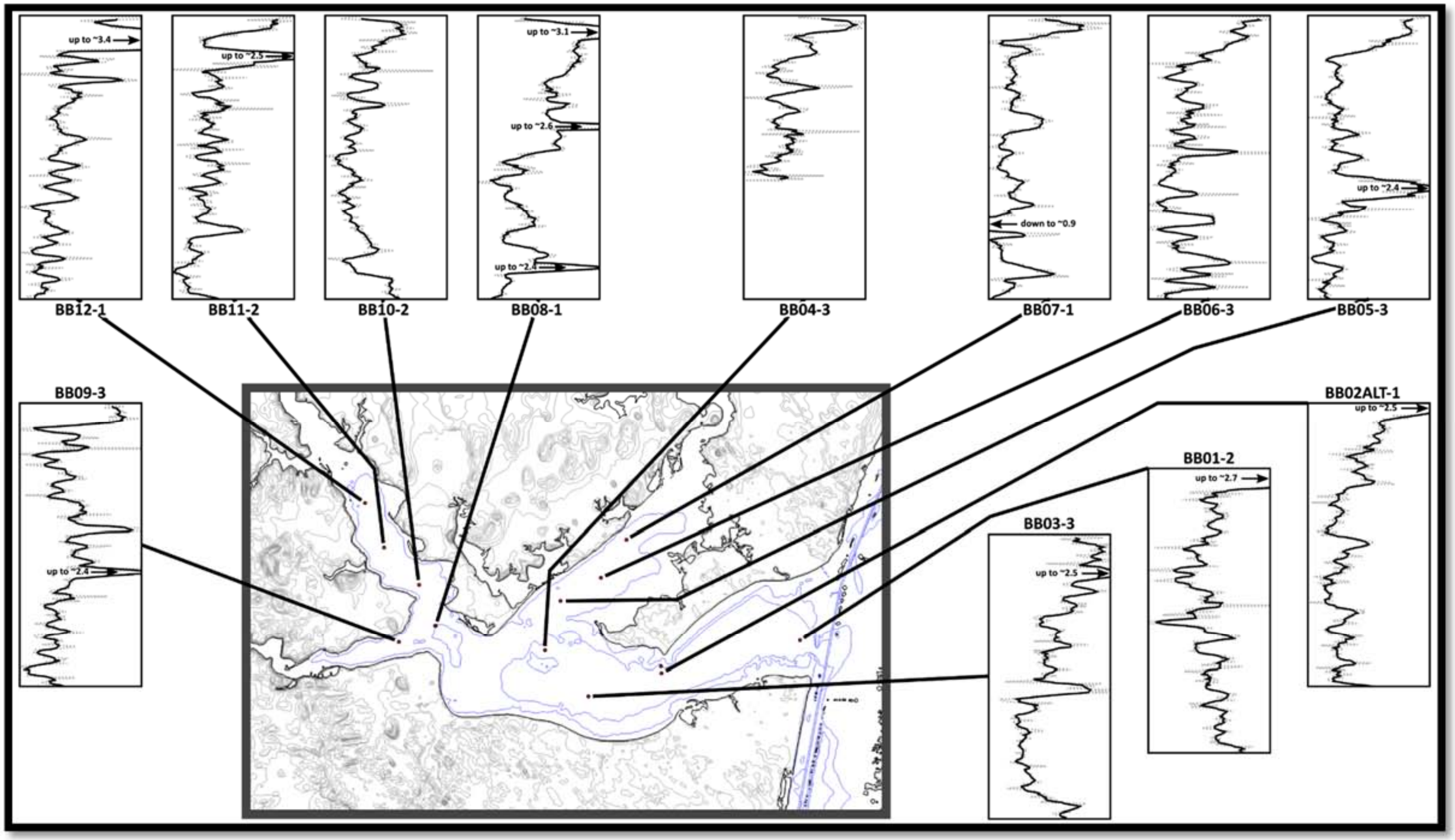

Figure 18—Synopsis Diagram of Inferred Chlorophyll Concentrations

These plots show the inferred chlorophyll concentrations down core to 1.2 m depth based on the surface reflectance scanning RABA$_{400\text{-}560}$ parameter (see text for more details). Reflectance spectra were gathered at 0.5-cm intervals down core (dotted light gray lines in background), but the results were smoothed by a 5-point centered running mean (solid black lines) to better show the trends. The width of each plot represents an identical scale ranging from 1.1 to 2.3 units (dimensionless). In instances where peaks significantly exceed the maximum scale value, arrows show the approximate peak value reached. Several long-term trends are noticeable including an initial decrease followed by a shift to increasing values in cores from the main basin, and neutral to generally increasing trends in the tributary bays. One common characteristic for almost all the cores is a strong increase towards the core top though the peak values for several of the cores fall a few centimeters below the actual sediment/water interface.

Several prominent trends can be noted in the results. In particular, sediment cores from the main basin (stations BB01, BB02ALT, BB03, and BB08), and from station BB10 show an initial trend towards decreasing values from 120 cm upwards, but around mid-core shift towards increasing values up to the present day. The three cores from Alazan Bay (stations BB05, BB06, and BB07) do not show strong trends for the majority of the core length from 120 cm upwards, but do show a strong increase in values starting at 20-25 cm depth up to the present day. Cores BB11-2 and BB12-1 from the Cayo del Grullo tributary show a show general increase from 120 cm upwards, and a very strong increase over the last 25 cm of accumulation. Finally, core BB09-3 shows an approximate opposite trend to the cores from the main basin—there is a trend towards progressively higher values to start, and shift and trend towards lower values, and then a very strong increase towards the top of the core. A common characteristic for almost all the cores is a strong increase towards the core top though the peak values for several of the cores fall a few centimeters below the actual sediment/water interface.

Inferred Carotenoid Content ($RABD_{510}$)

Inferred carotenoid content ($RABD_{510}$ parameter of Rein and Sirocko 2002) results are summarized graphically for all 12 sediment cores in Figure 19, and on a core-by-core basis in the Appendix section. Inferred carotenoid content was measured via diffuse color reflectance scanning as explained in the Sampling and Analysis Methods section above. The carotenoids are a group of red and yellow pigments that are found in all plants including aquatic and terrestrial vascular and non-vascular forms. As explained further below, chlorophyll and carotenoids initially covary in the sediment cores generally changing in unison. But this relationship breaks down in the latter part of the record, and they begin to vary inversely. This relationship is further examined in the Carotenoid Pigment Concentrations portion of the Discussion section below.

Inferred carotenoid content results are available at 0.5-cm resolution, but the results were smoothed by a 5-point centered running mean to reduce variability, and better show the trends. The $RABD_{510}$ values generally fall between 0.997 and 1.007 for all cores, but some higher value peaks are present generally towards core tops. These numbers are unitless/dimensionless because they are calculated as simple ratios between wavelengths.

Several prominent trends can be noted in the results. The three sediment cores from the eastern part of the main basin (stations BB01, BB02ALT, and BB03), show a very similar and marked trend, but with slight differences in the absolute $RABD_{510}$ values. There is a gradual trend towards decreasing values at the start of the record, a transition and shift towards higher values, and then another trend towards progressively decreasing value towards the present day. Core BB04-3 displays the same decreasing→increasing→decreasing trend, but in a much compressed form. Core BB08-1, which generally showed trends similar to the main basin cores in the other proxies, is a bit different here. It starts off with slightly elevated $RABD_{510}$ values of ~1.001, shows a maximum around mid-core like the other main basin cores, and then drops to slightly reduced $RABD_{510}$ values of around 0.999 for the remainder of the core. Cores BB10-2, BB11-2, and BB12-1 from the Cayo del Grullo tributary bay show a slow, general increase in $RABD_{510}$ values from 120 cm upwards with a shift towards lower values in the last 20-25 cm of sedimentation. BB10-2 and BB12-1 also show an initial decrease in values that is reminiscent of the main basin cores. Results from core BB09-3 show high variability with a strong decrease at the core top, but a long-term trend is not obvious.

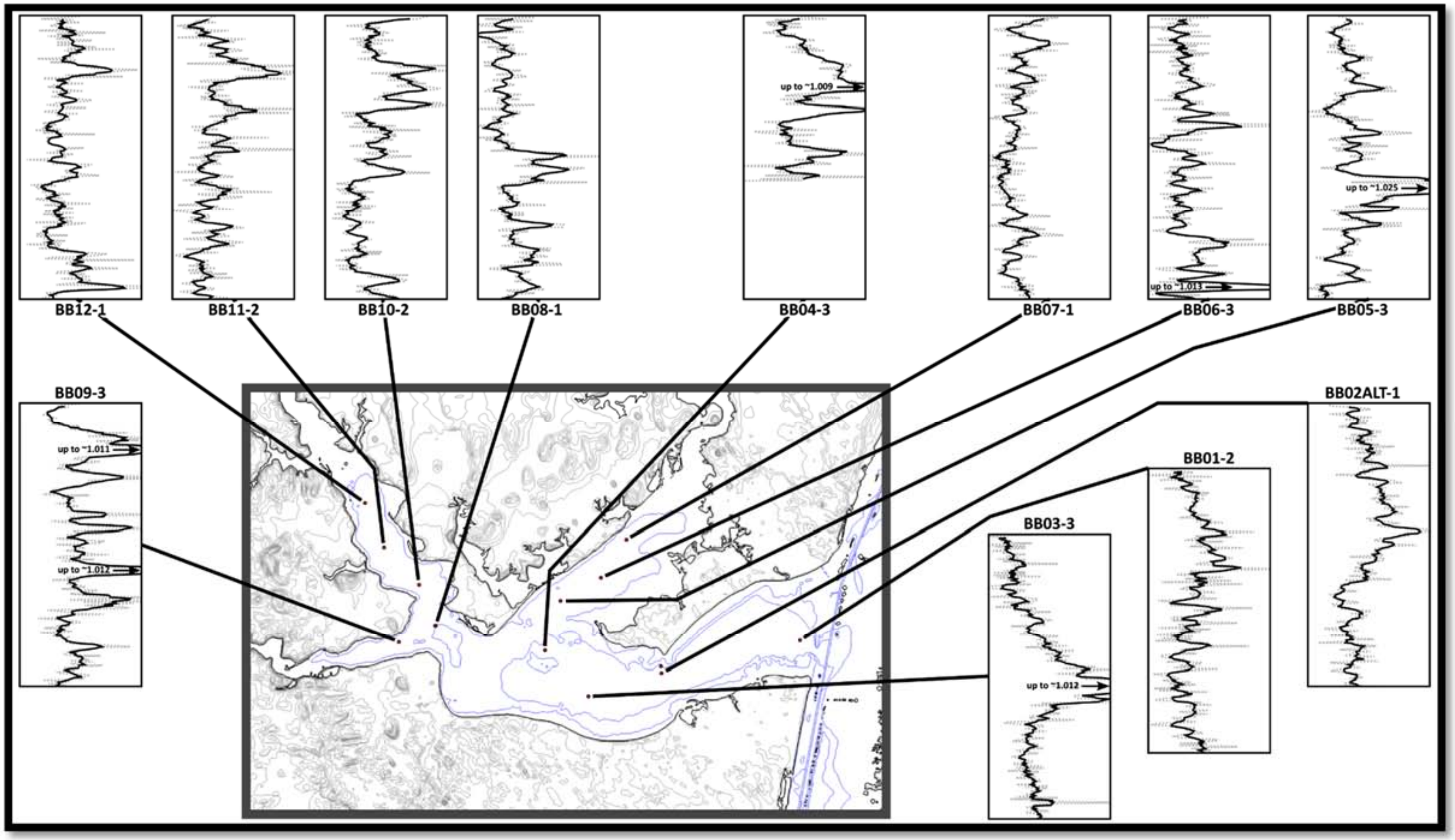

Figure 19—Synopsis Diagram of Inferred Carotenoid Pigment Concentrations

These plots show the inferred carotenoid pigment concentrations down core to 1.2 m depth based on the surface reflectance scanning $RABD_{510}$ parameter (see text for more details). The strongest carotenoid peaks in the records are coordinated with the presence of visible algal mats in the stratigraphy, but other aquatic algae (especially diatoms) and land plants are also potential sources for this pigment group. Reflectance spectra were gathered at 0.5-cm intervals down core (dotted light gray lines in background), but the results were smoothed by a 5-point centered running mean (solid black lines) to better show the trends. The width of each plot represents an identical scale ranging from 0.997 to 1.007 units (dimensionless). In instances where peaks significantly exceed the maximum scale value, arrows show the approximate peak value reached. A couple prominent trends can be recognized including an up core decreasing→increasing→decreasing trend for the main basin cores, and a slow general increase in values for the cores in the Cayo del Grullo tributary bay.

The results from the sediment cores taken along the length of Alazan Bay provide an interesting assemblage of trends. BB07-1, which is furthest into the tributary, shows a subtle trend towards decreasing values from 120 cm up to about mid-core, and then a shift, and trend towards slightly higher values towards the core top. Core BB05-3, which is positioned closest to the mouth of Alazan Bay on the main basin, displays an inverse trend to core BB07-1, but again, the shifts are subtle. Finally, core BB06-3 which falls intermediate to the other two cores, starts off with higher values, but then arguably displays a neutral trend with high/low variations around a mean $RABD_{510}$ value of 1.000.

Chlorophyll a Concentration via HPLC

Chlorophyll *a* concentration results as determined by HPLC are summarized graphically for all 12 sediment cores in Figure 20, on a core-by-core basis in the Appendix section. As with the inferred chlorophyll content results reported above, this measurement is interpreted to primarily reflect the amount of photosynthetic/algal biomass in the water column at the time a particular sediment layer was accumulated.

Given resource constraints, chlorophyll *a* concentrations were generally measured at 5-cm resolution down the length of the cores from 0-100 cm depth. This resulted in 21 samples for most cores (first sample at 0-1 cm for the modern sediment water interface, second sample at 4-5 cm depth, and then every 5-cm increment thereafter down to 100 cm). To verify the utility of the inferred chlorophyll content analysis measurement as determined by diffuse color reflectance scanning, we chose to analyze core BB02ALT-1 down its length via the HPLC technique at 1-cm resolution for comparison. Similarly, to develop a more detailed understanding of the influence of the Laguna Madre, core BB01-2 was analyzed at 1-cm resolution. Finally, resources allowed for the analysis of core BB06-3 in the Alazan Bay tributary at 1-cm resolution down to 71 cm depth.

It is important to note that the HPLC results are presented on a logarithmic axis because there is generally a very large increase in concentrations towards the core tops that makes any variation lower down in the cores almost imperceptible if a standard, linear axis is used for the scale. This necessitates a scale that visually accentuates the nature of the curves, and a scale from 10 to 10,000 (ng/g) was chosen. A consequence of this scale is that values measured as <10 ng/g do not appear, and leave gaps in the curves. These gaps are simply a function of the fact that a logarithmic scale was chosen to accommodate the range of the data—analysis was continuous down core at 5-cm resolution as mentioned above.

Regarding results from most of the 5-cm resolution data (cores BB04-3, BB05-3, BB07-1, BB08-1, BB09-3, BB10-2, and BB12-1), values generally fluctuate between 0-50 ng/g for the majority of the stratigraphy from 100 cm depth upwards, but a subtle increase begins around 15-20 cm depth, and a massive increase dominates the uppermost samples. The uppermost samples in these cores have peak chlorophyll values ranging from 740-12,342 ng/g, and the peaks average about 4,600 ng/g. Besides the very high core top values, there is some variation along the way from the base upwards, but it is very hard to discern given the low sampling resolution. Nonetheless, spikes in chlorophyll content are noted in cores BB07-1 (~145 ng/g at 34.5 cm depth, and 255 ng/g at 44.5 cm depth), BB09-3 (172 ng/g at 19.5 cm depth), and BB10-2 (488 ng/g at 49.5 cm depth).

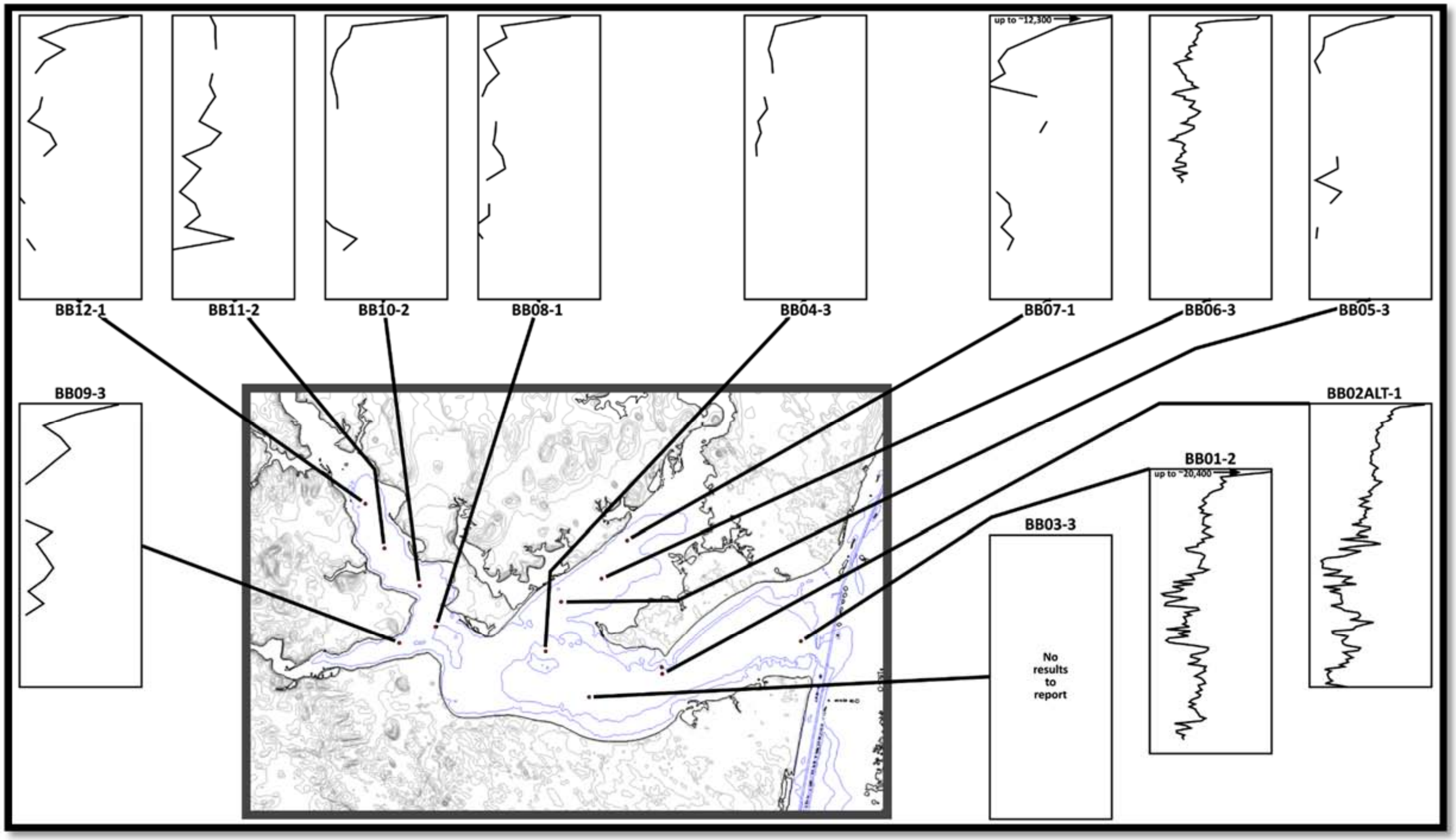

Figure 20—Synopsis Diagram of Chlorophyll *a* Concentrations via HPLC
These plots show the chlorophyll *a* concentrations down core to 1.2 m depth as determined via HPLC analysis. Cores BB01-2, BB02ALT-1, and BB06-3 were analyzed at continuous, 1-cm resolution down core, and thus, have very detailed profiles. The other cores were analyzed a 5-cm resolution down core leading to profiles with a blocky appearance. The width of each plot represents an identical, logarithmic scale ranging from 10 to 10,000 (ng/g of dry sediment). In instances where peaks significantly exceed the maximum scale value, arrows show the approximate peak value reached. The gaps in the 5 cm resolution data do not represent missing data, but instead represent very low measured values that fall below the minimum scale value. One common trend seen in the results from all core except core BB11-2 is a very strong increase in chlorophyll concentrations at the core tops.

Core BB11-2 was also analyzed at 5-cm resolution, but it shows a strong spike up to 332 ng/g at 94.5 cm depth, variability between 20-50 ng/g up to 60 cm depth, and then a jump to still variable, but higher levels between 50-150 ng/g from 60 cm depth to the top of the core. This core is the only one of the 12 that does not show a spike towards very high values at the top of the core.

Trends and variability in the 1-cm resolution data are much easier to recognize and quantify as expected. Cores BB01-2 and BB02ALT-1 show a very similar trend—values generally vary from small positive values up to about 200 ng/g initially. At about 72.5 cm depth, values in BB01-2 begin a gradual rise up core to about 13 cm depth at which point they begin a drastic rise to a peak value of 20,387 ng/g in the core top sample. It is noted that there is some flexibility about the starting depth of the trend in this core because different interpretations might be made given the many abrupt sand layers in this core. Core BB02ALT-1 shows a similar change, but starting at ~82 cm depth. The drastic rise in that core begins at 11.5 cm depth, and a peak value of 6840 ng/g is reached in the core top sample. Finally, core BB06-3 shows variability of chlorophyll values between ~20-180 ng/g from 71 cm up to 20 cm depth, then a gradual rise to ~200 ng/g at 6.5 cm depth, and lastly a drastic increase over the remainder of the core to a peak value of 4942 ng/g in the core top sample

It is important to note that the extra resolution provided by these 1-cm analyses shows that superimposed on the long-term trends that were just described, variability is also evident. This variability is also evident in the inferred pigment results from diffuse reflection scanning, and it probably represents real variability of photosynthetic/algal biomass in the water column at the time of accumulation of those strata.

Radioanalysis and Sediment Dating

<u>^{137}Cesium</u>

^{137}Cesium concentrations were measured based on the radionuclide 661-keV gamma ray line. The ^{137}Cs depth profiles are presented in Figure 21 for the three cores. For most of the cores, ^{137}Cs activities were below the detection limit of the instrumentation for the selected geometry and acquisition times. Minimum Detectable Activities (MDAs) were computed for all measurements following the methodology presented in the above Methods section. In Figure 21 the depth profile of the upper portion of the core are presented. The onset of ^{137}Cs is identified as year 1955 while the peak of the profile is identified as year 1964, the peak of the open air atomic bomb tests. Onsets of ^{137}Cs were detected at depths of 35 cm, 16 cm and 7 cm respectively for cores BB02ALT-1, BB06-3 and BB11-2. ^{137}Cs peaks were identified for depths of 29.5 cm, 12.5 cm and 6.5 cm for cores BB02ALT-1, BB06-3, and BB11-2. Average sedimentation rates for the upper portions of the cores were estimated based on these dates/core depths. The results are presented in Table 5. The sedimentation rates derived based on the onset of detectability of ^{137}Cs and peak ^{137}Cs activities were close. Resulting sediment rates vary substantially from 0.6 cm/yr for core BB02ALT-1 to 0.1 cm/yr for core BB11-2. Differences were expected considering the deeper waters and mid bay location of core BB02ALT-1 as compared to the locations of the other two cores in the tributary bays.

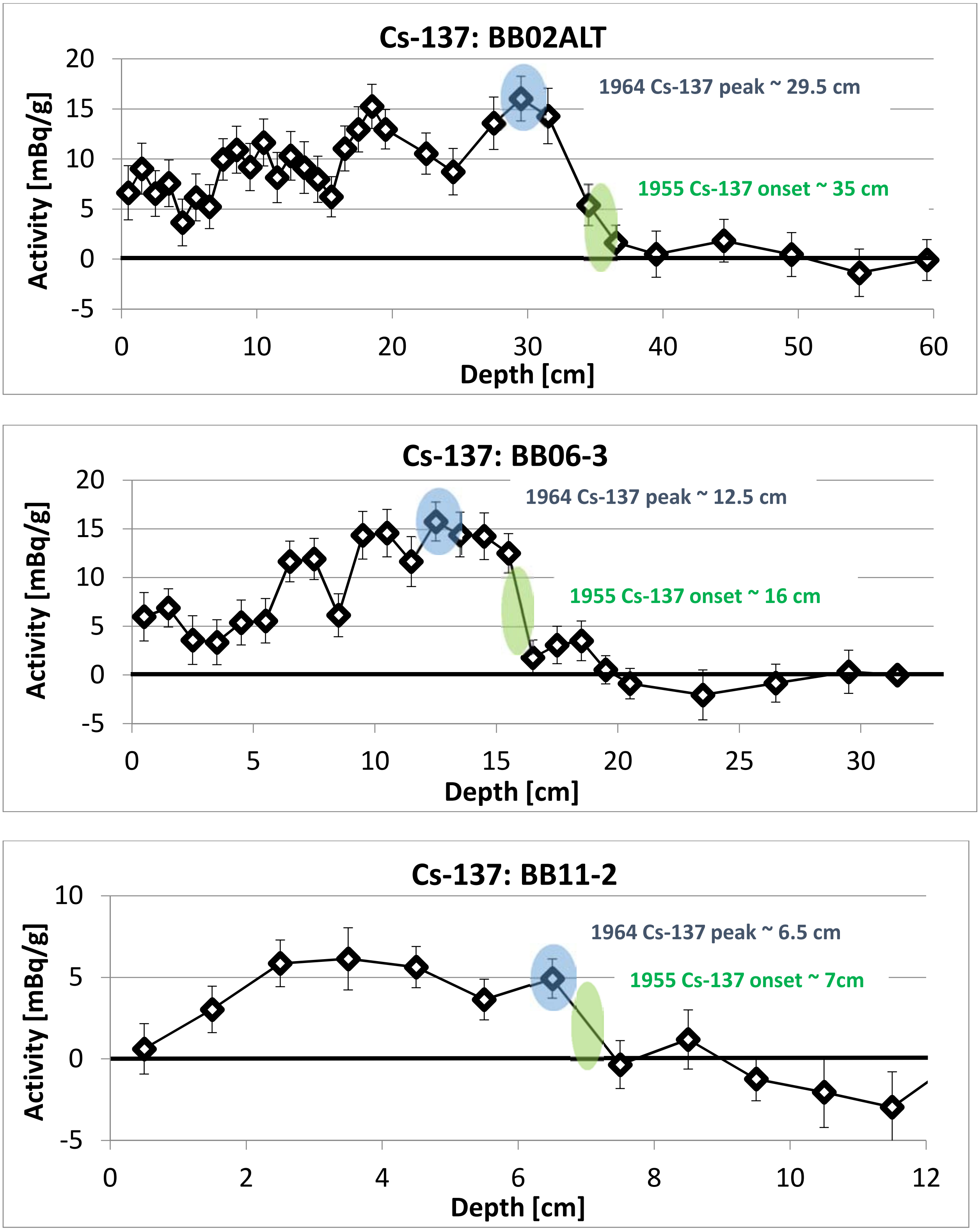

Figure 21—^{137}Cesium activity profiles for cores BB02ALT-1, BB06-3 and BB11-2
These plots show the ^{137}Cs activity profiles and include counting uncertainties. Note the large differences in the onset of detectable ^{137}Cs activities.

Table 5—Summary of Radiochronological Findings
This table summarizes the results of the ^{137}Cs and ^{210}Pb analyses used to date sediment cores BB02ALT-1, BB06-3, and BB11-2.

Core	**BB02-ALT-1**	**BB06-3**	**BB11-2**
Location	**Baffin Bay**	**Alazan Bay**	**Cayo Del Grullo**
^{137}Cs Onset (1955)	35 cm	16 cm	7.0 cm
^{137}Cs Peak (1964)	29.5 cm	12.5 cm	6.5 cm
^{137}Cs Derived Sed rate	0.57 cm/yr	0.25 cm/yr	0.10 cm/yr
^{210}Pb sed rate (dry mass)	0.55 g/cm^2/yr	0.25 g/cm^2/yr	0.09 g/cm^2/yr
^{210}Pb sed rate (for average sed density)	0.88 cm/yr	0.31 cm/yr	0.11 cm/yr
Selected Average Sed Rate	0.71 cm/yr	0.28 cm/yr	0.10 cm/yr
Core Estimated Time Span to 150 cm	AD 1800-2015	AD 1480-2015	AD 515-2015

^{210}Lead

^{210}Lead concentrations in the core samples were measured based on the 46-keV gamma ray line. The ^{210}Pb activity can be divided into geologically supported ^{210}Pb from the ^{238}U decay series content of the sediments and unsupported ^{210}Pb contributed by atmospheric deposition. The second contribution concentration will decrease with depth as excess ^{210}Pb is only contributed at the surface rather than generated continuously in the sedimentary materials. The decay with depth of the unsupported ^{210}Pb is based on its 22.3 years half-life and the location's sediment accumulation rate. Different methods can be used to estimate the unsupported ^{210}Pb concentrations. For this work the supported ^{210}Pb activity was estimated as the average activity in the deeper layers of the core. Based on the change with depth of the ^{210}Pb profile presented in Figure 22, Figure 23, and Figure 24 average supported ^{210}Pb activity were selected. Subtracting this component leads to estimated unsupported ^{210}Pb profiles. Some variability around the average supported concentration is to be expected related to the variability of the counting process and sedimentary materials.

The estimated unsupported ^{210}Pb was modeled using the usual exponential decay equation below:

$$^{210}\mathrm{Pb(z)} = {}^{210}\mathrm{Pb(surface)}e^{-\left(\frac{\lambda}{S}\right)z}$$

with λ (0.031 yr^{-1}) the ^{210}Pb decay constant, ^{210}Pb(surface) the surface unsupported ^{210}Pb concentration and S the dry mass sediment accumulation rate (g/cm^2/yr). The sedimentation rates were estimated from the graph of the logarithm of the unsupported ^{210}Pb activities versus depth for the upper portions of the cores prior to reaching depths no longer affected by unsupported ^{210}Pb. The estimated sedimentation rates are presented in the upper portions (a) of Figure 22 through Figure 24. The respective estimated sedimentation rates are 0.55, 0.25 and 0.09 g/cm^2/yr for cores BB02ALT-1, BB06-3, and BB11-2. These sedimentation rates are also expressed in cm/yr in Table 5 while factoring the average density of the core samples.

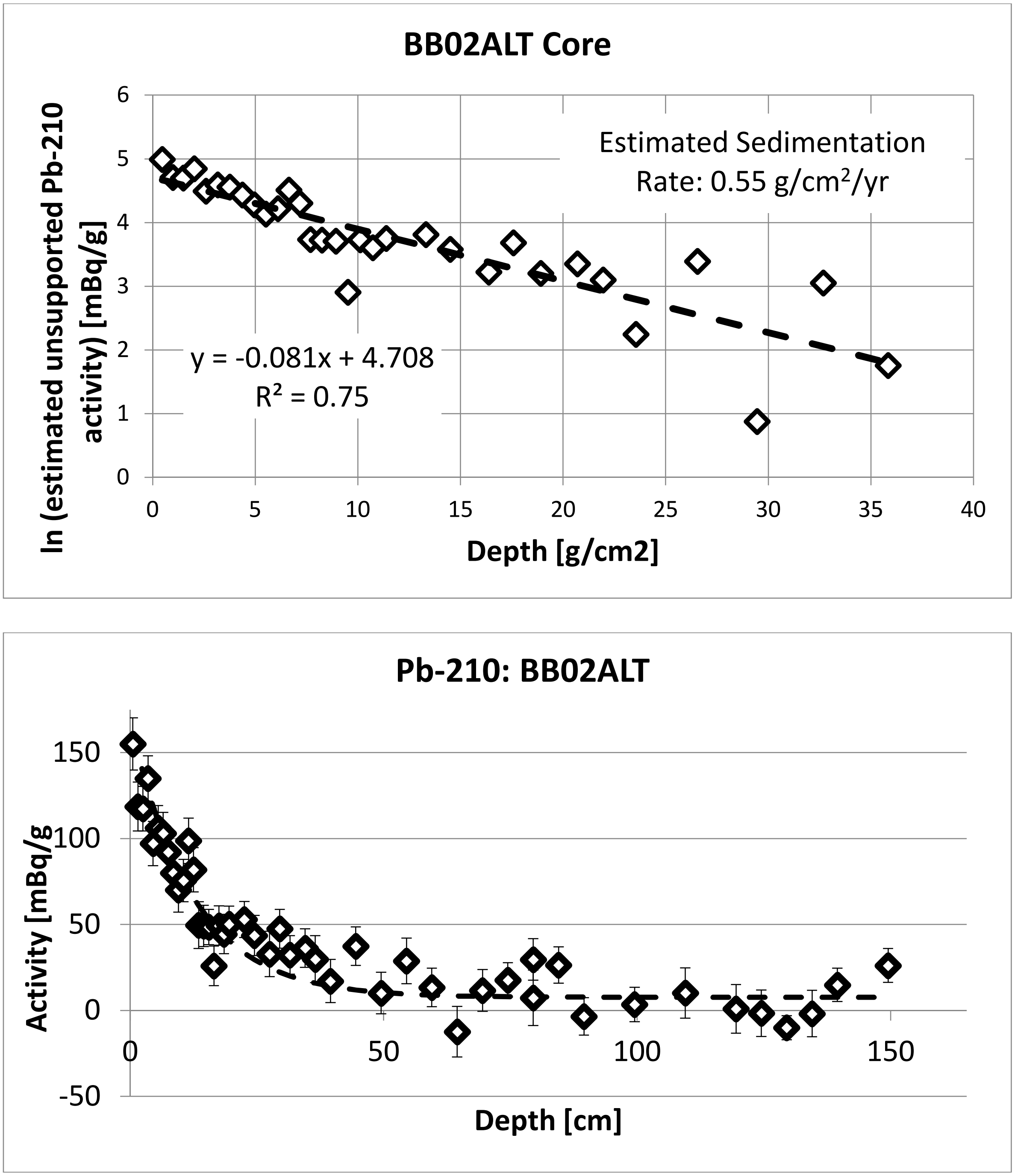

Figure 22—Core BB02ALT-1 Estimated Dry Mass Sedimentation Rate

These plots show the estimated dry mass sedimentation rate for core BB02ALT-1 based on the natural log of the unsupported ^{210}Pb activity profile (upper plot) and for an activity model including an estimated ^{210}Pb supported activity of 7.7 mBq/g (lower plot).

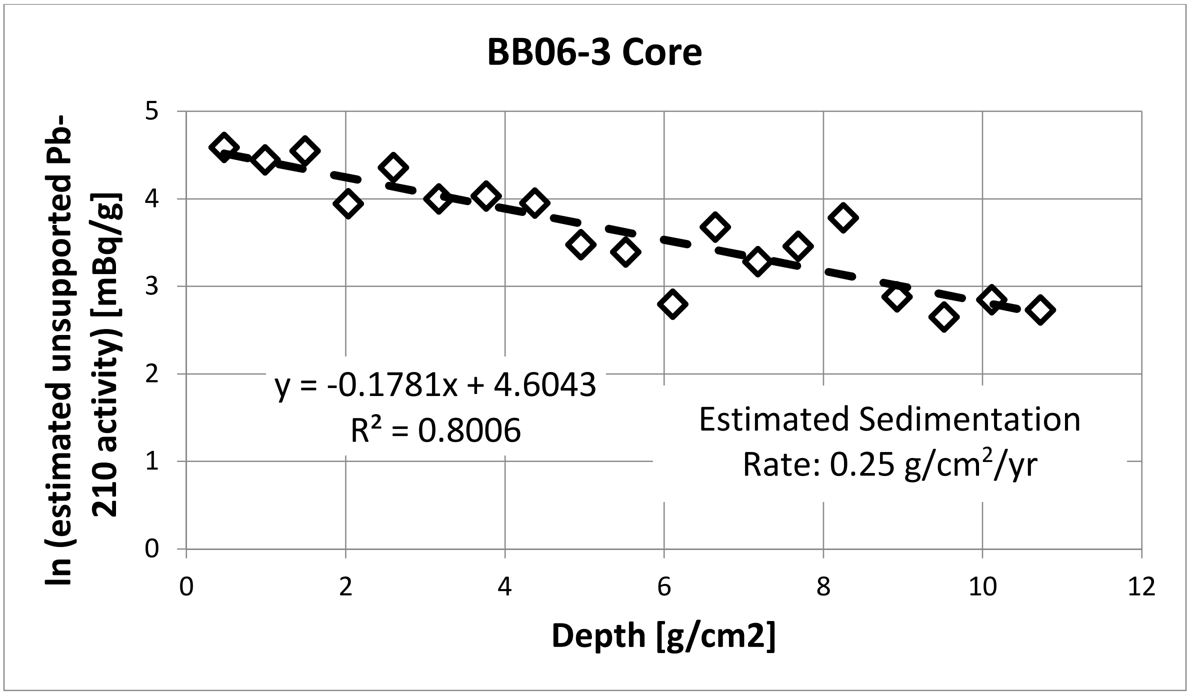

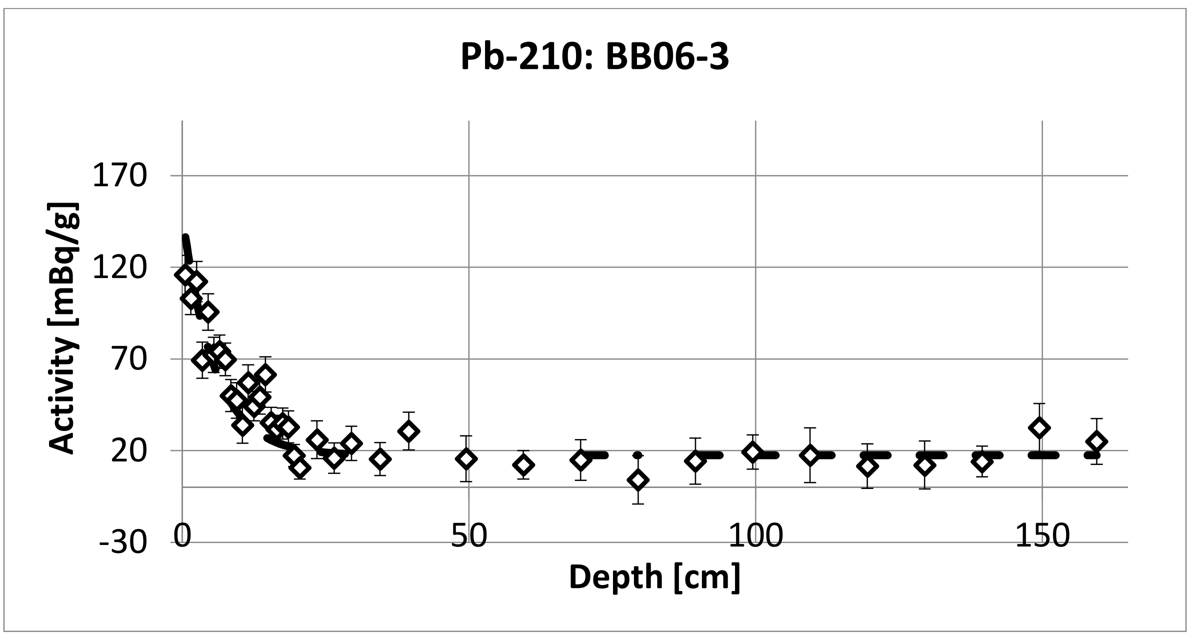

Figure 23—Core BB06-3 Estimated Dry Mass Sedimentation Rate

These plots show the estimated dry mass sedimentation rate for core BB06-3 based on the natural log of the unsupported ^{210}Pb activity profile (upper plot) and for an activity model including an estimated ^{210}Pb supported activity of 17.6 mBq/g (lower plot).

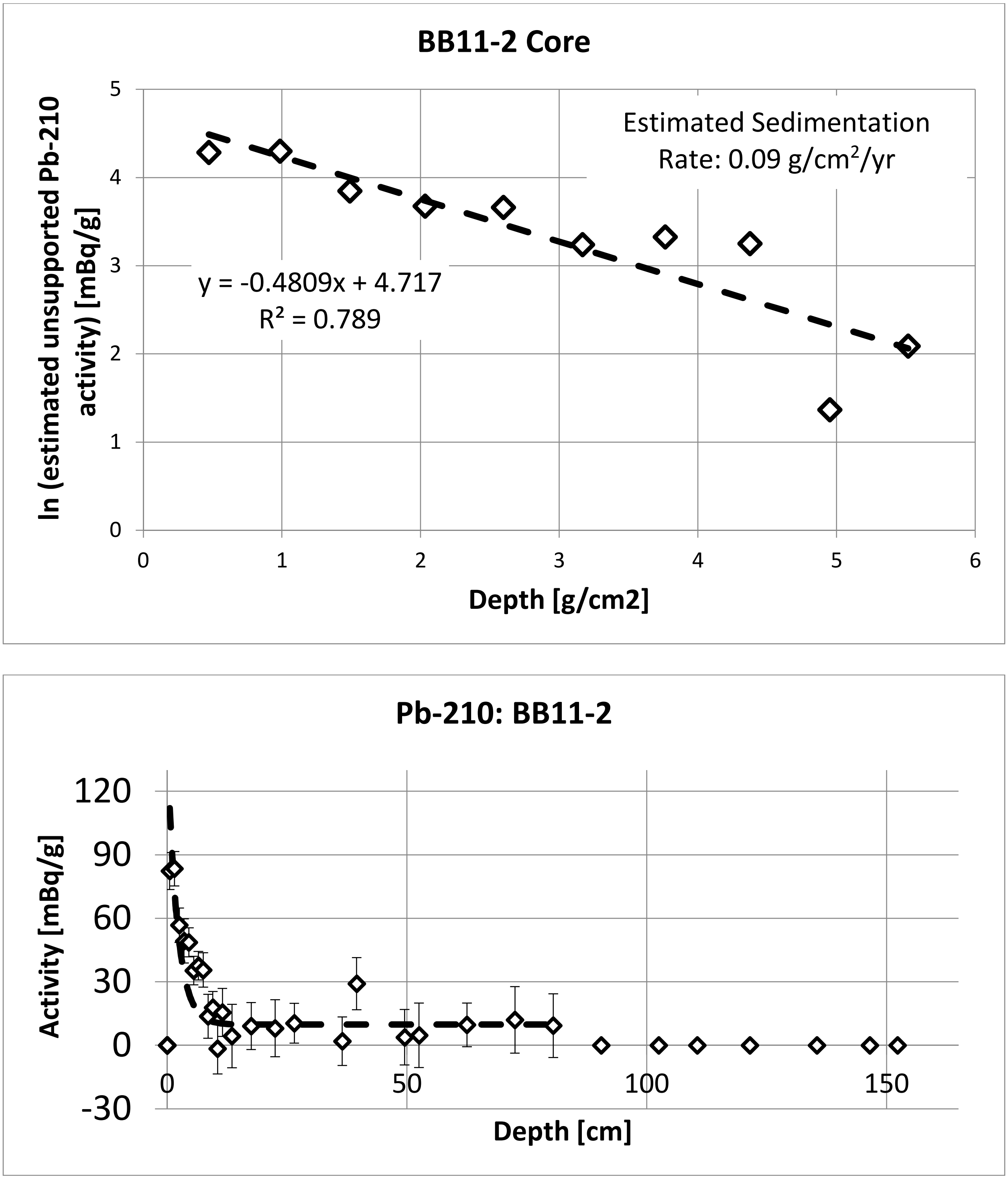

Figure 24—Core BB11-2 Estimated Dry Mass Sedimentation Rate
These plots show the estimated dry mass sedimentation rate for core BB11-2 based on the natural log of the unsupported ^{210}Pb activity profile (upper plot) and for an activity model including an estimated ^{210}Pb supported activity of 9.7 mBq/g (lower plot).

Sedimentation rates obtained by the ^{137}Cs and ^{210}Pb based methods are compared in Table 5. Sedimentation rates are similar for all cores with a bigger difference for core BB02ALT-1, 0.88 cm/yr for the ^{210}Pb method versus 0.57 cm/yr for the ^{137}Cs based method. While the difference is relatively large, the sedimentation rate is substantially larger than that of the other cores leading to a shorter time span for the core and a lesser impact of the uncertainty in sedimentation rate. For the rest of the analysis, the averages of the sedimentation rates derived by the ^{137}Cs and ^{210}Pb methods were selected for each core leading to estimated sedimentation rates of 0.71 cm/yr, 0.28 cm/yr and 0.10 cm/yr for cores BB02ALT-1, BB06-3, and BB11-2. Based on these estimated sedimentation rates and the length of the extracted cores, a tentative time span for the cores is computed and presented Table 5. It is important to keep in mind that a number of events, such as erosional events, can take place and disrupt the geochronology of the sediments. The variability of the sediment compositions is discussed in other sections of the report and is more prevalent in the upstream cores than the cores extracted in the mid or lower portion of Baffin Bay. Also material compaction will increase with core depths. While estimated sediment ages are considered quite good for the upper portions of the core, uncertainty increases considerably with core depths, particularly for core BB11-2 and its slow sedimentation rate. Hence, dates earlier than 1700-1800 are very uncertain and presented as a general guidelines prior to a further more detailed analysis that may identify other markers.

^{40}Potassium

The ^{40}Potassium activity was measured for all three cores through the ^{40}K 1,460 keV line. Results are presented in Figure 25. Activities were typically within a range of 600 to 900 mBq/g for core BB02ALT-1, in a range of 550 to 850 mBq/g for core BB06-3 and a little lower in a range of 450 to 750 mBq/g for core BB11-2. For all three cores occasional significant decreases in the ^{40}K activities are observed followed by a return to the general trend in activity. Approximate dates for the ^{40}K decreases are indicated on the graphs of Figure 25. Decreases in ^{40}K are tentatively correlated with the passage of large hurricanes with a substantial surge component such as the 1919 Corpus Christi Hurricane and possibly the 1837 Cat 4-5 Racers storm. The change in sediment composition around 1940 is tentatively correlated with the opening of the Intracoastal Waterway.

^{226}Radium

The ^{226}Radium activity was measured through the ^{214}Bi 609 keV gamma ray line. While the half-life of ^{226}Radium is 1600 years, its daughters decay in rapid succession starting with ^{222}Radon with a half-life of 3.82 days. The following elements in the decay chain are ^{218}P, ^{214}Pb, ^{214}Bi and ^{214}Po, all with half-lives shorter than 30 minutes up to the next element in the chain, ^{210}Pb, which has a half-life of 22 years.

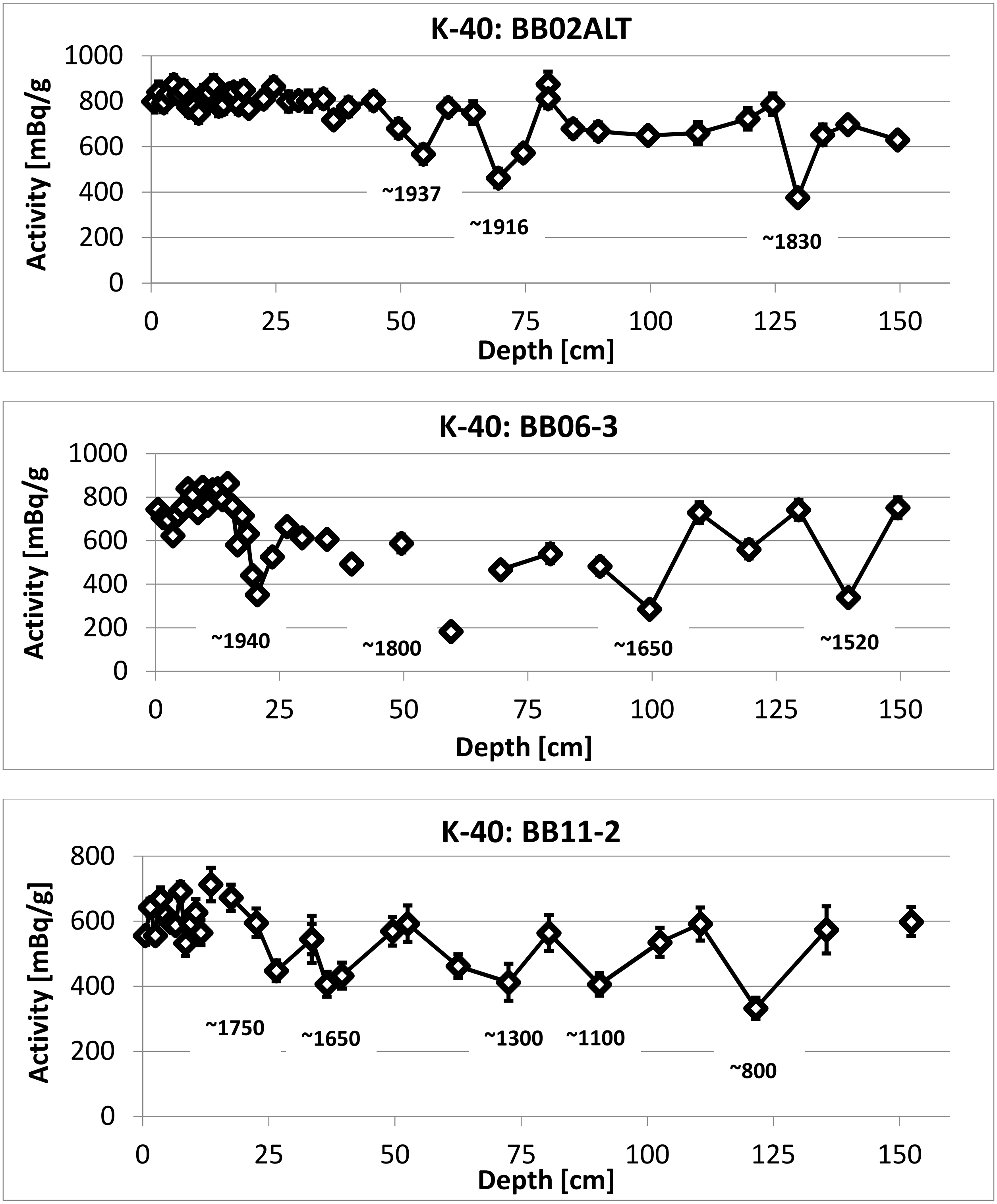

Figure 25—^{40}K activity profiles for cores BB02ALT-1, BB06-3 and BB11-2
These plots show ^{40}K activity profiles for cores BB02ALT-1, BB06-3 and BB11-2 including counting uncertainties. The approximate sediment age based on radiochronology is provided for features for general guidance with uncertainty increasing with depth.

In a sealed vial the elements will achieve decay equilibrium after a few half-lives of the longer lived radionuclide resulting in the same activity for all elements along the chain allowing to measure the ^{226}Radium activity based on radionuclides with more easily identified gamma ray signatures such as ^{214}Pb and ^{214}Bi. ^{226}Ra activities as measured through the ^{214}Bi vary between 0 and 75 mBq/g for core BB02ALT-1 with higher activities at the surface of the core. Three substantial increases in ^{214}Bi activities are observed in the core at depths of 45.5cm, 55.5cm and 119.5cm. The associated tentative dates associated with these increases in activity are displayed in Figure 26. The dates are relatively close to the events identified by the ^{40}K analysis and hence it is hypothesized that the changes in ^{226}Ra are also related to changes in sediment materials due to a large event, possibly a large hurricane with a substantial flood component. ^{214}Bi activities for core BB06-3 vary between 0 and about 50 mBq/g with several peaks at higher activities. Several of the peaks are located in the surface layers. Tentative dates are also associated with the peak with confidence in the estimates decreasing with core depth. For Core BB11-2, ^{214}Bi activities vary between 0 and 55 mBq/g with a surface peak with activity up to 63 mBq/g. Tentative dating of features is indicated on the graphs for Figure 26.

Higher resolution radiometric measurements will be required to further substantiate the potential relationship between the impact of hurricanes with a substantial flood component and ^{40}K and ^{226}Ra activities.

^{232}Thorium/^{208}Thalium

^{232}Thorium has a long half-life (1.41 x 10^{10} years) compared to its immediate decay products, ^{228}Ra has a half-life of 5.7 years and all other decay products have a half-life of less than 2 years. The activity of ^{232}Thorium is measured through the 583keV ^{208}Thallium (^{208}Tl) line. For all three cores the ^{208}Tl profiles did not show any substantial variability.

Core BB02ALT-1: 34.3 +/- 14.3 mBq/g
Core BB06-3: 29.4 +/- 11.8 mBq/g
Core BB11-2: 27.5 +/- 12.3mBq/g

While no specific dating information can be obtained from these measurements, the results show that the levels are low with substantial changes along core depth. Combined with other measurements this is a useful indication.

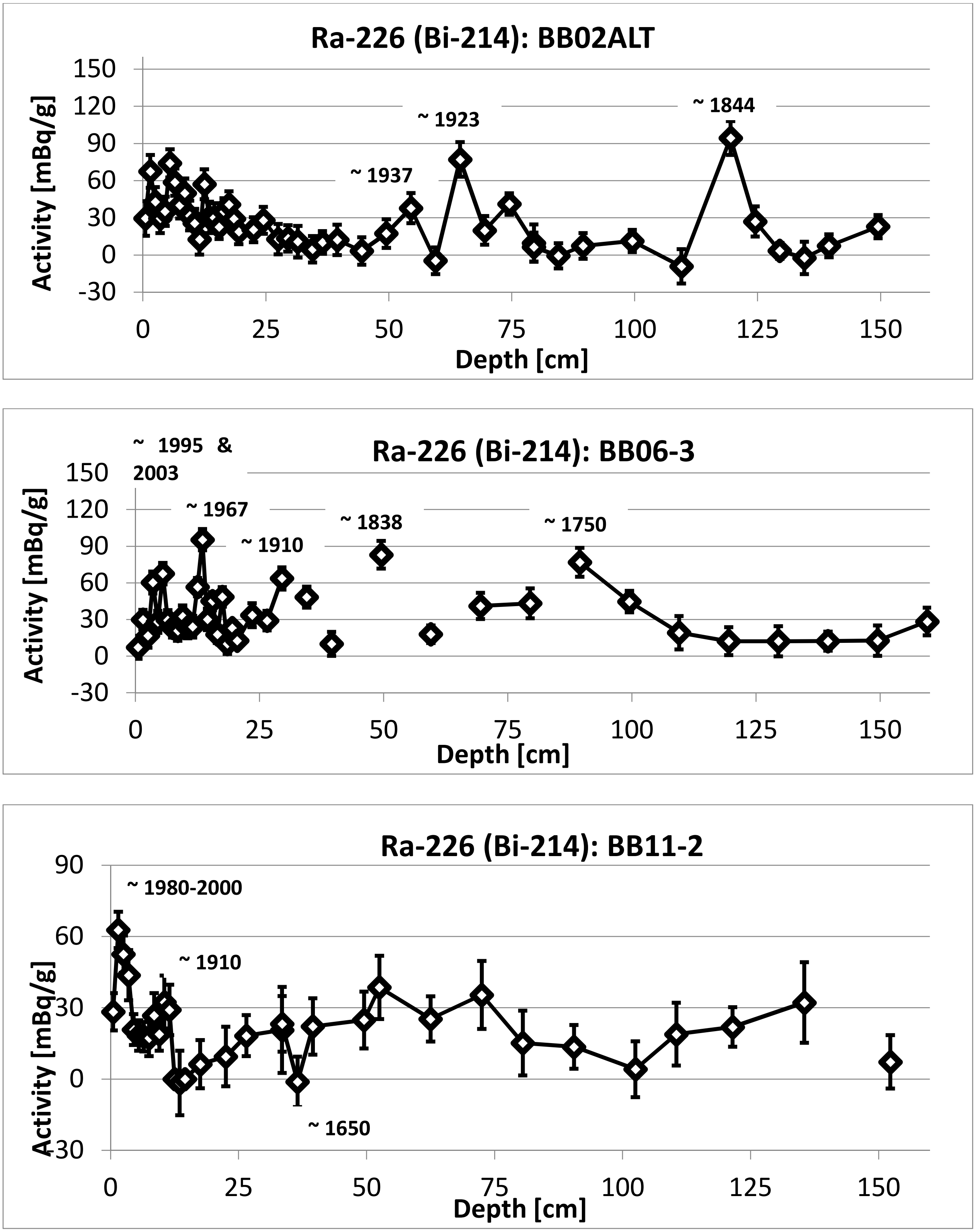

Figure 26—^{226}Ra activity profiles based on ^{214}Bi for cores BB02ALT-1, BB06-3 and BB11-2

These plots show the ^{226}Ra activity profiles based on ^{214}Bi for cores BB02ALT-1, BB06-3 and BB11-2 including counting uncertainties. Approximate sediment age based on radiochronology provided for features for general guidance with uncertainty increasing with depth.

G. Discussion

Chronology of the Sediments

A suite of evidence is used to help establish a time scale for the stratigraphy in the basin, and this includes results from the radioisotope data, and as well as the multiproxy analysis results in light of knowledge of the region's history. As discussed in the Nature of the Sedimentation and Stratigraphy section above, the sediment cores from the main basin appear to archive a more continuously complete record of sedimentation in the basin. This interpretation was simply based on the fact that sand/shell hash layers and erosional contacts are common in the sediment cores from the tributary bays. This is reinforced by calculated sedimentation rates based on the radioisotope analysis (Table 5). In particular, the calculated sedimentation rate for the main basin core (BB02ALT-1) ends up >2x larger than the rate calculated for Alazan Bay (core BB06-3), and >5x larger than the rated calculated for Cayo del Grullo (core BB11-2). With fluvial sediment load focused on the tributaries, it is expected that they would have similar or even greater sedimentation rates than the deeper waters of the main basin. In sum, while the stratigraphy is generally well-preserved throughout the basin, it is apparently much more continuously complete in the main basin. Nonetheless, results from the analyses of our multiproxy approach make correlation between the main basin and tributary bays possible.

Main basin core BB02ALT-1 was dated by ^{137}Cs and ^{210}Pb analysis. That core has at least one significant visible stratigraphic defect—the erosional/angular unconformity that runs diagonally across the core from 67-69 cm depth as pictured in Figure 17. There is also evidence of some core shortening at other points in the stratigraphy based on small offsets (i.e. microfaulting, see Figure 6) between distinctive beds, and this is probably due to compressive stress while coring, which is common. The net effect is that the sequence has been shortened, and some undetermined amount of the stratigraphic sequence is missing. Nonetheless, this core as well as BB01-2 and BB03-3 appear to be the most complete among the 12 stations.

Based on results of the ^{210}Pb and ^{137}Cs analyses for BB02ALT-1, low, average, and high estimates of the sedimentation rate were suggested as 0.55, 0.71, and 0.88 cm/year, respectively. The pigment and TOC results are particularly helpful for narrowing this down. The King Ranch was established in AD 1853, and marked the beginning of significant land use changes in parts of the Baffin Bay watershed that increased through time. Such changes would have lead to substantial, anthropogenic contributions in nutrient loading to the basin for the first time. Chlorophyll and carotenoid pigments show a prominent change at about 82 cm depth in the stratigraphy of core BB02ALT-1 (Figure 29). Both pigments are on a slowly decreasing trend from 120 cm depth upwards, but at 82 cm depth, they reverse trend, and start increasing. Similarly, TOC has a generally neutral trend from 120 cm depth upwards, but starts on an increasing trend at 82 cm depth. This would be the expected response with an increased nutrient loading to the system—an increase in pigments representative of an increasing algal biomass in the water column, and consequently, and increase in TOC being accumulated in the sediments.

This interpretation based on the pigments and TOC shows very good correspondence with the minimum sedimentation rate estimate provided by the ^{210}Pb and ^{137}Cs results (0.55 cm/year). Assuming 82 cm depth represents approximately AD 1860, this yields a sedimentation rate of approximately 0.53 cm/year. Given that some amount of the sequence is missing, and some core shortening has occurred, as mentioned above, this would certainly allow the proxy-based interpretation of AD 1860 to coincide with the radioisotope results. Therefore, the shift in pigment and TOC results is established as a marker for AD 1860. This pigment and TOC signal is clearly visible in the other main basin cores, and falls at ~72 cm depth in core BB01-2 (Figure 28), and ~92 cm depth in core BB03-3 (Figure 30). As for other proxy results, the common sand layers in core BB01-2 allow for some flexibility in the starting depth depending on interpretations.

Higher in the stratigraphy of core BB02ALT-1, the chronology is anchored by results of the ^{137}Cs analysis. The onset of ^{137}Cs sedimentation, which is linked to AD ~1955, is placed at ~35 cm depth, and the peak value representing AD ~1964 was encountered at ~29.5 cm depth (Figure 21). These two chronological anchors lead to several other interesting observations. First, the incombustible content shows an abrupt increase at about 43.5 cm depth in the core, and carbonate content shows a concomitant abrupt decrease at the same depth (Figure 29). This apparently corresponds with the mid to late 1940's given the onset of ^{137}Cs deposition. A very significant hydrological change affected the basin at this time—the Intracoastal Waterway (ICW) segment between Corpus Christi and Brownsville was under construction in the late 1940's, and finally opened in 1949 (TXDOT, 2006). This event significantly changed circulation patterns and flushing in the basin, and lead to a substantial change in the style of sedimentation. We speculate that the increased circulation would have lowered the alkalinity in the basin leading to a reduction of carbonate sedimentation, and this is further discussed in the Impact of the ICW Opening on Baffin Bay section below.

A follow-on interpretation is related to an anomalous, fine sandy deposit in the stratigraphy centered on ~54.5 cm depth (Figure 29). The fine sands have an oxic color, which is suggestive of a terrestrial source, but the magnetic susceptibility signal shows no spike as would be expected if this were the case. Instead, carbonate content shows a spike indicating this is carbonate sand. Core BB01-2 shows correlative sand beds centered on 52.5 and 56 cm depth. Thus, this deposit is interpreted as the result of hurricane overwash. The thicker, coarser sand bed in BB01-2 is the proximal facies given its location near the bay mouth close to the Laguna Madre, and the deposit in BB02ALT-1 is a finer, medial to distal facies equivalent. Given the overlying chronological anchors, this deposit can most likely be associated with the 1933 Brownsville Hurricane, which produced a ~4 m storm surge in Brownsville, and created more than 40 breaches in South Padre Island. A related interpretation is that the significant stratigraphic defect at 67-69 cm depth—the angular/erosional unconformity that runs diagonally across the core surface (Figure 17)—is potentially a product of the 1919 Florida Keys Hurricane, which made landfall near Baffin Bay as a large Category 3 storm. These interpretations are simply used as chronological control points given the goals of the present study, but they will be further explored in future research.

Thus, the interpreted chronology for core BB02ALT-1, is summarized in Table 6 below.

Evolution of Water Quality and Chlorophyll Concentrations in Baffin Bay Since AD 1850

This multiproxy study of the well-preserved sedimentary record in Baffin Bay provides an excellent opportunity to look back in time, and track how water quality and chlorophyll concentrations have evolved in the system through time. Core BB02ALT-1 serves as a key to this analysis given the completeness of that record, and the relatively strong chronological control.

Table 6—Interpreted Chronology for Core BB02ALT-1
This table shows the depth, ages, and interpretations for chronological control in core BB02ALT-1.

Depth in Core (cm)	Age (Year AD)	Interpretation
0	2015	modern sediment water interface
~29.5	~1964	peak of ^{137}Cs deposition
~35	~1955	onset of ^{137}Cs deposition
~43.5	1949	major change in circulation and sedimentation related to opening of ICW manifested in incombustible and carbonate content proxies
~54.5	1933	hurricane overwash from 1933 Brownsville Hurricane
~67-69	1919	erosional event related to 1919 Florida Keys Hurricane
~82	~1860	beginning of significant land use changes as manifested in pigments and TOC

Chlorophyll Pigment Concentrations

Diffuse color reflectance scanning and traditional HPLC analysis were used to develop high resolution, down core profiles of sediment chlorophyll concentrations for this project. As demonstrated in the Verification of Inferred Chlorophyll Content Versus HPLC-Determined Chlorophyll section above, the measurements from both types of analysis show a very strong correspondence. Thus, where funding constraints limited traditional HPLC chlorophyll determinations to a coarse, 5-cm resolution sampling, we instead consult the diffuse color reflectance scanning profiles, which are available at 0.5-cm resolution for all sediment cores. Furthermore, via the diffuse color reflectance scanning spectra, quantification of absorption troughs related to carotenoid pigments was also possible with the $RABD_{510}$ parameter (Rein and Sirocko, 2002). Including the carotenoids adds to the richness of the interpretations as discussed in the Carotenoid Pigment Concentrations section below.

Profile results from BB02ALT-1 (Figure 29) make it clear that farming, grazing, and other land use changes starting about AD 1860 (~82 cm depth in core) had a very strong impact on chlorophyll concentrations throughout the basin. Prior to this date, chlorophyll content showed variability between high/low values, but no long-term trend. Starting at ~82 cm depth in the core, chlorophyll content began a continuous, steady rise that has continued to the present day.

The progressive rise in chlorophyll content was not constant or linear, and shorter term variability is superimposed on the long-term trend. This implies that the basin probably saw periods of increased nutrient loading, which would have boosted primary productivity, and thus, increased pigment concentrations in the sediment. The largest prominent peak in chlorophyll content (excluding the present day one) is a peak centered on ~59 cm depth, which according to the interpreted chronology for this core (Table 6) probably represents around AD 1926-1927. Human populations in the region showed rapid growth during the decade of the 1920's, and nearly tripled in size from 4,470 up to 12,451 (Texas State Historical Association, online Handbook of Texas, URL: https://tshaonline.org/handbook/online/articles/hck10). It is possible that this rapid expansion of population increased the nutrient load delivered to the system, and boosted primary productivity. Additional historical research may help point to a more directly causal mechanism.

The second most prominent peak superimposed on the main trend is very obvious in the inferred chlorophyll content record from reflection scanning. The event is still recognizable, but less obvious, in the HPLC results. This feature starts developing at ~36 cm depth, and reaches its peak value at ~33 cm depth. According to the interpreted chronology for this core (Table 6), simple linear interpolation between the surrounding anchor points yields a suggested age of AD 1954-1958 for these two depths. This range exactly corresponds with the peak of the regional, catastrophic drought in the 1950's, and this response in chlorophyll content is almost certainly related to that event by a very straightforward mechanism. The suggested mechanism is that decreased fresh water flow through the system due to a reduction in river input reduced flushing within the basin. The result was an increase in nutrient accumulation that drove primary productivity levels higher, and thus, resulted in an increase in chlorophyll concentrations as recorded in the sediments.

Several other peaks in chlorophyll content are recognizable in the post AD ~1860 part of the record including at ~75.5 cm, ~70 cm, ~46 cm, ~26.5 cm, ~20.5, ~16.5 cm, and ~11 cm depth. As the chronology and interpretations of the data are refined, it may be possible to associate these chlorophyll peaks with historical/climatological events that are known to have affected the basin and watershed.

The modern chlorophyll peak in the basin is impressive (Figure 18 and Figure 20). Actual HPLC measured values of chlorophyll in dry sediment reach 6,840 ng/g in core BB02ALT-1. But they reach even higher values of 20,387 ng/g in BB01-2, 12,342 ng/g in BB07-1, and 8,813 ng/g in BB10-2. This is undoubtedly related to an increasing nutrient load to the basin, but it is also very probable that the strong drought which started in 2010 has significantly reduced fresh water flow to the basin. Just as reduced fresh water flow during the catastrophic 1950's drought probably led to accumulation of nutrients due to reduced flushing, and thus, drove primary productivity in the system, the recent drought is probably involved with the modern chlorophyll peak seen at the tops of the cores throughout the basin. One appreciated implication of this observation is that as this drought recedes, chlorophyll values will probably be reduced, too, due to increased flushing.

Carotenoid Pigment Concentrations

Spectra from the diffuse color reflection scanning work also allowed for the tracking of carotenoid pigment concentrations (Figure 19). This pigment group is found in all plants including aquatic and terrestrial vascular and non-vascular forms, and thus, it can also be used to track algal biomass in the water column. But what is particularly more enlightening is to compare the long-term trends of this group with those of the chlorophylls for the following reason. The chlorophylls are generally much more susceptible to alteration and breakdown by factors such as light, increased temperatures, and also the presence of oxygen. In turn, the carotenoids are generally more resistant. Thus, the relative variation of both pigment groups can be viewed as sort of a preservation index in the water column.

In the early part of the BB02ALT-1 record, it can be seen that the long-term trends of the inferred chlorophyll and carotenoid pigment concentrations generally co-vary in unison. As one increases, so does the other. However, there is a change in this relationship starting at about ~60 cm depth, which probably represents AD ~1930 according to the interpreted chronology (Table 6). At this point, the long-term trends diverge, and begin to show an inverse response. Given the difference in the susceptibility of alteration for the two pigment groups as mentioned above, this long-term shift towards increasing chlorophyll values, and decreasing carotenoids, can be interpreted as a long-term shift towards better preservation conditions, which favors chlorophyll. Indeed, given that light and temperature have been approximately constant over the period of record (if anything, temperature has been increasing since the 1850's), this divergence of curves may represent a progressive, long-term decrease in oxygenation of the water column due to eutrophication of the basin.

<u>Impact of the ICW Opening on Baffin Bay</u>

Regarding the opening of the ICW in AD 1949, which is linked to ~43.5 cm depth in BB02ALT-1, what effect did that have on the Baffin Bay system? With respect to water quality and chlorophyll content in the basin, it appears that the ICW opening did at least initially produce a lowering of the chlorophyll values. This is based on the observation that there is a chlorophyll peak at ~46 cm depth on the reflectance scanning curve, and the opening of the ICW sits at a local minimum on the same curve. But the effect was short-lived, and chlorophyll concentration values continued to rise.

This may not be a fair assessment of ICW's impact because the boundary conditions of the system were also constantly changing. In particular, soon after the ICW opened, the regional catastrophic drought of the 1950's began to develop. And furthermore, while the opening would have certainly improved flushing of the basin and helped stabilize salinities, the nutrient loading to the watershed and basin was on an ever increasing upward trajectory. Indeed, the population quickly grew from 7,782 in 1940 to 16,857 in 1950 to 30,052 in 1960 (Texas State Historical Association, online Handbook of Texas, URL: https://tshaonline.org/handbook/online/articles/hck10).

There is no doubt, however, that the opening of the ICW provoked a substantial change in the style of sedimentation in the main basin, and probably Alazan Bay, too. The change probably affected the Laguna Salada and Cayo del Grullo tributary bays, too, but to a lesser extent based on what is visible in the sedimentary record. In the Chronology of the Sediments section above, it was speculated that the ICW opening increased circulation, and lowered the alkalinity in the basin, thus, leading to a reduction of carbonate sedimentation. This was based on a clear, mode-like shift in the incombustible content (Figure 13) and carbonate content (Figure 14) results from the main basin—carbonate content abruptly drops while incombustible content abruptly increases.

This change could be interpreted as either a reduction in carbonate sedimentation, or potentially an increase in siliciclastic sedimentation, as both scenarios lead to the same relative change. For the latter scenario, siliciclastic material is generally delivered by the fluvial system so a significant boost in fluvial input would be required—this seems unlikely. Instead, there is strong evidence to suggest that the former interpretation is correct, and core BB04-3 shows almost direct evidence for this assertion. In that core, spectacular, carbonate-rich laminae (~20-27% carbonate by weight) are being accumulated at that station, and then at 20 cm depth, a drastic change in sedimentation style occurs (Figure 27). The laminae disappear, and carbonate content plummets to just ~7-11% by weight. This transition is exactly correlative with the opening of the ICW as interpreted from sediment core BB02ALT-1. Thus, we suggest this shift is not simply due to greater fluvial input, but instead, a large reduction in alkalinity that reduced the production of carbonate sedimentation in the basin.

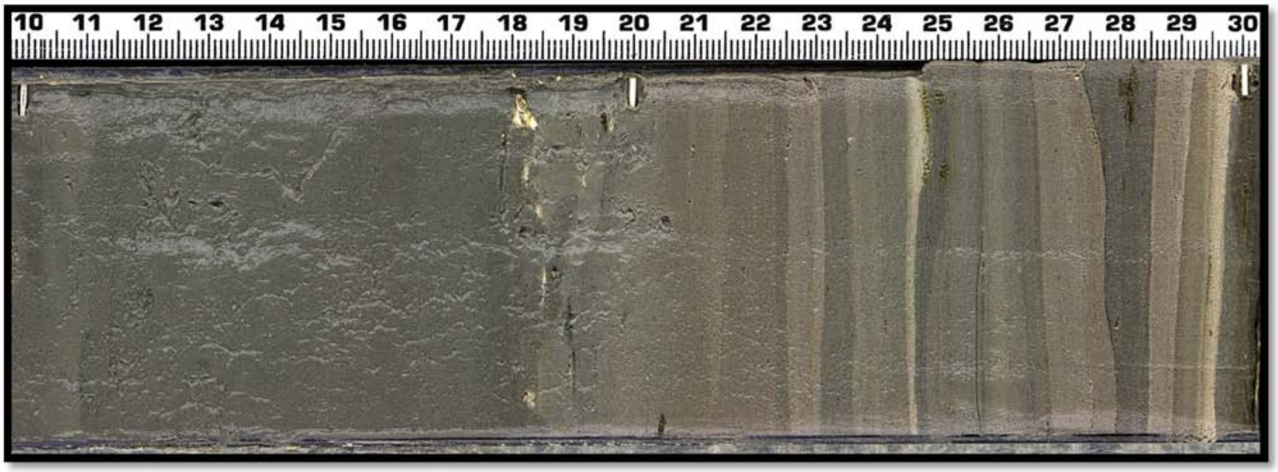

Figure 27—Effect of ICW Opening on Core BB04-3 Sedimentation Style
The above image shows the drastic change in sedimentation style in core BB04-3 related to the opening of the ICW in 1949. Note that the contrast in the image has been enhanced to accentuate visibility of the stratigraphy. Beautiful carbonate laminae deposition (20-27% carbonate by weight) is abruptly replaced by non-laminated sedimentation (7-11% carbonate by weight) at about ~20 cm depth. This suggests increased flushing drastically decreased the alkalinity needed for carbonate-rich sedimentation.

TOC Variations

Long-term trends in TOC throughout the basin are presented in Figure 15. As reported in the Total Orga*n*ic Carbon portion of the Results section, the three sediment cores in the main basin show a general long-term trend towards increasing TOC values from 120 cm depth upwards. But around mid-core, the general trend reverses, and the values become progressively lower upwards to the core tops. This shift occurs at about ~60 cm depth in core BB02ALT-1, which probably represents AD ~1930 according to the interpreted chronology (Table 6). This is the same depth at which the long-term trends of the chlorophyll and carotenoid pigment curves begin to diverge as discussed above, and that was interpreted to represent a progressive, long-term decrease in oxygenation of the water column due to eutrophication of the basin. Thus, an initial, intuitive expectation is that TOC values should increase, too, but this does not seem to the case.

This relationship seems puzzling, but as the question was explored, it became clear that the initial, intuitive expectation was not necessarily correct. While chlorophyll and TOC trends often mirror each other, it is recognized that this is not the case in all estuaries, especially those with high TOC values. For example, such mirroring breaks down in the Schuylkill River estuary and some of the western tributary branches of the Chesapeake Bay where results show very high TOC values, but low chlorophyll values (EPA, 1998). Like the systems mentioned above, the Baffin Bay sediments have high TOC values with 0-120 cm averages for all 12 cores ranging from 4.10-6.66% (Table 4). This might explain why TOC values do not display progressively increasingly value up core like is seen with chlorophyll content—TOC is already elevated along the length of the cores due to very good preservation.

General Observations About the How the System Functions

Based on the sediment cores and results from this report, it is possible to make some general comments about how the system functions as a whole with respect to water quality and sedimentation in the main basin and secondary bays.

The sediment cores from the eastern main basin (BB01-2, BB02-ALT-1, and BB03-3) show similar responses to events witnessed throughout the basin, and show the greatest impact, at least with respect to changes in sediment composition, as related to the opening of the ICW. Core BB01-2 also includes, superimposed on the main basin trends, the common influence of sediment contributions from the Laguna Madre given its location.

Core BB04-3 bottomed out in shell hash, but the ~60 cm of muddy sediment that caps the sequence shows very similar trends in most of the analyses as the main basin cores, but just in a compressed vertical section. Nonetheless, the carbonate-rich laminae that were being deposited at that location prior to the opening of the ICW (Figure 27) are only present in cores from the Laguna Salada and Cayo del Grullo tributary bays. Therefore, the water column at this location appears to have some affinity for what is happening in the tributary bays, too. This affinity may be less directly related to the tributary bays themselves, and simply a function of the bathymetric highs that surround the station (Figure 2).

Cores BB05-3, BB06-3, and BB07-1 are located along the length of the Alazan Bay with the latter being located the farthest into the bay away from the main basin. Results for cores BB05-3 and BB06-3 suggest their records reflect events happening in that tributary bay, but curiously, core BB07-1 often shows analysis results that are similar to the cores from the main basin. This is unexpected especially given the reef at the mouth of the bay which partially restricts exchange with the main basin. Nonetheless, it does indicate that water quality changes seen in the main basin may also be clearly noted deep into Alazan Bay.

Core BB08-1, located at the western end of the main basin at the confluence of the Laguna Salada and Cayo del Grullo tributaries, usually shows trends in analysis results that are similar to the main basin. But the response are not quite as marked, and this probably reflects a greater impact of the water masses in the adjacent tributary bays.

Cores BB10-2, BB11-2, and BB12-1 are located along the length of the Cayo del Grullo tributary bay with the latter being located the farthest into the bay away from the main basin. The cores provide a tributary-centric record of water-quality and sedimentation history that is strongly influenced by contributions from fluvial activity.

Finally, core BB09-3 from the Laguna Salada shows trends in analysis results that sometimes are similar to the other tributary bays, but are also frequently different (for example, the results for carbonate content and inferred pigment concentration). This may have some significance with respect to the initiation of algal blooms such as brown tide because such blooms do not seem to be initiated in the main basin, but instead, presumably spread there from the tributary bays. Given that core BB07-1 from Alazan Bay does reflect water quality changes seen in the main basin, it may not be the most likely candidate bay for the initiation of these blooms. Instead, the Laguna Salada, which functions somewhat independently, might serve as the initiator.

H. Suggestions for Future Work

Several suggestions for future work emerge from this study.

It would be very helpful to prepare a detailed examination of natural, climatological, and historical events that affected the basin, but specifically focused on events that would strongly be linked to water quality or sedimentation. This includes, for example, drought events, hurricanes, better tracking of the growth of populations, urbanization, and other industries in the watershed, and similar. This would provide guidance to help firm up the chronology, and provide better explanations for the proxy evidence.

Additional chronologic control would be helpful because it is clear that there are substantial differences in sedimentation rates throughout the basin. Together with a tighter transect of sediment cores that runs from the main basin into one of the tributary bays, this would be especially helpful for better defining the relationship between these two areas.

An expansion of proxy analyses would be very useful. The true strength of a multiproxy study has hopefully emerged in the pages of this report. By looking at just one or a couple of proxies, we develop an extremely limited picture of the basin as a whole. But via this multiproxy study, it is clear that no single proxy is enough by itself. Where one proxy is indefinite or equivocal about a particular event, we can cast light on the event from multiple proxies, and provide more robust interpretations.

Finally, while additional sediment cores from sites throughout the system could help fill in the picture, one particular area to focus on would be the Laguna Salada tributary bay. This could potentially provide important information about the origin point for brown tide blooms.

I. Acknowledgements

The success of this project is due to the support and help of many different people, and we offer our thanks here.

From the Coastal Bend Bays and Estuaries Program, Jace Tunnell took a great interest in this project, and helped give us liftoff. And when Jace moved on to MANERR, Rosario Martinez ably stepped in, and continued to support this work with great flexibility. We sincerely thank you Jace, Rosario, the CBBEP for your support with this project!

Bobby Duke (TAMUCC Center for Coastal Studies) made our field work and time on the water a breeze—he let us focus on the science while he took care of everything else. Thank you, Bobby!

Several folks with the TAMUCC Earth System Science Lab helped either in the field, or in the lab, or both. This includes Grace Davila, Rifat Ilhan, Mark McKay, and Chasidy Palmer. Special thanks go to Grace and Chasidy who helped with much of the tedious work that is associated with high resolution analyses, and similarly to Mark for his help with this project.

I-Shuo "Wade" Huang (TAMUCC Center for Coastal Studies) was the critical force behind actually running the HPLC pigment analyses. Thank you, Wade!

Whitney Rutledge stepped in to run the gamma ray spectroscopy station on several occasions to keep things going. Thank you, Whitney!

And finally, DeAnna Greer (TAMUCC Conrad Blucher Institute) did a tremendous job with helping to take care of the budget and all the related administrative matters so we could stay focused on the science. Thank you, DeAnna!

J. Literature Cited

Dean, W.E. Jr., 1974. Determination of carbonate and organic matter in calcareous and sedimentary rocks by loss on ignition: comparison with other methods, Journal of Sedimentary Petrology, v. 44, no. 1, p. 242-248.

Environmental Protection Agency. 1998. Mid-Atlantic Integrated Assessment Estuaries (MAIA-E), Summary Report, Environmental Conditions in the Mid-Atlantic Estuaries. 115 pp.

Nueces River Authority. 2013. 2013 Basin Summary Report, 201 pp.

Pribyl, D.W. 2010. A critical review of the conventional SOC to SOM conversion factor. Geoderma, v. 156, p. 75-83.

Rein, B. and Sirocko, F. 2002. In-situ reflectance spectroscopy–analysing techniques for high-resolution pigment logging in sediment cores. International Journal of Earth Sciences, v. 91, p. 950-954.

Texas Department of Transportation. 2006. Gulf Intracoastal Waterway, 2005-2006 Legislative Report, 14 pp.

Zimba, P.V., Dionigi, C.P., Millie, D.F. 1999. Evaluating the relationship between photopigment synthesis and 2-methylisoborneol accumulation in cyanobacteria. Journal of Phycology 35, p. 1422-1429.

Zimba, P.V., Tucker, C.S., Mischke, C.C., Grimm, C.G. 2002. Short-term effects of diuron on catfish pond ecology. North American Journal of Aquaculture 64, p. 16– 23.

K. Appendix: Complete Results Panels for Baffin Bay Sediment Cores

This appendix contains the complete results panels for all the sediment cores that were examined for this project.

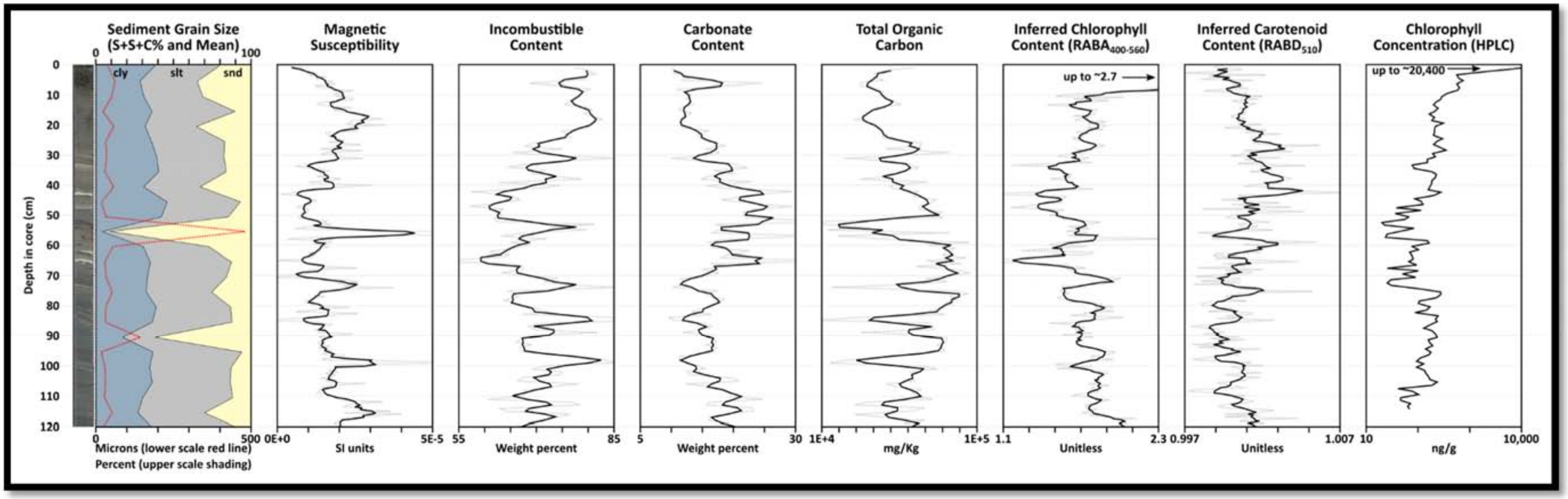

Figure 28—Sediment Core BB01-2 Results Panel

This figure shows a thumbnail image of sediment core BB01-2 from 0-120 cm depth followed by analysis results. Sediment grain size was analyzed at 5-cm resolution, and sand, silt, and clay percentages totaling 100% are represented by the blue, gray, and yellow shading, respectively. The mean grain size from 0-500 microns diameter is represented in the same plot by the red line. Magnetic susceptibility, inferred chlorophyll content ($RABA_{400-560}$), and inferred carotenoid content ($RABD_{510}$) analyses were performed at 0.5-cm resolution. Incombustible content, carbonate content, and total organic carbon analyses were undertaken at 1-cm resolution. For both groups of analyses, the full resolution results are represented by the light gray lines in the background of the plots. To better see the trends in the data, results from both the 0.5-cm and 1-cm resolution analyses were filtered by 5- and 3-point centered running means, respectively, and this smoothed data is represented by the black lines in each plot. Chlorophyll *a* concentrations as determined by HPLC were analyzed at 1-cm resolution down the length of this core. A common plot scale for each set of analysis results was used for all cores (with a few noted exceptions) to make comparisons between cores easy. A byproduct of this common scale is that in a few cases, peak/trough values of results fall outside of the common scale range. In these cases, arrows with numbers show the maximum peak/trough values that were reached.

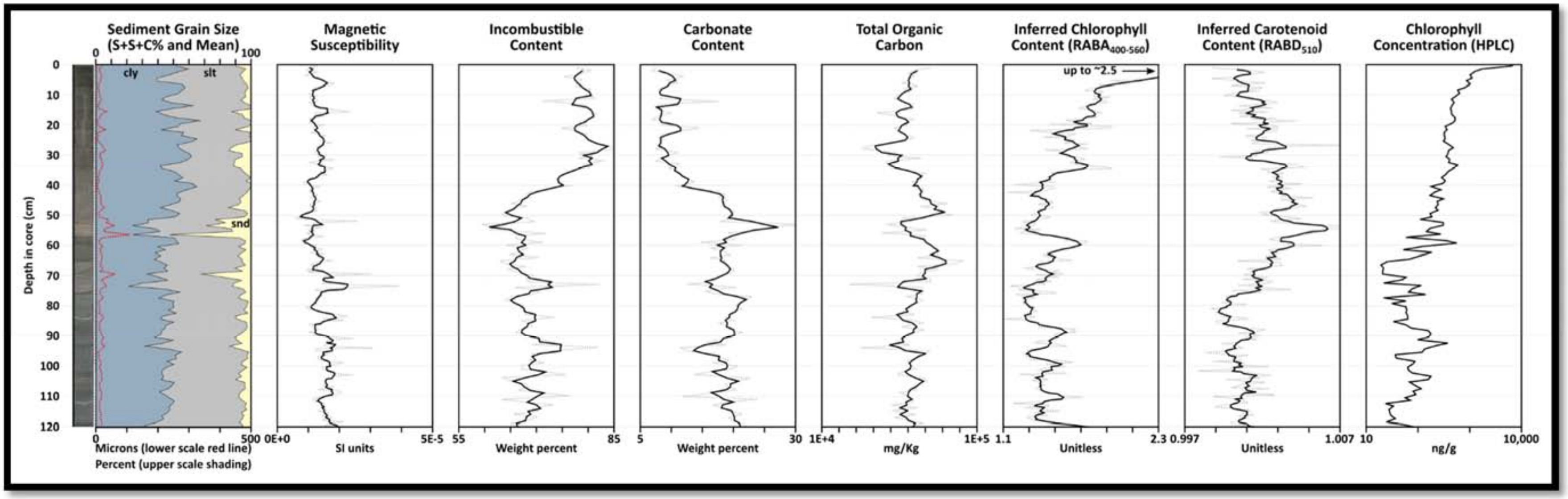

Figure 29—Sediment Core BB02ALT-1 Results Panel

This figure shows a thumbnail image of sediment core BB02ALT-1 from 0-120 cm depth followed by analysis results. Sediment grain size was analyzed at 1-cm resolution, and sand, silt, and clay percentages totaling 100% are represented by the blue, gray, and yellow shading, respectively. The mean grain size from 0-500 microns diameter is represented in the same plot by the red line. Magnetic susceptibility, inferred chlorophyll content ($RABA_{400\text{-}560}$), and inferred carotenoid content ($RABD_{510}$) analyses were performed at 0.5-cm resolution. Incombustible content, carbonate content, and total organic carbon analyses were undertaken at 1-cm resolution. For both groups of analyses, the full resolution results are represented by the light gray lines in the background of the plots. To better see the trends in the data, results from both the 0.5-cm and 1-cm resolution analyses were filtered by 5- and 3-point centered running means, respectively, and this smoothed data is represented by the black lines in each plot. Chlorophyll *a* concentrations as determined by HPLC were analyzed at 1-cm resolution down the length of this core. A common plot scale for each set of analysis results was used for all cores (with a few noted exceptions) to make comparisons between cores easy. A byproduct of this common scale is that in a few cases, peak/trough values of results fall outside of the common scale range. In these cases, arrows with numbers show the maximum peak/trough values that were reached.

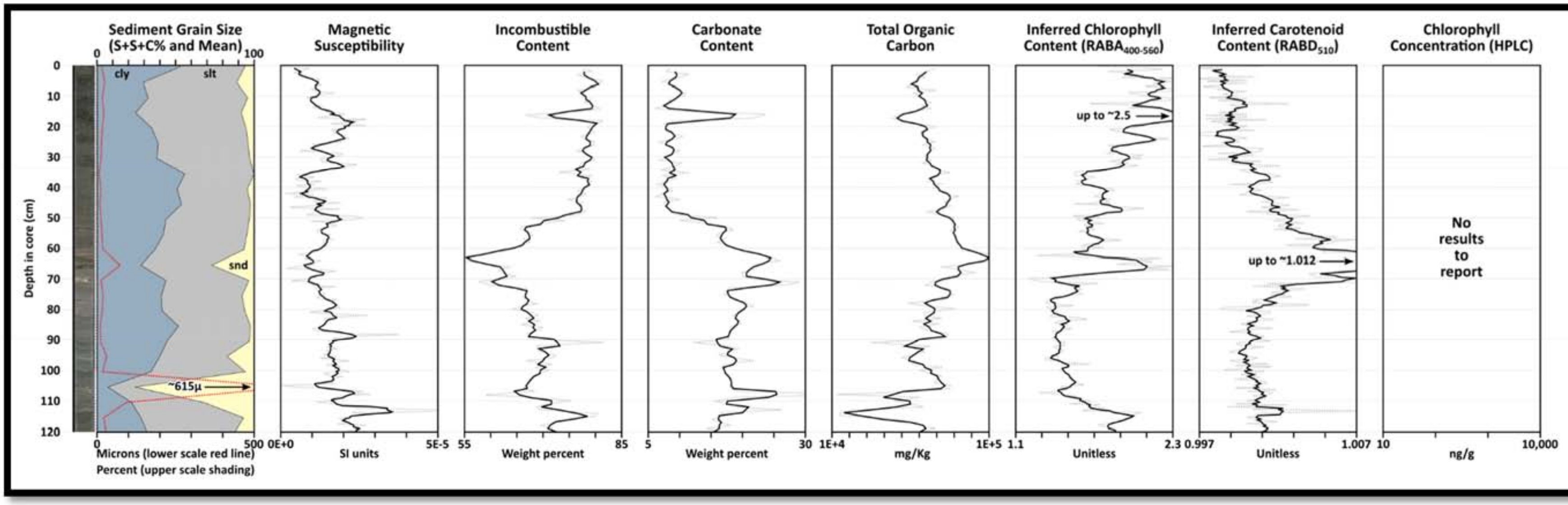

Figure 30—Sediment Core BB03-3 Results Panel

This figure shows a thumbnail image of sediment core BB03-3 from 0-120 cm depth followed by analysis results. Sediment grain size was analyzed at 5-cm resolution, and sand, silt, and clay percentages totaling 100% are represented by the blue, gray, and yellow shading, respectively. The mean grain size from 0-500 microns diameter is represented in the same plot by the red line. Magnetic susceptibility, inferred chlorophyll content ($RABA_{400\text{-}560}$), and inferred carotenoid content ($RABD_{510}$) analyses were performed at 0.5-cm resolution. Incombustible content, carbonate content, and total organic carbon analyses were undertaken at 1-cm resolution. For both groups of analyses, the full resolution results are represented by the light gray lines in the background of the plots. To better see the trends in the data, results from both the 0.5-cm and 1-cm resolution analyses were filtered by 5- and 3-point centered running means, respectively, and this smoothed data is represented by the black lines in each plot. Analysis of chlorophyll *a* concentrations as determined by HPLC was not undertaken for this core. A common plot scale for each set of analysis results was used for all cores (with a few noted exceptions) to make comparisons between cores easy. A byproduct of this common scale is that in a few cases, peak/trough values of results fall outside of the common scale range. In these cases, arrows with numbers show the maximum peak/trough values that were reached.

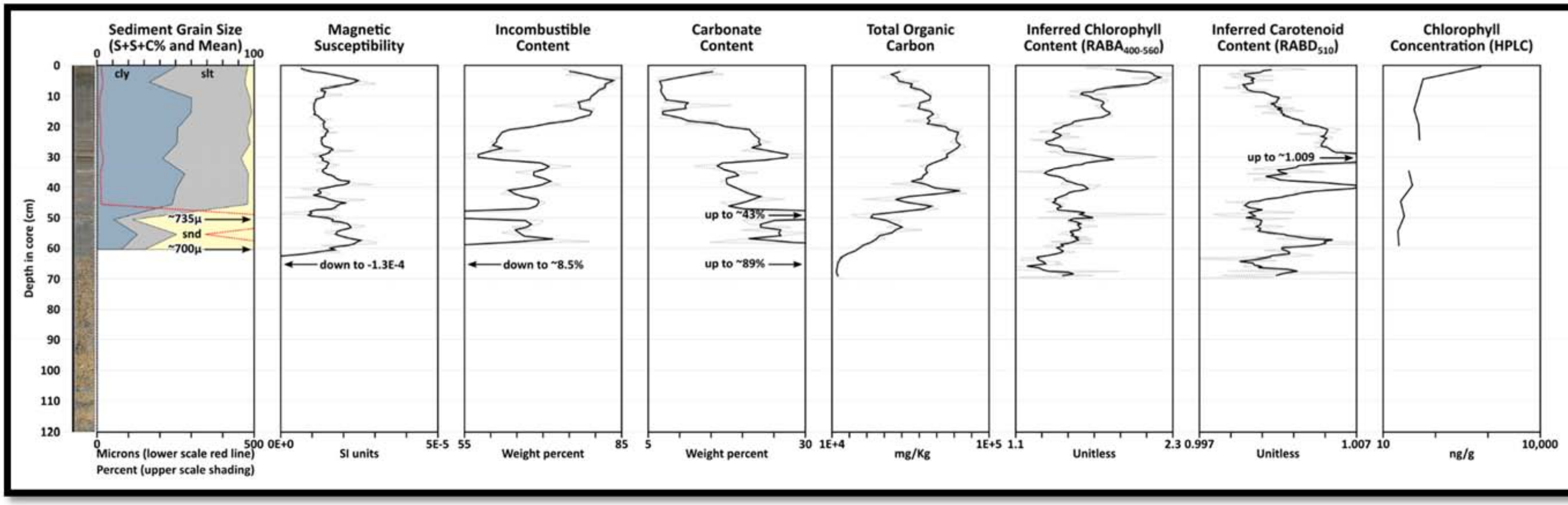

Figure 31—Sediment Core BB04-3 Results Panel

This figure shows a thumbnail image of sediment core BB04-3 from 0-120 cm depth followed by analysis results. This core transitions to essentially pure shell hash at about 63 cm depth, thus sediment grain size and chlorophyll *a* concentration analyses were only undertaken down to 60 cm depth, while the other analyses were performed down to 70 cm depth. Sediment grain size was analyzed at 5-cm resolution, and sand, silt, and clay percentages totaling 100% are represented by the blue, gray, and yellow shading, respectively. The mean grain size from 0-500 microns diameter is represented in the same plot by the red line. Magnetic susceptibility, inferred chlorophyll content ($RABA_{400-560}$), and inferred carotenoid content ($RABD_{510}$) analyses were performed at 0.5-cm resolution. Incombustible content, carbonate content, and total organic carbon analyses were undertaken at 1-cm resolution. For both groups of analyses, the full resolution results are represented by the light gray lines in the background of the plots. To better see the trends in the data, results from both the 0.5-cm and 1-cm resolution analyses were filtered by 5- and 3-point centered running means, respectively, and this smoothed data is represented by the black lines in each plot. Chlorophyll *a* concentrations as determined by HPLC were analyzed at 5-cm resolution for this core, but only down to 60 cm depth. The gaps in this curve do not represent missing data, but instead represent very low measured values that fall below the minimum scale value of 10 ng/g concentration. A common plot scale for each set of analysis results was used for all cores (with a few noted exceptions) to make comparisons between cores easy. A byproduct of this common scale is that in a few cases, peak/trough values of results fall outside of the common scale range. In these cases, arrows with numbers show the maximum peak/trough values that were reached.

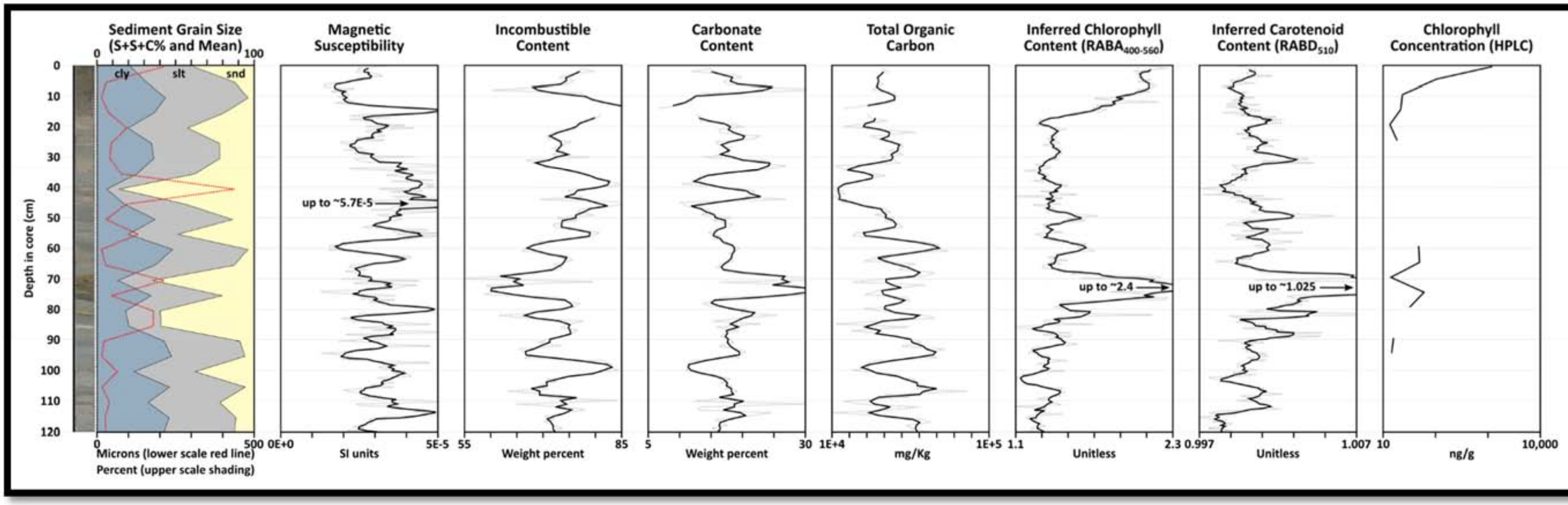

Figure 32—Sediment Core BB05-3 Results Panel

This figure shows a thumbnail image of sediment core BB05-3 from 0-120 cm depth followed by analysis results. Sediment grain size was analyzed at 5-cm resolution, and sand, silt, and clay percentages totaling 100% are represented by the blue, gray, and yellow shading, respectively. The mean grain size from 0-500 microns diameter is represented in the same plot by the red line. Magnetic susceptibility, inferred chlorophyll content ($RABA_{400-560}$), and inferred carotenoid content ($RABD_{510}$) analyses were performed at 0.5-cm resolution. Incombustible content, carbonate content, and total organic carbon analyses were undertaken at 1-cm resolution. For both groups of analyses, the full resolution results are represented by the light gray lines in the background of the plots. To better see the trends in the data, results from both the 0.5-cm and 1-cm resolution analyses were filtered by 5- and 3-point centered running means, respectively, and this smoothed data is represented by the black lines in each plot. The small gap centered on 15 cm depth, and seen in the incombustible content, carbonate content, and total organic carbon curves represents a single sample that was lost during analysis. As the results are filtered by a 3-point centered running mean, it makes the gap appear larger (3 samples) than it really is (1 sample). Chlorophyll *a* concentrations as determined by HPLC were analyzed at 5-cm resolution for this core down to 100 cm depth. The gaps in this curve do not represent missing data, but instead represent very low measured values that fall below the minimum scale value of 10 ng/g concentration. A common plot scale for each set of analysis results was used for all cores (with a few noted exceptions) to make comparisons between cores easy. A byproduct of this common scale is that in a few cases, peak/trough values of results fall outside of the common scale range. In these cases, arrows with numbers show the maximum peak/trough values that were reached.

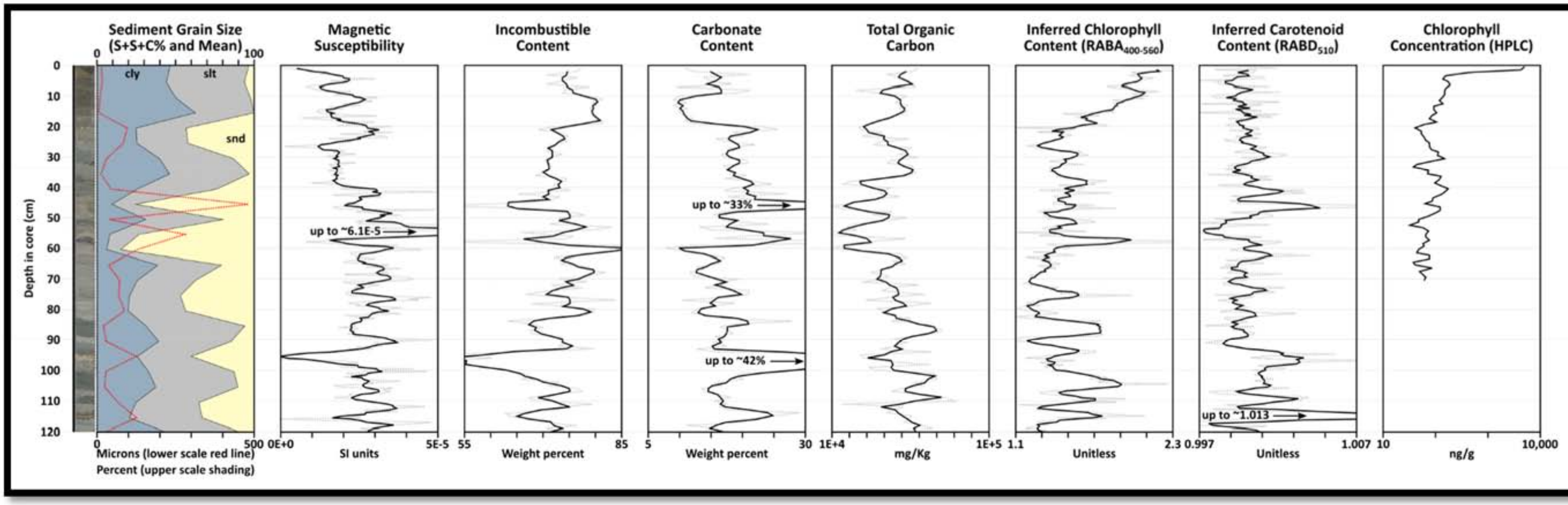

Figure 33—Sediment Core BB06-3 Results Panel

This figure shows a thumbnail image of sediment core BB06-3 from 0-120 cm depth followed by analysis results. Sediment grain size was analyzed at 5-cm resolution, and sand, silt, and clay percentages totaling 100% are represented by the blue, gray, and yellow shading, respectively. The mean grain size from 0-500 microns diameter is represented in the same plot by the red line. Magnetic susceptibility, inferred chlorophyll content ($RABA_{400-560}$), and inferred carotenoid content ($RABD_{510}$) analyses were performed at 0.5-cm resolution. Incombustible content, carbonate content, and total organic carbon analyses were undertaken at 1-cm resolution. For both groups of analyses, the full resolution results are represented by the light gray lines in the background of the plots. To better see the trends in the data, results from both the 0.5-cm and 1-cm resolution analyses were filtered by 5- and 3-point centered running means, respectively, and this smoothed data is represented by the black lines in each plot. Chlorophyll *a* concentrations as determined by HPLC were analyzed at 1-cm resolution for this core, but only down to 71 cm depth. A common plot scale for each set of analysis results was used for all cores (with a few noted exceptions) to make comparisons between cores easy. A byproduct of this common scale is that in a few cases, peak/trough values of results fall outside of the common scale range. In these cases, arrows with numbers show the maximum peak/trough values that were reached.

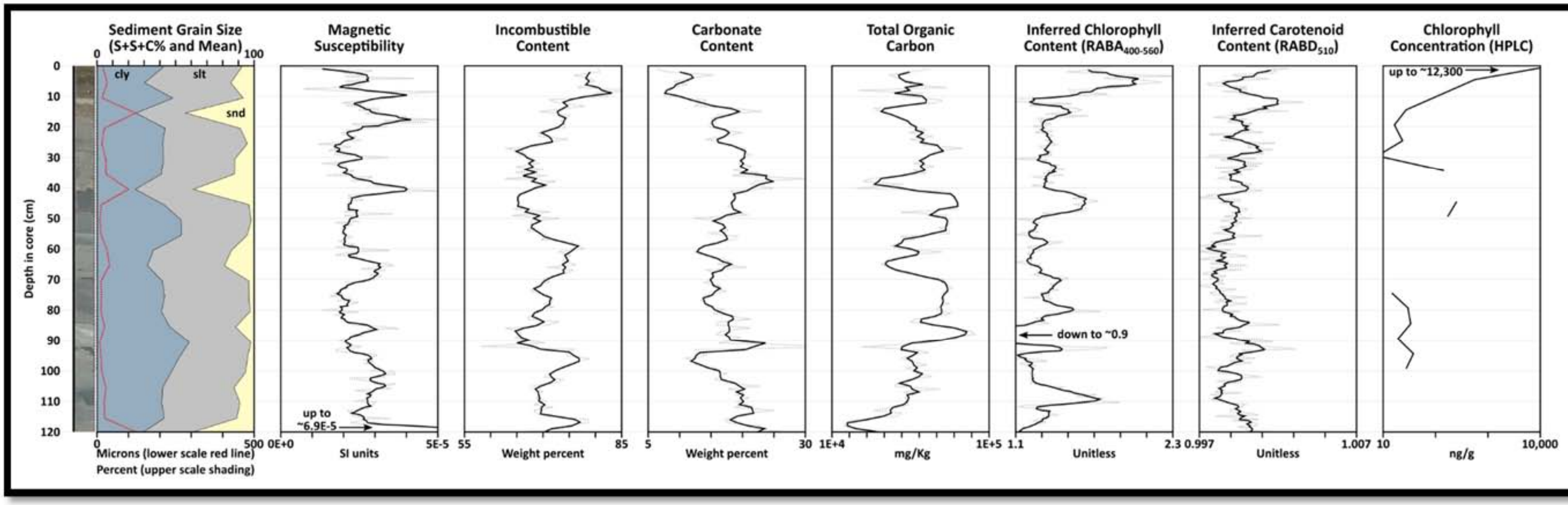

Figure 34—Sediment Core BB07-1 Results Panel

This figure shows a thumbnail image of sediment core BB07-1 from 0-120 cm depth followed by analysis results. Sediment grain size was analyzed at 5-cm resolution, and sand, silt, and clay percentages totaling 100% are represented by the blue, gray, and yellow shading, respectively. The mean grain size from 0-500 microns diameter is represented in the same plot by the red line. Magnetic susceptibility, inferred chlorophyll content ($RABA_{400\text{-}560}$), and inferred carotenoid content ($RABD_{510}$) analyses were performed at 0.5-cm resolution. Incombustible content, carbonate content, and total organic carbon analyses were undertaken at 1-cm resolution. For both groups of analyses, the full resolution results are represented by the light gray lines in the background of the plots. To better see the trends in the data, results from both the 0.5-cm and 1-cm resolution analyses were filtered by 5- and 3-point centered running means, respectively, and this smoothed data is represented by the black lines in each plot. Chlorophyll *a* concentrations as determined by HPLC were analyzed at 5-cm resolution for this core down to 100 cm depth. The gaps in this curve do not represent missing data, but instead represent very low measured values that fall below the minimum scale value of 10 ng/g concentration. A common plot scale for each set of analysis results was used for all cores (with a few noted exceptions) to make comparisons between cores easy. A byproduct of this common scale is that in a few cases, peak/trough values of results fall outside of the common scale range. In these cases, arrows with numbers show the maximum peak/trough values that were reached.

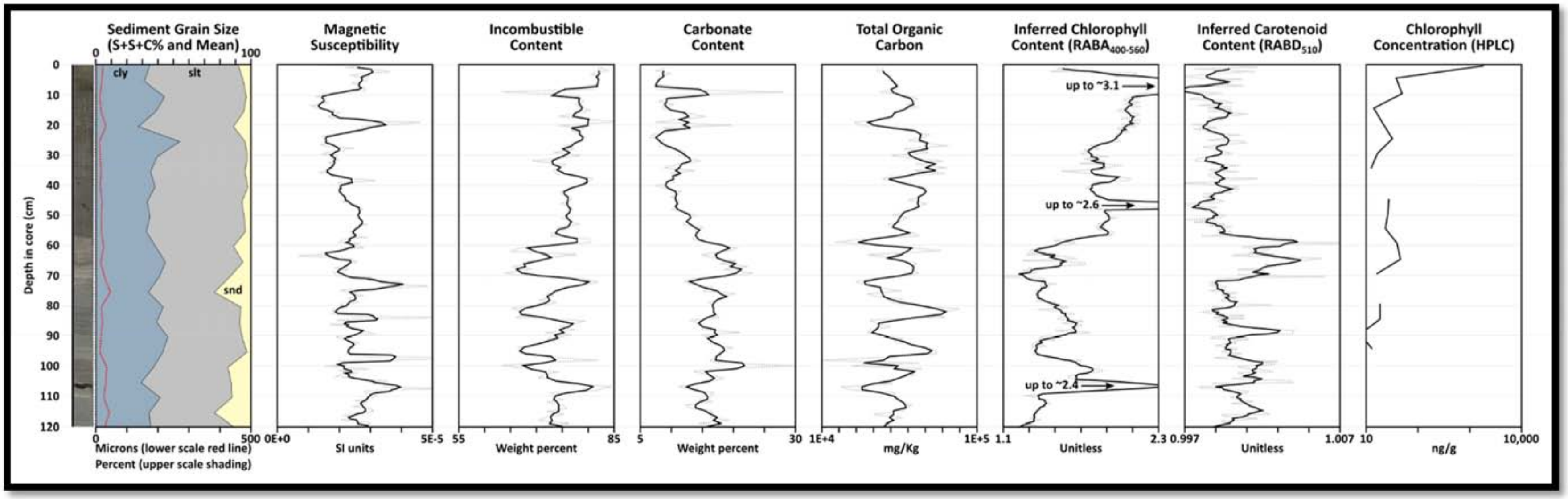

Figure 35—Sediment Core BB08-1 Results Panel

This figure shows a thumbnail image of sediment core BB08-1 from 0-120 cm depth followed by analysis results. Sediment grain size was analyzed at 5-cm resolution, and sand, silt, and clay percentages totaling 100% are represented by the blue, gray, and yellow shading, respectively. The mean grain size from 0-500 microns diameter is represented in the same plot by the red line. Magnetic susceptibility, inferred chlorophyll content ($RABA_{400\text{-}560}$), and inferred carotenoid content ($RABD_{510}$) analyses were performed at 0.5-cm resolution. Incombustible content, carbonate content, and total organic carbon analyses were undertaken at 1-cm resolution. For both groups of analyses, the full resolution results are represented by the light gray lines in the background of the plots. To better see the trends in the data, results from both the 0.5-cm and 1-cm resolution analyses were filtered by 5- and 3-point centered running means, respectively, and this smoothed data is represented by the black lines in each plot. Chlorophyll *a* concentrations as determined by HPLC were analyzed at 5-cm resolution for this core down to 100 cm depth. The gaps in this curve do not represent missing data, but instead represent very low measured values that fall below the minimum scale value of 10 ng/g concentration. A common plot scale for each set of analysis results was used for all cores (with a few noted exceptions) to make comparisons between cores easy. A byproduct of this common scale is that in a few cases, peak/trough values of results fall outside of the common scale range. In these cases, arrows with numbers show the maximum peak/trough values that were reached.

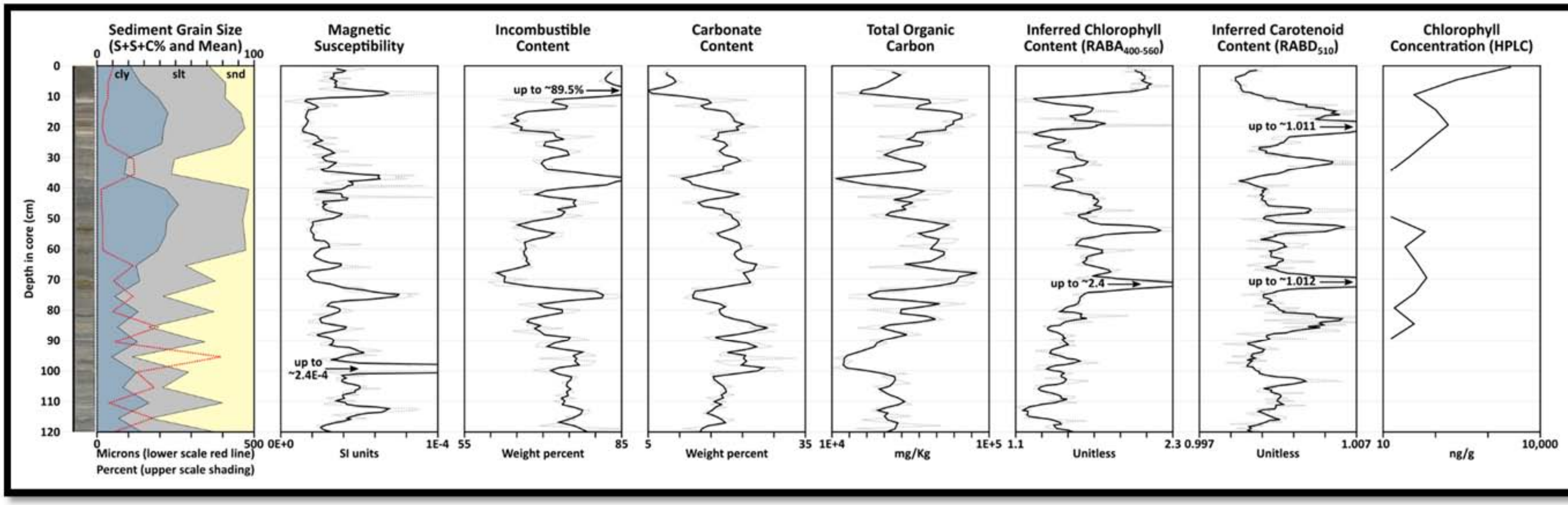

Figure 36—Sediment Core BB09-3 Results Panel

This figure shows a thumbnail image of sediment core BB09-3 from 0-120 cm depth followed by analysis results. Sediment grain size was analyzed at 5-cm resolution, and sand, silt, and clay percentages totaling 100% are represented by the blue, gray, and yellow shading, respectively. The mean grain size from 0-500 microns diameter is represented in the same plot by the red line. Magnetic susceptibility, inferred chlorophyll content ($RABA_{400-560}$), and inferred carotenoid content ($RABD_{510}$) analyses were performed at 0.5-cm resolution. Incombustible content, carbonate content, and total organic carbon analyses were undertaken at 1-cm resolution. For both groups of analyses, the full resolution results are represented by the light gray lines in the background of the plots. To better see the trends in the data, results from both the 0.5-cm and 1-cm resolution analyses were filtered by 5- and 3-point centered running means, respectively, and this smoothed data is represented by the black lines in each plot. Chlorophyll *a* concentrations as determined by HPLC were analyzed at 5-cm resolution for this core down to 100 cm depth. The gaps in this curve do not represent missing data, but instead represent very low measured values that fall below the minimum scale value of 10 ng/g concentration. A common plot scale for each set of analysis results was used for all cores (with a few noted exceptions) to make comparisons between cores easy. A byproduct of this common scale is that in a few cases, peak/trough values of results fall outside of the common scale range. In these cases, arrows with numbers show the maximum peak/trough values that were reached.

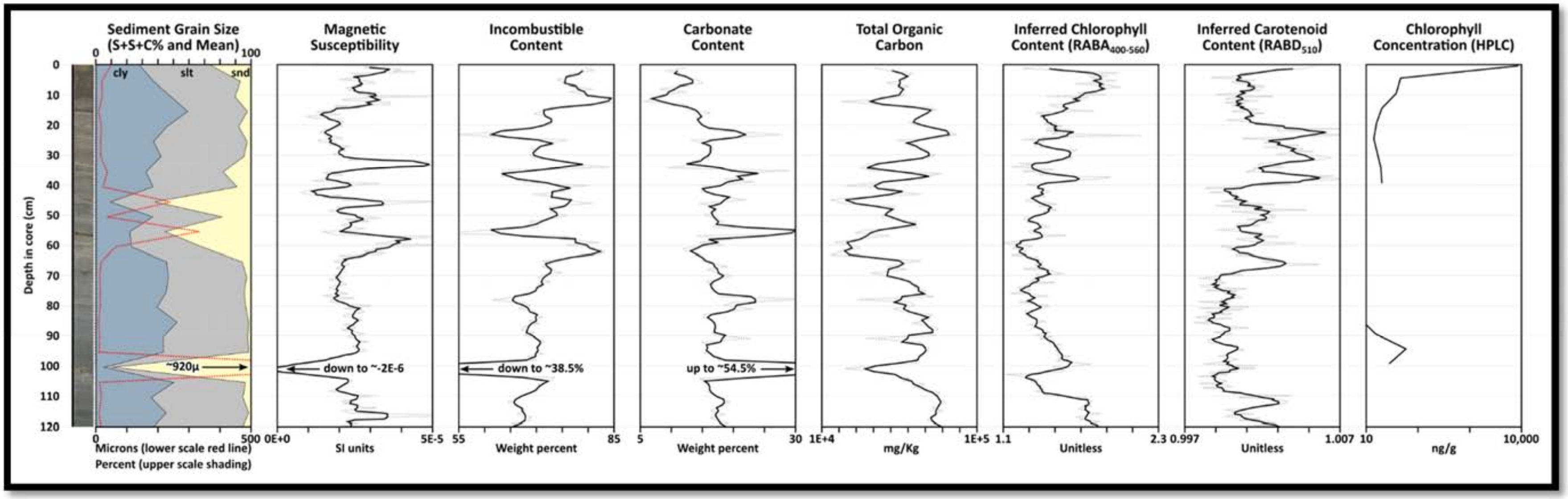

Figure 37—Sediment Core BB10-2 Results Panel

This figure shows a thumbnail image of sediment core BB10-2 from 0-120 cm depth followed by analysis results. Sediment grain size was analyzed at 5-cm resolution, and sand, silt, and clay percentages totaling 100% are represented by the blue, gray, and yellow shading, respectively. The mean grain size from 0-500 microns diameter is represented in the same plot by the red line. Magnetic susceptibility, inferred chlorophyll content ($RABA_{400\text{-}560}$), and inferred carotenoid content ($RABD_{510}$) analyses were performed at 0.5-cm resolution. Incombustible content, carbonate content, and total organic carbon analyses were undertaken at 1-cm resolution. For both groups of analyses, the full resolution results are represented by the light gray lines in the background of the plots. To better see the trends in the data, results from both the 0.5-cm and 1-cm resolution analyses were filtered by 5- and 3-point centered running means, respectively, and this smoothed data is represented by the black lines in each plot. Chlorophyll *a* concentrations as determined by HPLC were analyzed at 5-cm resolution for this core down to 100 cm depth. The gaps in this curve do not represent missing data, but instead represent very low measured values that fall below the minimum scale value of 10 ng/g concentration. A common plot scale for each set of analysis results was used for all cores (with a few noted exceptions) to make comparisons between cores easy. A byproduct of this common scale is that in a few cases, peak/trough values of results fall outside of the common scale range. In these cases, arrows with numbers show the maximum peak/trough values that were reached.

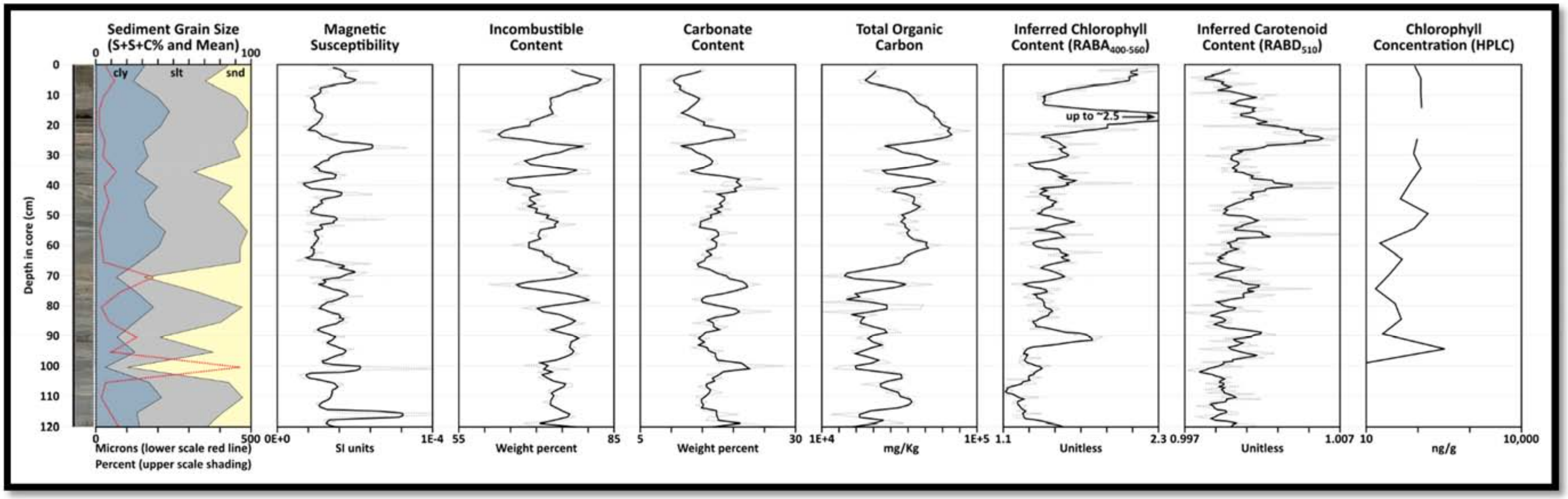

Figure 38—Sediment Core BB11-2 Results Panel

This figure shows a thumbnail image of sediment core BB11-2 from 0-120 cm depth followed by analysis results. Sediment grain size was analyzed at 5-cm resolution, and sand, silt, and clay percentages totaling 100% are represented by the blue, gray, and yellow shading, respectively. The mean grain size from 0-500 microns diameter is represented in the same plot by the red line. Magnetic susceptibility, inferred chlorophyll content ($RABA_{400-560}$), and inferred carotenoid content ($RABD_{510}$) analyses were performed at 0.5-cm resolution. Incombustible content, carbonate content, and total organic carbon analyses were undertaken at 1-cm resolution. For both groups of analyses, the full resolution results are represented by the light gray lines in the background of the plots. To better see the trends in the data, results from both the 0.5-cm and 1-cm resolution analyses were filtered by 5- and 3-point centered running means, respectively, and this smoothed data is represented by the black lines in each plot. Chlorophyll *a* concentrations as determined by HPLC were analyzed at 5-cm resolution for this core down to 100 cm depth. The gaps in this curve do not represent missing data, but instead represent very low measured values that fall below the minimum scale value of 10 ng/g concentration. A common plot scale for each set of analysis results was used for all cores (with a few noted exceptions) to make comparisons between cores easy. A byproduct of this common scale is that in a few cases, peak/trough values of results fall outside of the common scale range. In these cases, arrows with numbers show the maximum peak/trough values that were reached.

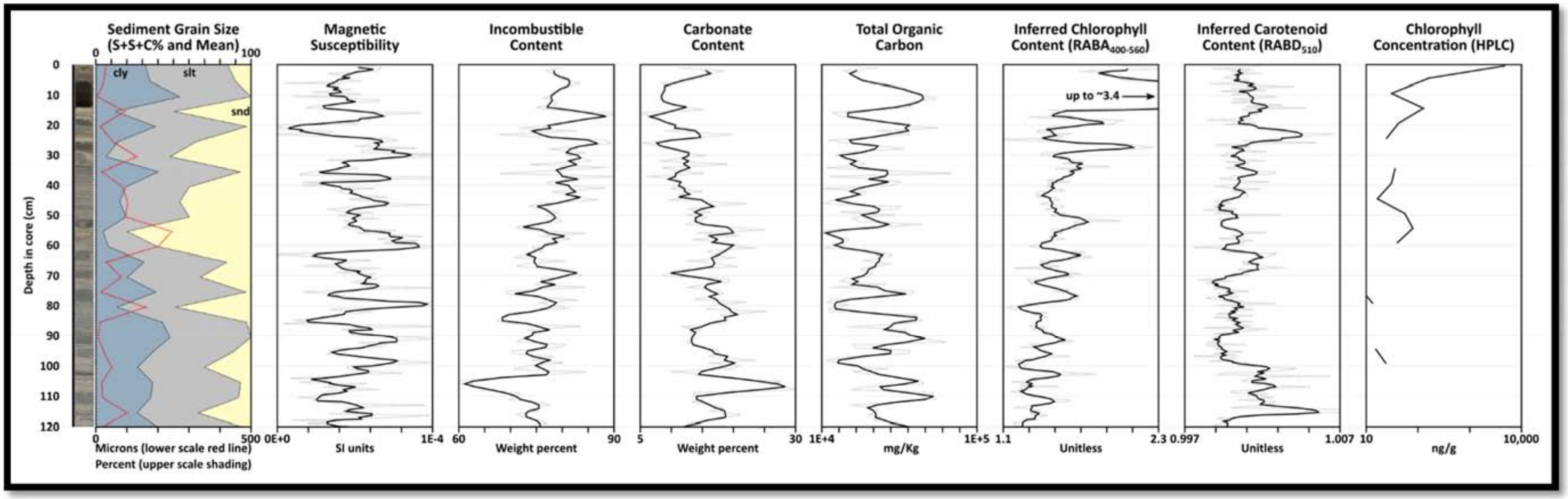

Figure 39—Sediment Core BB12-1 Results Panel
This figure shows a thumbnail image of sediment core BB12-1 from 0-120 cm depth followed by analysis results. Sediment grain size was analyzed at 5-cm resolution, and sand, silt, and clay percentages totaling 100% are represented by the blue, gray, and yellow shading, respectively. The mean grain size from 0-500 microns diameter is represented in the same plot by the red line. Magnetic susceptibility, inferred chlorophyll content ($RABA_{400-560}$), and inferred carotenoid content ($RABD_{510}$) analyses were performed at 0.5-cm resolution. Incombustible content, carbonate content, and total organic carbon analyses were undertaken at 1-cm resolution. Note that the plot scale for incombustible content for this core runs from 60-90% whereas for the other 11 cores, it runs from 55-85%. For both groups of analyses, the full resolution results are represented by the light gray lines in the background of the plots. To better see the trends in the data, results from both the 0.5-cm and 1-cm resolution analyses were filtered by 5- and 3-point centered running means, respectively, and this smoothed data is represented by the black lines in each plot. Chlorophyll *a* concentrations as determined by HPLC were analyzed at 5-cm resolution for this core down to 100 cm depth. The gaps in this curve do not represent missing data, but instead represent very low measured values that fall below the minimum scale value of 10 ng/g concentration. A common plot scale for each set of analysis results was used for all cores (with a few noted exceptions) to make comparisons between cores easy. A byproduct of this common scale is that in a few cases, peak/trough values of results fall outside of the common scale range. In these cases, arrows with numbers show the maximum peak/trough values that were reached.